International Scientific-Technical and Production Journal

# The Paton WELDING JOURNAL

May 2003 # 5

English translation of the monthly «Avtomaticheskaya Svarka» (Automatic Welding) journal published in Russian since 1948

**Founders:** *The E.O. Paton Electric Welding Institute of the NAS of Ukraine*
*International Association «Welding»*

**Publisher:** *International Association «Welding»*



***Address:***
*E.O. Paton Electric Welding Institute,*
*International Association «Welding»,*
*11, Bozhenko str., 03680, Kyiv, Ukraine*
*Tel.: (38044) 227 67 57*
*Fax: (38044) 268 04 86*
*E-mail: journal@paton.kiev.ua*
*http://www.nas.gov.ua/pwj*

State Registration Certificate
KV 4790 of 09.01.2001

***Subscriptions:***
$460, 12 issues per year,
postage and packaging included.
Back issues available.



## CONTENTS

# APPLICATION OF ACTIVE FLUXES AND ACTIVE GASES TO INCREASE EFFICIENCY OF ARC AND PLASMA WELDING

**B.E. PATON, M.M. SAVITSKY, V.S. GVOZDETSKY, I.V. KRIVTSUN, A.M. SAVITSKY, Yu.E. GODLIS** and **A.F. LUPAN**
E.O. Paton Electric Welding Institute, NASU, Kyiv, Ukraine

Considered are probable causes of increase in the penetration depth in plasma and arc welding by the MIG and TIG methods using activating fluxes. It is shown that deep penetration of metal is caused by contraction of the arc and increase in the concentration of thermal and mechanical effects of plasma on metal with a simultaneous decrease in its surface tension at the presence of elements that have a high surface activity and susceptibility to formation of negative or positive ions.

***Keywords:*** *plasma and arc welding in inert-gas atmosphere, activating fluxes, metal and tungsten electrodes, arc pressure, surface tension, penetration, mechanical properties, welded joint*

Activation of processes occurring in the weld pool and arc burning in inert gases by using microadditions of chemical elements is an advanced area of development of welding [1–3]. Addition of 0.10–0.01 % (of mass of metal melted) of elements which have a high surface activity and susceptibility to formation of negative or positive ions to the welding zone allows values of the weld form factor to be varied over wide ranges with no changes in welding conditions. For example, narrow welds with deep penetration (down to 12 mm) or wide welds with low penetration (about 1–2 mm) can be produced in argon-arc welding by the TIG method [4].

Technologies of argon-arc welding of steels and titanium alloys by the TIG method, developed by the E.O. Paton Electric Welding Institute, were widely applied, starting from 1970, in aircraft and rocket engineering, nuclear power generation and other industries of the former Soviet Union. Some of them, collectively called A-TIG welding, after they were tested by TWI in 1993–1995, became the subject of investigation and application in different countries of Europe, Asia and America. The efforts made separately and at different times in the USA and Japan on adaptation of the above technologies to local conditions and their improvement were included into the lists of priority directions of development of welding [6, 7].

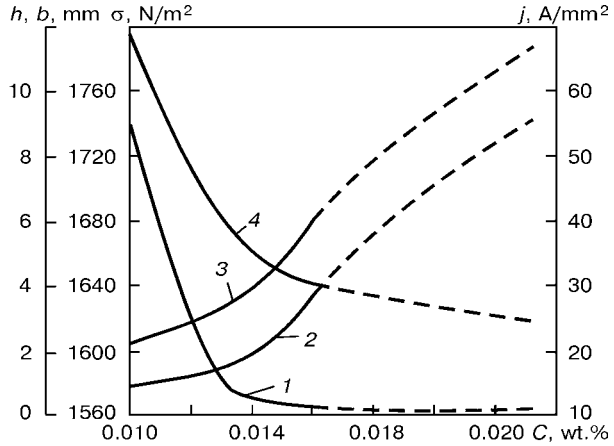


**Figure 1.** Effect of the total content $C$ of sulphur and oxygen in steel (solid curves), as well as sulphur and oxygen in steel and shielding gas (dashed curves), on $\sigma$ (*1*), $j$ (*2*), $h$ (*3*) and $b$ (*4*) in argon-arc welding

Analysis described in [8] showed the absence of a single opinion on this matter. Existing hypotheses can be conditionally subdivided into two main groups. The first group includes those which give preference to metallurgical and thermal processes occurring in liquid and solid metal, whereas the second group includes hypotheses which suggest that physical processes in the welding arc are of a primary importance.

However, the most typical situation is that in which both groups of the processes participate, with some of them prevailing over the other depending upon the conditions. Thus, it was established that in argon-arc welding by the TIG method the certain correlation exists between variations in surface tension coefficient $\sigma$ of liquid steel and weld width $b$, as well as between current density $j$ in the active spot at anode and penetration depth $h$, depending upon the total sulphur and oxygen content of steel or of steel and shielding gas (Figure 1). These elements are known to have a high surface activity and energy of affinity for electron, i.e. they can simultaneously initiate metallurgical processes in the weld pool and physical processes in the arc.

It can be seen from the Figure that as the total content $C$ of these elements in steel grows from 0.010 to 0.014 wt.%, the surface tension coefficients and width of the weld substantially decrease, which is accompanied by increase in the current density and penetration depth. Further increase in the total content of sulphur and oxygen in steel, or an extra amount of oxygen added to the shielding gas leading to increase in the total content of these elements in the welding zone to 0.02 wt.% of the molten metal, has a lower effect on the surface tension coefficient and

width of the weld than on the current density and penetration depth in steel.

Therefore, it can be assumed that at an insignificant content (up to 0.014 %) of sulphur and oxygen in steel the metallurgical processes are dominant within the welding zone. With the content of these elements in excess of 0.014 wt.% the physical processes in the arc become more active, thus leading to increase in the current density and penetration depth of metal, probably because of a more intensive thermal and mechanical impact on the weld pool by the arc.

Arc pressure $P_a$ on the surface of the weld pool in TIG welding is attributable to interaction of two forces. The effect of one of them is caused by retardation near the anode surface of the plasma flow formed in the arc column as a result of interaction of the electric current of the arc with a natural magnetic field [9], whereas the effect of the other is caused by a reactive pressure of the jet of metal vapours from the anode spot of the arc [10]. As proved by the experimental and calculation data, both components of the arc pressure are a function of current density $j$, and, since the distribution of the current density in the anode spot is described by the curve with maximum at the centre [11], the arc pressure has a similar distribution (Figure 2). As shown by experiments, increase in the sulphur and oxygen content of steel is accompanied by increase in the arc pressure on metal, while after extra activation by oxygen its value becoms commensurable with the value of surface tension (compare Figures 1 and 2).

Contraction of the arc by activators and reduction in transverse size of the weld pool surface seem to lead to increase in resistance of molten metal to penetration of the arc. However, the effect of this factor is compensated for by decrease in surface tension of metal at the metal–slag interface.

If the first component of the arc pressure is dominant in TIG welding, this leads to formation of a crater in metal, in which the plasma flow is subjected to additional contraction by the metal pressed out from the crater. This results in choking of the vapour flow, causing increase in the kinetic energy of the flow and, hence, the penetrating power of the arc.

Geometric sizes of a weld and characteristics of the plasma flow vary in a similar way. It can be seen from transverse macrosection of the weld shown in Figure 3 that the penetration zone, while going deeper into metal, first narrows and then gradually widens. If in this case the bottom of the crater is broken out, this leads to formation of a channel in metal, in which a secondary plasma flow is formed. This process is identical to that occurring in the plasmatron [12, 13]. The above-said seems to be the factor which makes the plasma flows formed by the activated arc and plasmatron closer to each other in energy and technological characteristics.

It should be noted that during the plasma welding process the plasma flow rapidly widens at its exit from the plasmatron nozzle as a result of the pressure

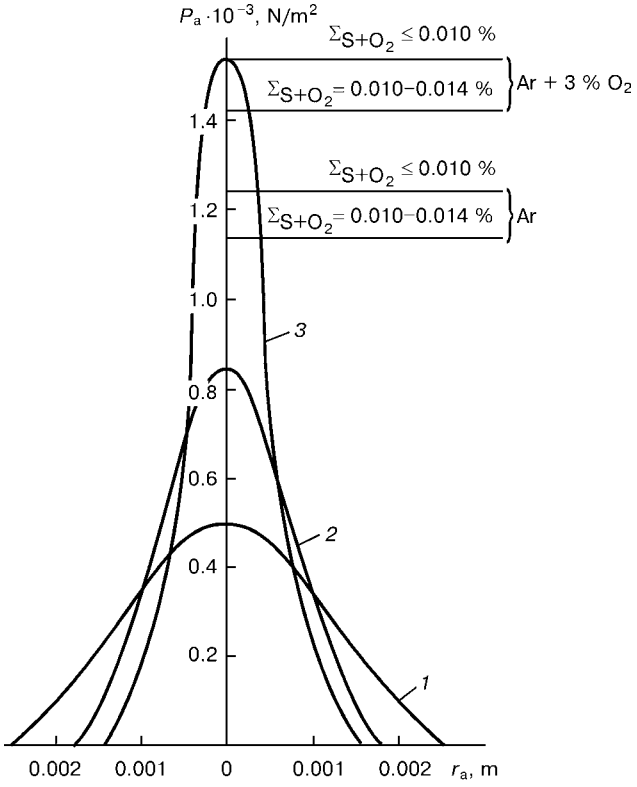


**Figure 2.** Distribution of excess pressure on anode by the arc in argon-arc welding of steel with $\sum_{S+O_2} \le 0.010$ (*1*), equal to 0.010–0.014 (*2*) and ≥ 0.014 (*3*) % (horizontal lines show levels of resistance of metal to penetration of the arc caused by surface tension $P_{s.t}$ and hydrostatic pressure $P_h$ of metal during welding in argon and Ar + 3 % $O_2$ mixture; $r_a$ is the anode spot radius)

drop, which usually leads to decrease in the intensity of heating and penetrating power of plasma. To add to it, there are easily ionised elements near the surface of the metal welded, which are contained in the base metal vapours. These elements favour widening of the plasma flow and increase resistance of metal to the penetration of plasma into the weld pool because of a high surface tension of molten metal in argon. Values of the required characteristics of plasma are usually maintained by increasing the welding current, flow rate of the plasma gas and contraction of plasma using hydrogen, as well as by decreasing the nozzle to workpiece distance [13]. Little consideration has been given so far to the effect exerted by easily ionised and surface-active elements in plasma welding. The investigation results [4] are indicative of the fact that al-

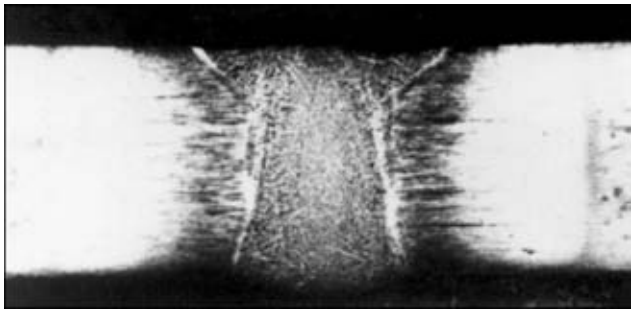

**Figure 3.** Transverse macrosection of the weld made by argon-arc welding by the TIG method with activation in steel 6 mm thick

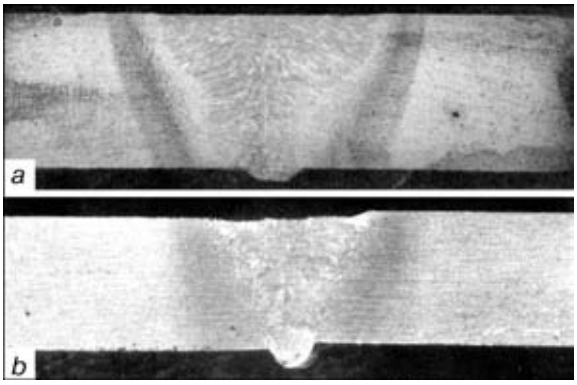


**Figure 4.** Macrosections of welds made on steel 6 mm thick by plasma welding without (*a*) and with (*b*) activation

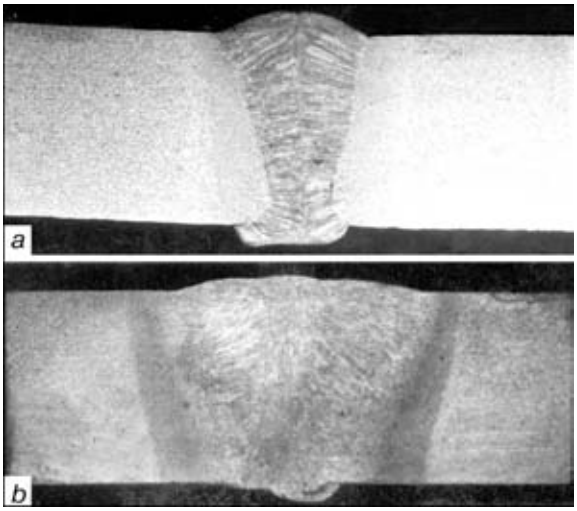


**Figure 5.** Macrosections of welds made by MIG welding on steel VSt3kp 10 mm thick in $CO_2$ (*a*) and argon with activation (*b*)

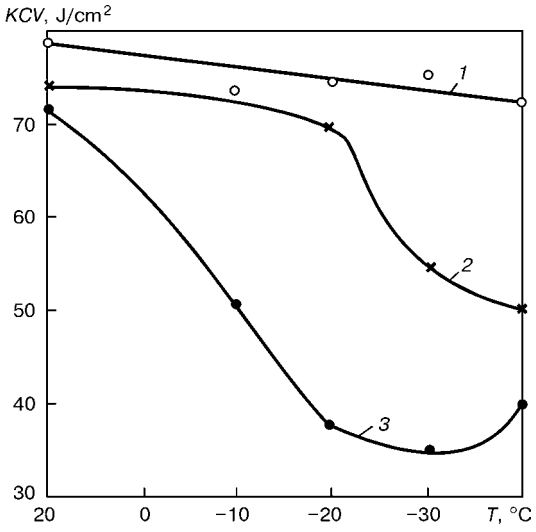


**Figure 6.** Temperature dependence of impact toughness of metal in different zones of a welded joint made by MIG welding with activation: *1* — weld; *2* — HAZ; *3* — base metal

**Table 1.** Parameters of arc and plasma welding with activation

| *Welding method* | $I_w$, *A* | $U_a$, *V* | $v_w$, *m/h* |
|---|---|---|---|
| A-TIG with flux VS-2e | 165 | 10 | 6 |
| Plasma: | | | |
| with flux VS-2e | 110 | 22 | 12 |
| without flux | 150 | 22 | 12 |

lowance for these factors would open up new opportunities for further increase in the efficiency of this welding method. Macrosections of the welds made by plasma welding on steel 6 mm thick without and with activation under conditions indicated in Table 1 are shown in Figure 4. As it can be seen from this Figure, application of an activating flux which contains materials with an increased surface activity and affinity for electron enables the plasma flow in the near-anode region to be additionally contracted and its penetrating power to be increased by a factor of 1.5–2 in welding at low currents. In this case mechanical properties of welded joints are improved and the full-strength joints are provided.

Interesting results were obtained also in MIG welding using wire Sv-08G2S, performed in argon, $CO_2$ or their mixture (Ar + 15 % $CO_2$) with or without activating fluxes. Plates 10 mm thick of steel VSt3kp (rimming) were used as the base metal [14].

The effect of increase in the penetration depth is more pronounced in welding performed in pure argon. As shown by the results of the investigations conducted (Table 2), application of an activator in this case allows the penetration depth to be increased almost 1.6 times compared with welding in $CO_2$ and in a mixture of Ar + 15 % $CO_2$, and 1.8 times compared with welding in argon without an activator. The shape of the weld is also changed in this case. The finger-shaped penetration characteristic of weld-

**Table 2.** Effect on penetration depth by activators*

| *Welding method* | *Shielding atmosphere* | *Penetration depth, mm* |
|---|---|---|
| Without activator | Ar | 3.8 |
| | Ar + 15 % $CO_2$ | 4.5 |
| | $CO_2$ | 4.5 |
| With activator | Ar | 7.0 |
| | Ar + 15 % $CO_2$ | 6.8 |
| | $CO_2$ | 4.8 |

*Welding conditions used were as follows: $I_w$ = 280 A; $U_a$ = 28 V; $v_w$ = 25 m/h.

**Table 3.** Effect of an activator on energy parameters of gas-shielded welding of steel VSt3kp 10 mm thick

| *One-pass welding* | $I_w$, *A* | $U_a$, *V* | $v_w$, *m/h* | *q/v* |
|---|---|---|---|---|
| In Ar with activator | 400 | 34 | 40 | 8654 |
| In $CO_2$ without activator | 550 | 40 | 25 | 22190 |

**Table 4.** Effect of activator on mechanical properties of welded joint

| *Welding process* | *Welded joint region* | $\sigma_y$, *MPa* | $\sigma_t$, *MPa* | *KCV, J/cm²* | |
|---|---|---|---|---|---|
| | | | | *+20 °C* | *−20 °C* |
| In Ar with activator | Weld | 510 | 680 | 79 | 70 |
| | HAZ | N/D | N/D | 74 | 74 |
| In $CO_2$ without activator | Weld | 368 | 570 | 61 | 33 |
| | HAZ | N/D | N/D | 80 | 75 |

*Note.* Welding was performed on metal with the following mechanical properties: $\sigma_y$ = 349 MPa, $\sigma_t$ = 476 MPa, $KCV_{20}$ = 71 and $KCV_{-20}$ = = 37 J/cm$^2$.

ing in pure argon becomes wedge-shaped under the effect of an activator (Figure 5).

Comparison of technological capabilities of welding in argon with an activator and in $CO_2$ without an activator showed that in one-pass welding with full penetration of metal of the same thickness the heat input $q/v$ in the first case was approximately 2.6 times as low as in the second case (Table 3).

This fact is one of the probable causes of improvement of mechanical properties of welded joints. This can be well illustrated by an example of variations in impact toughness of the weld and HAZ metal specimens with a sharp notch (Charpy) tested at −20 °C (Table 4).

As established, values of impact toughness of the base and HAZ metal tend to monotonously decrease, the value of impact toughness of the weld metal remaining almost unchanged (Figure 6).

It should be noted in conclusion that activation of physical-chemical processes occurring in TIG, MIG and plasma welding under the effect of microadditions of chemical elements creates preconditions for a more efficient utilisation of energy of the arc and performing welding at a decreased heat input, as well as for controlling the weld metal melting and solidification processes and the kinetics of structural transformations in the HAZ to improve mechanical properties and performance of welded joints. In addition, this will provide a substantial improvement in culture of welding production and its environmental safety.


1. Paton, B.E., Makara, A.M., Medovar, B.I. et al. (1977) Weldability of structural steels subjected to refining remelting. *Avtomatich. Svarka*, **6**, 1–4.
2. Makara, A.M., Savitsky, M.M., Kushnirenko, B.N. et al. (1977) Influence of refining on metal penetration in arc welding. *Ibid.*, **9**, 7–10.
3. Zamkov, V.N., Prilutsky, V.P., Gurevich, S.M. (1977) Influence of flux composition on non-consumable electrode welding process. *Ibid.*, **3**, 49–71.
4. Savitsky, M.M., Leskov, G.I. (1980) Mechanism of influence of electronegative elements on penetrating power of the arc with tungsten cathode. *Ibid.*, **9**, 17–22.
5. Jushchenko, K.A., Savitsky, M.M., Kovalenko, O.V. (1993) A-TIG welding of carbon-manganese and stainless steel. In: *Proc. of Int. Conf. on Welding Technology of Paton Institute*, Cambridge, Oct. 1993. Cambridge: Abington Publ.
6. Gordon, J.R. (1995) Perspectives on welding research and development in the USA. *Welding Rev. Int.*, August, 95–106.
7. (2001) Technologies of welding and joining in the 21st century. *J. JWS*, **3**, 6–18.
8. Savitsky, M.M., Kushnirenko, B.N., Olejnik, O.I. (1999) Peculiarities of tungsten electrode welding of steels with active fluxes (A-TIG process). *Avtomatich. Svarka*, **12**, 20–29.
9. Voropaj, N.M., Krivtsun, I.V. (1978) Gas-dynamic characteristics of plasma flows in welding arcs. *Magnitnaya Gidrodinamika*, **1**, 132–136.
10. Paton, B.E., Zamkov, V.N., Prilutsky, V.P. et al. (2000) Contraction of the welding arc caused by the flux in tungsten-electrode argon-arc welding. *The Paton Welding J.*, **1**, 5–11.
11. Savitsky, M.M., Gvozdetsky, V.S., Skrypnik, V.I. et al. (1979) Current density in anode spot during welding of conventional and refined steels. *Avtomatich. Sbarka*, **7**, 17–20.
12. Savitsky, M.M., Kushnirenko, B.N., Lupan, A.F. et al. (1981) Peculiarities of weld formation in welding with activating flux. *Ibid.*, **2**, 18–21.
13. (1979) *Microplasma welding*. Ed. by B.E. Paton. Kyiv: Naukova Dumka.
14. Dudko, D.A., Savitsky, A.M., Savitsky, M.M. (1996) Consumable electrode gas-shielded welding with activating flux. *Avtomatich. Svarka*, **10**, 54–55.

# STRUCTURE AND PROPERTIES OF WELDED JOINTS OF NICKEL-BASED HEAT-RESISTANT ALLOY

**A.A. SLIVINSKY**[1] and **P. VEIT**[2]
[1]Institute of Joining and Beam Technologies, Otto-von-Guericke University, Magdeburg, Germany
[2]Institute of Experimental Physics, Otto-von-Guericke University, Magdeburg, Germany

Results of metallographic examinations of different regions of the NiCr25FeAlY high-nickel alloy welded joints, made by tungsten electrode in inert gas, consumable electrode in mixture of gases and under the flux layer, are given. Susceptibility of the alloy to the formation of hot cracks was evaluated and the presence of ductility dip in it near 700 °C temperature after heat treatment was found. The relationship was established between the decreased ductility of the alloy and formation of phase and chemical heterogeneity.

***Keywords:*** *arc welding (TIG, MAGMS, SAW, MMAW), high-nickel alloy, welded joints, structure, technological strength, curve of ductility*

Nickel-based alloy of NiCr25FeAlY type (commercial designation Nicrofer® 6025 HT — 602 CA), developed by the specialists of Krupp VDM GmbH in 1992, is widely used in manufacture of equipment for the metallurgical, ceramic and chemical industries, units for waste recycling [1–3]. Chemical composition of alloy NiCr25FeAlY is as follows, %: Ni — base; 24–26 Cr; 8–11 Fe; 0.15–0.25 C; ≤ 0.1 Mn; ≤ 0.5 Si; ≤ 0.1 Cu; 1.8–2.4 Al; 0.1–0.2 Ti; 0.05–0.12 Y; 0.01–0.10 Zr. From the data of company-producer the material possesses a high heat resistance and high-temperature strength and can be used at temperature up to 1200 °C in carburizing, oxygen-containing and nitriding medium [1].

To attain the high-temperature strength of the alloy the developers used the principles of a solid-solution, carbide and dispersion hardening that provides the presence of a complex phase structure in the material, including a solid γ-solution of carbon in Ni–Cr–Fe-matrix [1]; strengthening carbide $Me_{23}C_6$, where Me = (Cr, Fe, Ni) [1, 4–6]; intermetallic γ′-phase $Ni_3(Al, Ti)$ [1, 7–9].

The same as many other austenitic dispersion-hardened alloys, the alloy NiCr25FeAlY is characterized by a satisfactory weldability, with a manifestation of susceptibility to the formation of hot cracks in welding and heat treatment [9–15]. The possible changes in structure of material caused by the processes of welding or heat treatment and leading to the loss in technological strength can be as follows:

- growth of austenitic grain in HAZ metal;
- agglomeration of primary carbides (tendency of carbides to the formation of coarse grain-boundary precipitations during heating at the unchanged total share of precipitated carbides);
- formation of a carbide chain (process, opposite to the above-described), i.e. precipitation of numerous fine carbide phases along the grain boundaries;
- formation of brittle topologically close-packed μ-, σ-, Laves-phases.

Similar structural transformations for some alloys on nickel base can cause not only the formation of hot cracks in welding, but also to reduce significantly the serviceability of welded structures, made from these materials, under the action of high temperatures.

At the Institute of Joining and Beam Technologies a series of experiments was performed, including welding of high-resistant nickel alloy NiCr25FeAlY, test for susceptibility to hot cracking, mechanical-technological tests and analysis of microstructure of the welded joint. The latter was performed at the assistance of Methodological-Diagnostic Center of Materials Science of Magdeburg University. It included the optical microscopy (microscopes «Nikon-Epiphot» and «Leica Reichert MeF3A»), scanning electron microscopy (electron microscope JEOL JSM 5410) and transmission electron microscopy (electron microscope Philips CM200).

Welding was performed on 500 × 150 mm plates of 6 and 10 mm thickness with V-shaped groove preparation. In the scope of investigations the plasma welding without filler material was used for filling root welds, and next passes were made using four different methods: tungsten electrode in inert gas (TIG), consumable electrode gas-mixture shielded (MAGMS) and submerged arc welding under the flux layer (SAW), and also with covered electrodes (MMAW). In all cases a filler metal was used, which is similar to parent metal (PM) in chemical composition. The main welding parameters are given in the Table. To increase the productivity and to decrease the number of passes the TIG welding on 10 mm thick plates was performed with transverse arc oscillations.

The quantitative analysis of grain size in HAZ metal and PM showed that the thermal cycle of welding influences negligibly the growth of the matrix grain. Only in the direct vicinity of the fusion line (up to 0.2 mm) some coarsening of structure by one number of grain is observed. At some distance from the fusion line, for more than by 0.2 mm, the grain preserves stable sizes. The processes of agglomeration of carbides and formation of a carbide chain in HAZ

Parameters of welding for filling passes on 10 mm thick plates

| *Parameter* | *Method of welding* | | |
|---|---|---|---|
| | *TIG* | *MAGMS* | *SAW* |
| Diameter of filler material, mm | 1.2 | 1.2 | 1.6 |
| Welding current, A | 180 | 148 | 220–250 |
| Arc voltage, V | 10 | 23 | 35 |
| Welding speed, cm/min | 20 | 33 | 50 |
| Oscillations of arc: | | | |
| amplitude of oscillstions, mm | 5 | – | – |
| rate of oscillations, cm/min | 10 | – | – |
| Shielding gas/flux: | | | |
| kind | Ar + 1 % $N_2$ | Ar + 5 % $N_2$ + 5 % He + 0.05 % $CO_2$ | SAW flux 50-11 |
| consumption, l/min | 12 | 20 | – |

metal were not observed in HAZ metal. Carbide phase in PM and HAZ metal is presented by carbides of two types, precipitated both at the boundaries and also inside the austenitic grain. The first group includes the carbides of mainly round or globular shape with an average diameter of about 2–5 μm, the second group includes the coarser carbide inclusions of irregular shape with an 12–18 μm average length, elongated in the direction of rolling PM plates (Figures 1 and 2).

The electron microanalysis of carbide phase showed that the structure of welded joints of alloy NiCr25FeAlY includes the particles of carbides $Me_{23}C_6$ and $Me_7C_3$, where Me = (Cr, Ni, Fe). Dominating role in the formation of carbide phase is played by the atoms of chromium, i.e. separate particles of carbide represent in principle the pure compounds of chromium and carbon. The presence of carbides of $Me_{23}C_6$ and $Me_7C_3$ types in the alloy structure was confirmed also by the measurements of microhardness. Microhardness of grains of γ-matrix was on average *HV* 0.03-320–350 (*HV* 0.04-230–270). Values of microhardness of carbide particles prove the presence of two groups of carbides with different levels of microhardness: *HV* 0.03-880–980 (*HV* 0.04-500) and *HV* 0.03-1350 (*HV* 0.04-680–750). With allowance for the reference data on microhardness of carbides $Cr_7C_3$ and $Cr_{23}C_6$ [16] the conclusion can be made about the presence of both types of carbides in the alloy structure in initial state and after welding. In general, this phenomenon, widely spread for high-temperature high-strength materials on nickel base [9], is confirmed also for NiCr25FeAlY by data of [17]. In parallel with investigations of a carbide phase in regions adjacent directly to the fusion line (in HAZ metal and along the boundaries of dendrites in weld), the areas with eutectoid structure of phase precipitations were observed (Figures 2–4).

The presence of the eutectoid phase near the fusion line can serve a negative factor, intensifying the formation of hot cracks during welding-technological treatment of alloy NiCr25FeAlY. This is due to a higher fusibility of eutectic with respect to PM and its clearly expressed brittle (lamellar) morphology (Figure 4). The microhardness of the eutectoid phase 3 times exceeds that of γ-matrix on average and amounts to *HV* 0.04-510–680. In its turn, the distribution of eutectoid formations along the grain boundaries around the matrix carbides indicates the process of redistribution of elements of the carbide phase and γ- matrix, formation of eutectoid composition, its pre-fusion and subsequent crystallization in

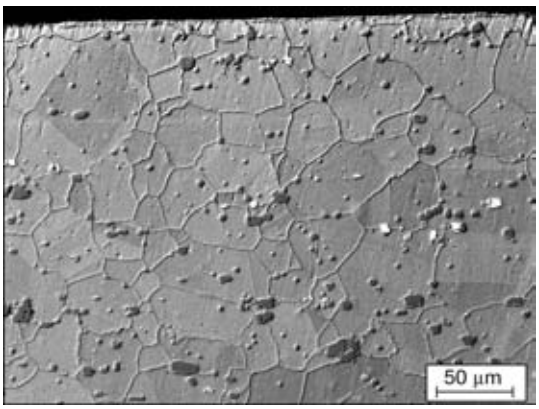


**Figure 1.** Microstructure of parent metal of TIG welded joint of NiCr25FeAlY alloy at the distance of about 5 mm from fusion line (dark particles — carbide phase; light particles — yttrium and zirconium; SEM, back scattered electrons)

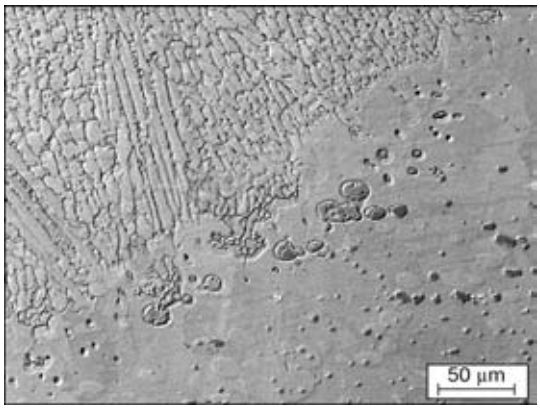


**Figure 2.** Microstructure of HAZ metal of TIG welded joint of NiCr25FeAlY alloy near the fusion line. Typical are the eutectoid formations along the fusion line from the side of HAZ metal (SEM, back scattered electrons)

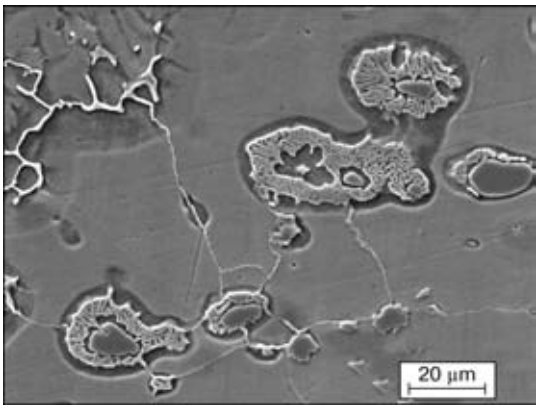


**Figure 3.** Microstructure of HAZ metal of TIG welded joint of NiCr25FeAlY alloy near the fusion line (SEM, absorbed electrons)

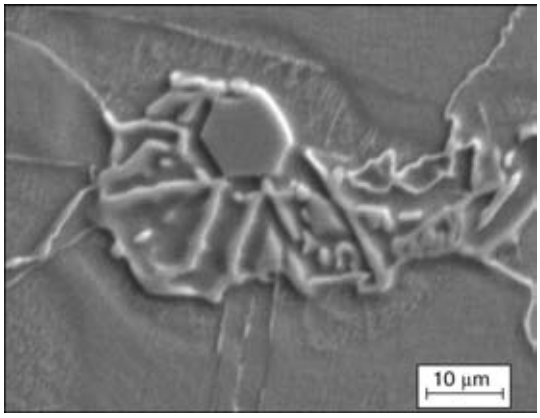


**Figure 4.** Eutectoid phase around carbide particle, area of HAZ metal near the fusion line (SEM, absorbed electrons)

the form of eutectoid phase, arranging only around the carbide.

To establish the effect of above-described structural transformations in the material on its technological strength a series of tests was made for resistance of alloy NiCr25FeAlY against hot cracking in welding. Tests (PVR-test) were performed in accordance with a standard document DVS 1004-1. The test principle is shown schematically in Figure 5.

Welding torch was displaced along the axis of a $200 \times 40 \times 10$ mm flat specimen at a constant welding speed, providing its penetration for some depth, depending on the welding parameters. Simultaneously, with the beginning of the welding process the specimen began to be subjected to tension in the direction of arc movement with a constantly increasing speed. Here, the definite value of tension rate $v_{tens}$ corresponds to each point in the weld. The quantitative criterion for determination of material susceptibility to hot crack formation is a critical rate of tension $v_{cr}$ (rate of tension at which the first cracks are observed at the specimen surface).

During tests the argon TIG welding without filler wire was used as the most preferable method of welding from the point of view of resistance against hot cracking. The welding speed for different test specimens varied within 10.6–22.2 cm/min at other parameters being constant. The processed test data are given in Figure 6.

Critical rate of tension is inversely proportional to linear energy, i.e. with increase of the latter in welding the hazard of formation of hot cracks is also increased. According to [18] the conclusion can be made, on the basis of criteria established experimentally, about the satisfactory resistance of alloy NiCr25FeAlY against the hot crack formation as material indicating the critical rate of tension, locating in the interval of 30–70 mm/min during the PVR-test. Thus, in welding at low values of linear energy ($\approx$ 6 kJ/cm) the material possesses the high enough crack resistance and makes it possible to produce the quality welded joints. At the same time when the linear energy reaches 8.5 kJ/cm and more the alloy possesses unsatisfactory resistance against the hot crack formation in shielded-gas arc welding.

Hot cracks formed in welds during PVR-test have a clearly expressed interdendritic nature and formed, first of all, in periphery zones of welds near the fusion line. An additional factor promoting initiation and propagation of hot cracks in these regions, in particular, is the presence of an eutectic liquid in the intergrain and interdendritic space below the solidus temperature. The transition of hot cracks from the weld to the HAZ metal was observed in some cases by this reason (Figure 7).

To check the serviceability of welded joints of heat-resistant alloy NiCr25FeAlY at high temperatures a number of investigations was carried out, including heating and holding of welded specimens made by different methods of welding in the range of critical temperatures with a subsequent mechanical technological tests and metallographic examinations of structural changes.

Some references [19, 20] indicate the hazard of formation of the so-called cracks of a repeated heating for heat-resistant alloys on nickel base at their heat

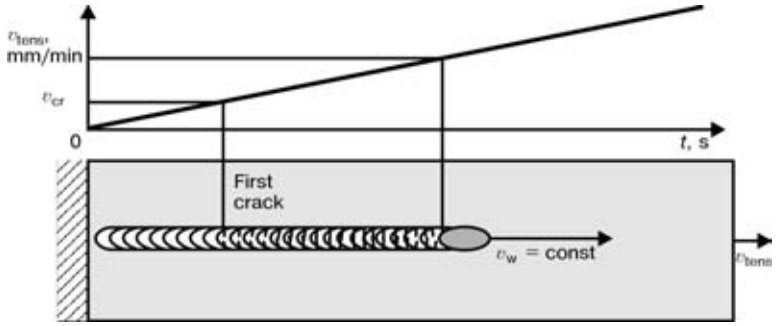


**Figure 5.** Schematic diagram of PVR-test

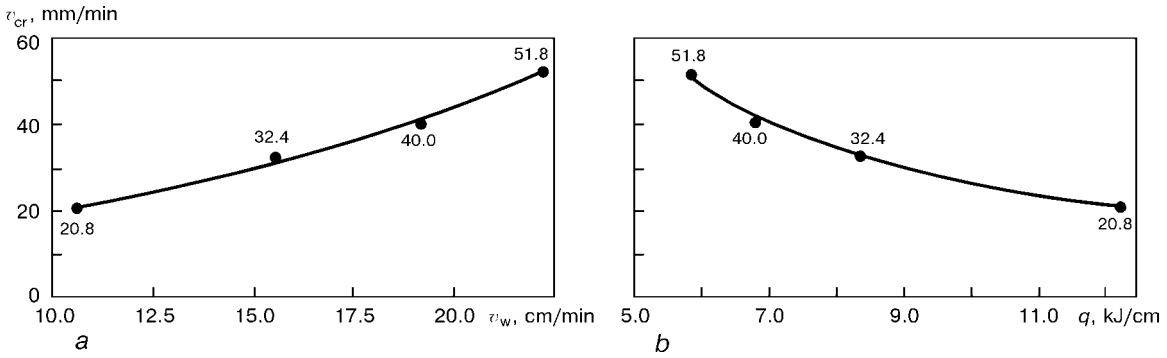


**Figure 6.** Dependence of critical rate of tension $v_{cr}$ for NiCr25FeAlY alloy on welding speed (*a*) and linear energy (*b*)

treatment or in the operating conditions under the action of high temperatures. Interval of temperatures 600–800 °C is most hazardous here. The decisive factor stipulating the reduction in ductility of the material within this temperature interval is accepted to be considered its dispersion hardening as a result of precipitation of γ'-phase $Ni_3(Al, Ti)$ [13, 19, 21, 22].

The study of fine structure of heat-treated welded specimens of alloy NiCr25FeAlY (heating up to 700 °C, holding for 100 h, air cooling) showed the presence of γ'-phase in its structure, which was not observed in study of material structure in the initial state. Particles of γ'-phase are precipitated in the weld, HAZ metal and PM and have a rounded shape (diameter of about 21–31 nm) (Figures 8 and 9). As the grain boundaries of the as-delivered PM were almost free from the carbide precipitations (Figure 10), the study of a fine structure of the welded joints after heating showed the presence of numerous precipitations of a fine-dispersed carbide phase both along the grain boundaries in the PM (Figure 11) and HAZ metal, and also along the interdendritic boundaries in weld (Figure 21).

To establish the effect of temperature load and caused structural transformations by it in the material on its mechanical-technological properties the comparative tests were made on transverse tension, bending and impact strength of welded specimens from NiCr25FeAlY alloy. Results of impact strength tests are shown in Figure 12. Samples with V-notch for tests were cut out from welded joints made by TIG, MAGMS welding and SAW (root weld was filled with a plasma welding). The notch was located on PM, along weld axis in transverse section, fusion line and in HAZ metal. Energy of fracture $A_v$ at impact strength test for specimens from PM and typical regions of the welded joint was approximately similar and equal to 75–80 J. Here, the noticeable advantage of any method of welding was not observed. At the same time the provoking heating up to 700 °C and holding for 100 h has led to the decrease in fracture energy almost by 30 % both in PM and also in HAZ metal. However, the highest drop in material toughness due to low-temperature holding was observed in the weld. In this case the fracture energy was 4 times reduced and equal to 18–20 J for the welds.

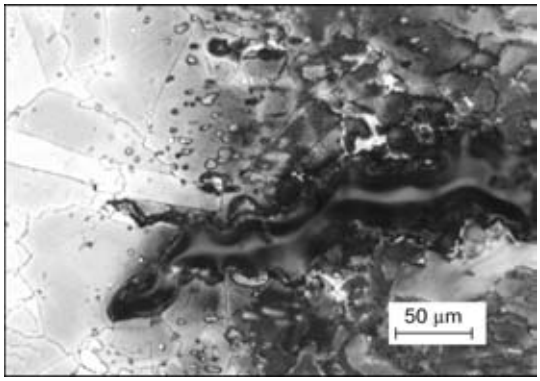


**Figure 7.** Illustration of hot crack «coming out» from weld metal to HAZ metal (optical microscopy, etching according to Bloech and Wedl II)

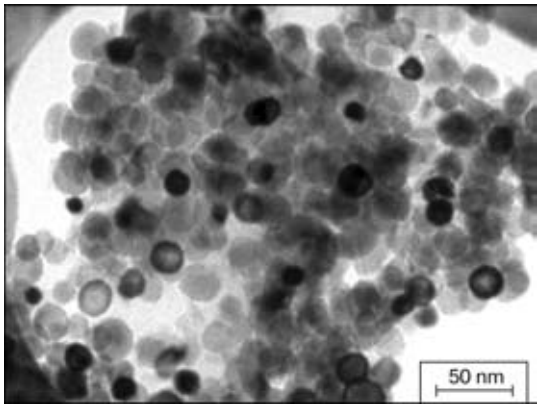


**Figure 8.** Particles of γ'-phase in weld after low-temperature holding (electron transmission microscopy)

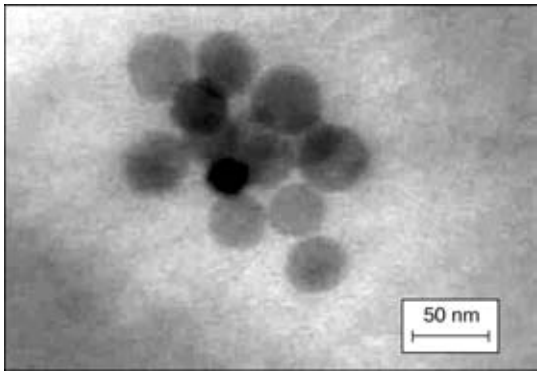


**Figure 9.** Particles of γ'-phase in parent metal after low-temperature holding (electron transmission microscopy)

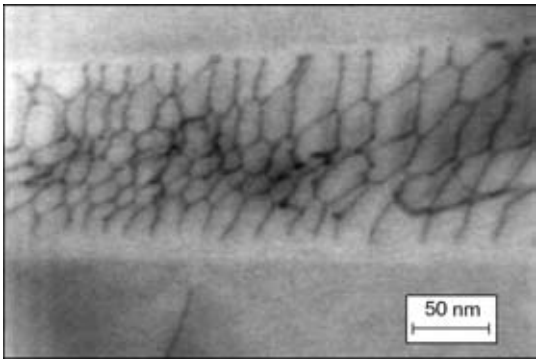


**Figure 10.** Intergrain boundary in parent metal before low-temperature holding. Dislocation network and separate carbide microparticles are typical (electron transmission microscopy)

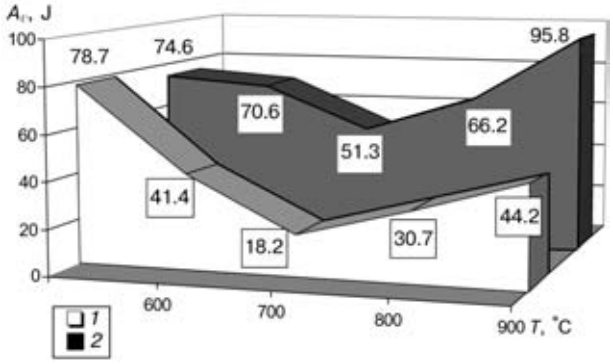


**Figure 13.** Change in fracture energy of NiCr25FeAlY alloy depending on temperature of provoking heating for welds made by TIG (*1*), and for PM (*2*)

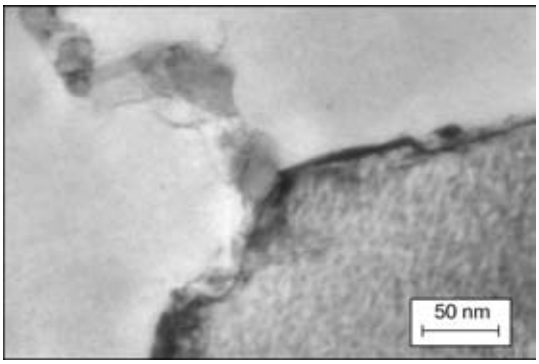


**Figure 11.** Microstructure of parent metal after low-temperature holding. Grain boundaries are covered with carbide precipitations. Right grain with contrast precipitations of $\gamma'$-phase (electron transmission microscopy)

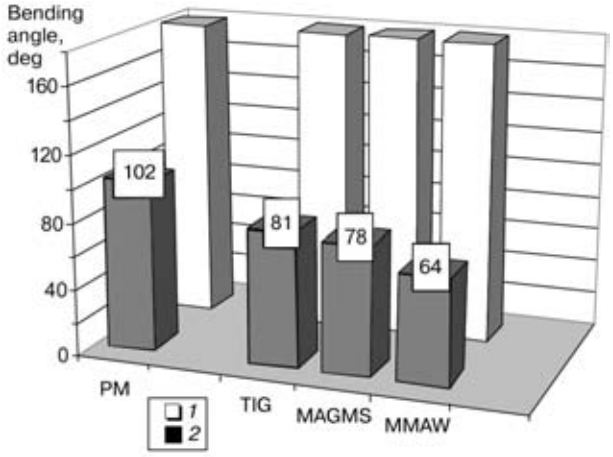


**Figure 14.** Change in ductility of NiCr25FeAlY alloy in typical regions of welded joints: PM and welds made by different methods of welding in initial state after welding (*1*) and after low-temperature holding (*2*)

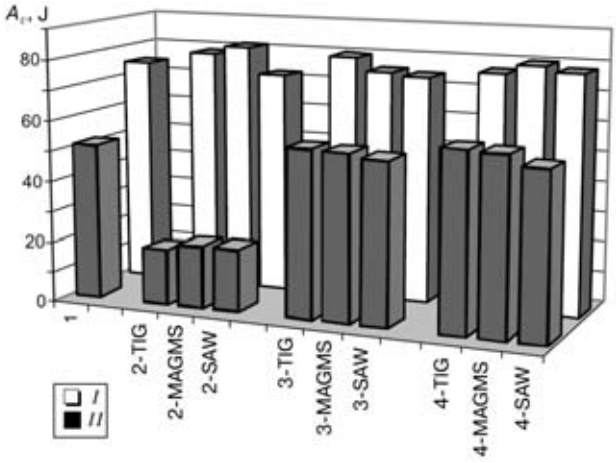


**Figure 12.** Fracture energy $A_i$ of NiCr25FeAlY alloy in typical regions of welded joints: PM (*1*), weld (*2*), fusion line (*3*) and HAZ metal (*4*) made by different methods of welding in initial state after welding (*I*) and after low-temperature holding (*II*)

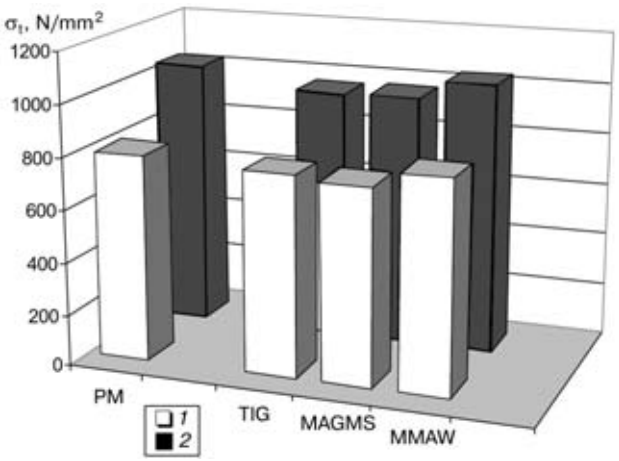


**Figure 15.** Change in strength of NiCr25FeAlY alloy in typical regions of welded joints: PM and welds made by different methods of welding in initial state after welding (*1*) and after high-temperature holding (*2*)

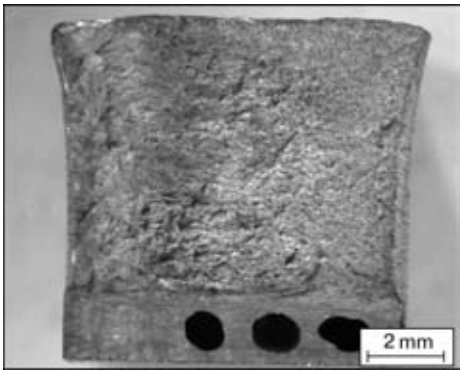


**Figure 16.** General view of fracture surface containing TIG weld after impact strength test

The further tests of welded specimens of NiCr25FeAlY alloy at different temperatures of the provoking heating showed that the range of temperatures near 700 °C is most hazardous from the point of view of reduction in the impact strength (Figure 13). The holding duration was not changed and equal to 100 h for all cases. Similar results were obtained also at comparative testing of specimens of PM and alloy NiCr25FeAlY for transverse bending (Figure 14). Bending angle of samples, not subjected to heat action, made from PM and containing welds, was 180°. The initiation of the first cracks was observed in samples from PM, heated to 700 °C and subjected to holding for 100 h at 102° angle of bending. When testing welded samples, whose root weld was filled by a plasma welding, the tensile forces were transferred to filling passes made by TIG, MAGMS welding and MMAW. In this case, a brittle fracture in weld at bending angles 81, 78 and 64° at different methods of welding was observed in samples subjected to the provoking heating.

Thus, tests for transverse bending also confirmed the presence of a significant drop in ductility of material of welds of NiCr25FeAlY alloy welded joints, subjected to heating and holding in the range of temperatures near 700 °C.

Tests for transverse tension of samples from PM and containing welded TIG, MAGMS and MMAW welds, also confirmed the material hardening due to the above-described temperature treatment (Figure 15). Here, the samples were fractured in PM in all cases.

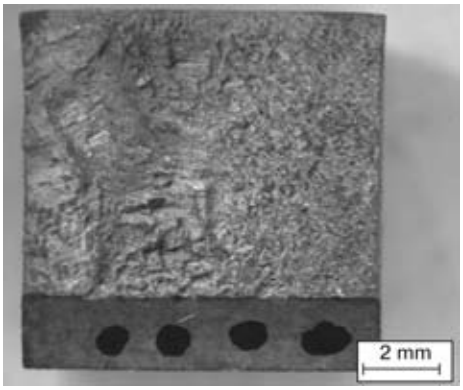


**Figure 17.** General view of fracture surface of sample containing TIG weld after impact strength test. Before the sample test the low-temperature holding (700 °C, 100 h) was used

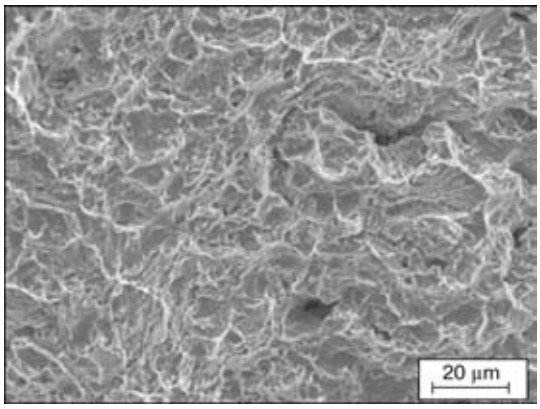


**Figure 18.** Fractographic pattern of fracture of TIG weld after impact strength test (SEM)

Study of fracture surfaces of welded samples after impact strength tests reveals the higher ductility of the structure of root welds made by the plasma welding (Figures 16, 17, *right part*), in comparison with filling passes made by different arc methods of welding, in particular with a TIG (Figures 16, 17, *left part*). In addition, the comparison of a shape of sections of fracture surfaces shows the much higher level of a plastic deformation in non-heated samples (Figure 16), as compared with the more brittle pattern

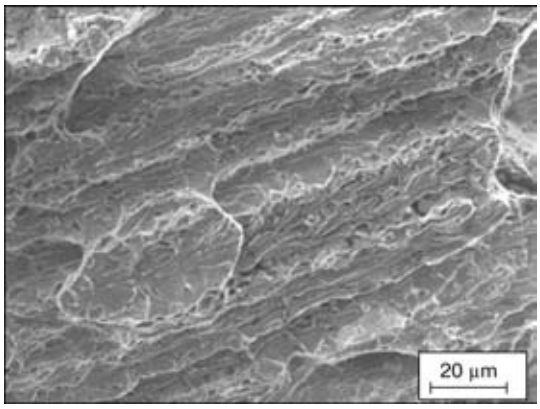


**Figure 19.** Fractographic pattern of fracture of TIG weld after impact strength test. Before sample test the low-temperature holding (700 °C, 100 h) was used (SEM)

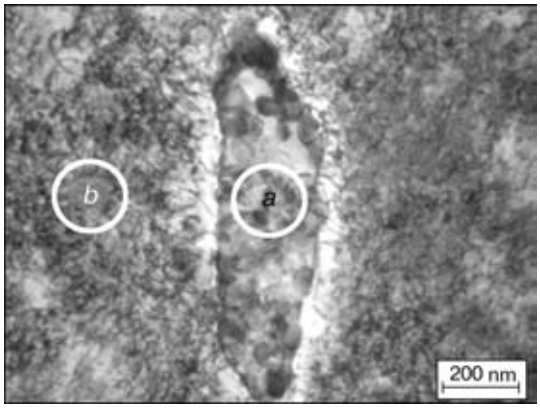


**Figure 20.** Microstructure of HAZ metal of TIG welded joint of NiCr25FeAlY alloy after thermal holding (700 °C, 100 h). Typical regions: polycrystal chromium carbide (*a*), matrix with a dislocation network (*b*) (electron transmission microscopy)

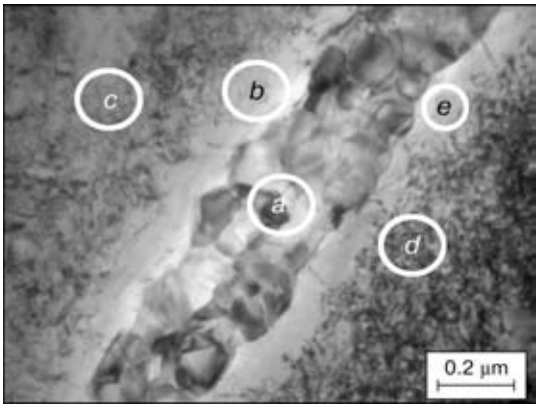


**Figure 21.** Microstructure of TIG weld of NiCr25FeALY alloy after thermal holding (700 °C, 100 h). Typical regions: *a* — interdendritic boundary covered with carbide precipitations; *b* — «fringing», adjacent to it, being free from precipitations; *c* — matrix with a dislocation network (electron transmission microscopy)

of fracture in samples, subjected preliminary to the provoking heating (Figure 17). The more comprehensive investigation of fracture surfaces in welds shows the cellular (honeycomb) structure of fracture typical of ductile materials in samples, which were not subjected to thermal action after welding (Figure 18), as compared with brittle (shear) structure of fracture surface of welds subjected to a low-temperature holding (Fi-gure 19).

Thus, the results of mechanical-technological tests of welded joints of NiCr25FeAlY alloy indicate adequately the essential decrease in ductility and toughness of the material due to even comparatively short-time holding in the region of 700 °C that is, in its turn, caused directly by the $\gamma'$-phase precipitation. Here, the most weakened zone of the welded joint is the weld. This fact cannot be grounded only due to the $\gamma'$-phase precipitation.

During examinations using the method of electron transmission microscopy the presence of «fringing», free of hardening particles and dislocations near the interphase carbide–matrix boundary was revealed in the microstructure of metal of HAZ and weld of thermally-affected samples (Figures 20 and 21). The width of «fringing» is about 0.1 μm. In Figures 20 and 21 the presence of $\gamma'$-phase is designated by dislocation lines, i.e. on areas, being free of dislocations, there are no also the particles of the $\gamma'$-phase. Moreover, the electron microanalysis of structure showed some depletion of «fringing» metal with chromium as compared with the matrix. This phenomenon can be explained by the fact that in the conditions of formation of the hardening carbide $Me_{23}C_6$ (760–980 °C according to [9]) the matrix is depleted with chromium that increases, in turn, the solubility of $\gamma'$-phase near the boundary of grain or dendrite, and, more clearly, elements of $\gamma'$-hardeners, resulting in the formation of the above-described zones, being free from precipitations. These were samples, in which the intensive precipitation of fine-dispersed carbide phase along the boundaries of grains and dendrites was observed after the low-temperature holding (700 °C, 100 h).

Thus, the significant decrease in ductility of the welded joints caused by the temperature effect, is the result of a phase and chemical inhomogeneity, stipulated by complex structural transformations, such as precipitation of hardening $\gamma'$-phase in the matrix, precipitation of fine-dispersed carbide phase $Me_{23}C_7$ along the boundaries of dendrites and partial homogenization (dissolution of $\gamma'$-phase) in the near-boundary region. Here, the weld with its dendritic structure is the most weakened zone because of the anisotropy of its mechanical properties as compared with PM or HAZ metal.


1. (1999) Hochtemperaturwerkstoffe der Krupp VDM fuer den Anlagenbau. *VDM Report*, **25**, 64.
2. Brill, U. (1995) Praktische Erfahrungen mit dem neuen Werkstoff Nicrofer 6025 HT im Ofen- und Waermebehandlungsanlagenbau. *Stahl*, **6**, 37–40.
3. Brill, U. (1999) Neue Ergebnisse mit dem Werkstoff Nicrofer 6025 HT im Ofen- und Waermebehandlungsanlagenbau. *Ibid.*, **3**, 54–56.
4. Baar, B., Brill, U. (1994) Gefuegecharakterisierung der neuen karbidhaertenden, hochwarmfesten Nickelbasislegierung Nicrofer 6025 HT (2.4633). *Prakt. Metallographie*, **25**, 331–341.
5. Brill, U. (1994) Eigenschaften und Einsatzgebiete der neuen warmfesten Legierung Nicrofer 6025 HT. *Stahl*, **3**, 32–35.
6. Brill, U. (1992) Neue warmfeste und korrosionsbestaendige Nickel-Basis-Legierung fuer Temperaturen bis zu 1200 °C. *Metall-Wissenschaft + Technik*, **8**, 778–782.
7. Anik, S., Dorn, L. (1983) Metallphysikalische Vorgaenge beim Schweißen von Nickelwerkstoffen — Waermebehandlung und Schweissverfahren. *Schweißen und Schneiden*, **11**, 540–544.
8. Durand-Charre, M. (1997) *The microstructure of superalloys*. Amsterdam: Gordon&Breach.
9. Sims, Ch.T. et al. (1987) *Superalloys II.* John Wiley and Sons.
10. Anik, S., Dorn, L. (1983) Metallphysikalische Vorgaenge beim Schweißen von Nickelwerkstoffen — Einfluß der Werkstoffzusammensetzung. *Schweißen und Schneiden*, **9**, 445–450.
11. Savchenko, V.S., Yushchenko, K.A., Savolej, N.I. et al. (1993) Some fundamentals of hot cracking in welding of cast heat-resistant nickel alloys. *Avtomatich. Svarka*, **3**, 13–16.
12. Savchenko, V.S., Yushchenko, K.A., Savolej, N.I. (1987) Influence of deformation rate on susceptibility of stable-austenitic welds to hot cracking in low-temperature range of brittleness. *Ibid.*, **10**, 9–12.
13. Yushchenko, K.A., Lipodaev, V.N., Belchuk, M.V. et al. (1986) Resistance of welded joints from heat-resistant nickel alloy of Hastelloy N type to hot cracking. *Ibid.*, **9**, 10–12.
14. Kvasnitsky, V.F. (1985) Welding and brazing of heat-resistant alloys in shipbuilding. *Ibid.*, **10**, 26–30.
15. Morochko, V.P., Fyodorov, B.M., Andreev, V.D. (1983) Comparison of laser, electron beam and argon-arc processes of welding of heat-resistant nickel alloy KhN68VMTYuK. *Svarochn. Proizvodstvo*, **6**, 13–16.
16. Goldschmidt, H.J. (1967) *Interstitial alloys*. London: Butterworths.
17. Brill, U. (1996) Einfluß des C-Gehaltes auf die Gefuegeausbildung der hochwarmfesten Nickelbasislegierung NiCr25Fe10AlY, *Metall*, **12**, 798–804.
18. Klug, P. (1980) *Beitrag zur Pruefung der Heißrißanfaelligkeit von hochlegierten Schweißzusatzwerkstoffen mit dem PVR-Test der VEW-Kapfenberg.* Diss. Graz.
19. Sorokin, L.I., Tupikin, V.I. (1985) Classification of heat-resistant nickel alloys in conformity with their resistance to crack formation during heat treatment of welded joints. *Avtomatich. Svarka*, **5**, 23–25.
20. Skvortsov, E.A., Golubev, E.N. (1978) About cracking of welded joints of austenitic dispersion-hardening alloys in heat treatment. *Svarochn. Proizvodstvo*, **4**, 9–10.
21. Ibas, O., Brill, U. (1998) *Einfluß der Auslagerungstemperatur und -zeit auf die Zaehigkeit von ausgewaehlten Ni-Basis-Legierungen. Konferenz «Werkstoffpruefung».* Einzelbericht.
22. Yushchenko, K.A., Pinchuk, N.I., Nakonechny, A.A. et al. (1985) Investigation of weldability of cast heat-resistant nickel alloys with 6 % Al. *Avtomatich. Svarka*, **10**, 18–24.

# PECULIARITIES OF CRYSTALLINE STRUCTURE OF WELDED JOINTS IN SINGLE CRYSTALS

**B.A. ZADERY**[1], **S.S. KOTENKO**[1], **E.P. POLISHCHUK**[1], **K.A. YUSHCHENKO**[1], **O.M. BARABASH**[2] and **O.P. KARASEVSKAYA**[2]
[1]E.O. Paton Electric Welding Institute, NASU, Kyiv, Ukraine
[2]G.V. Kurdyumov Institute for Metal Physics, NASU, Kyiv, Ukraine

Crystallographic texture and microstructure of fusion welded joints were studied. Criteria were selected for estimation of the degree of inheritance of structural state of the base metal by the weld metal. Factors determining the degree of such inheritance were established, and conditions for a minimum distortion of the structural state were identified.

***Keywords:*** *fusion welding, metal solidification, crystallographic orientation, single-crystal state, X-ray examinations, disorientation, dislocation density, inheritance of structure, welding conditions*

Structural state of the weld metal is one of the main factors determining physical-mechanical properties and performance of welded joints [1–3]. The latter greatly depends upon how precisely the structural state of the base metal is inherited by the weld metal.

Proceeding from basic postulates of the metal solidification theory [4–6], it can be presumed that the degree of inheritance is determined cumulatively by the initial crystallographic orientation, perfection of structure of a material welded and parameters of the thermal effect of a welding heat source (welding conditions and parameters).

Publications dedicated to this issue are not numerous, and those available often contain contradictory results [1, 6–11]. They focus mainly on just a statement and illustration of the fact of inheritance of orientation of melted grains of the base metal by the weld metal, as well as on peculiarities of a coarse-crystalline macrostructure of the weld metal. How precisely at different scale (structural) levels the weld metal can inherit crystallographic orientation and structure of the base metal, as well as which factors this inheritance depends upon — these are the issues the present study is dedicated to.

The object of the package of investigations in this study is an initial crystallographic orientation and microstructure of the single-crystal base metal, as well as their variations under the effect of the thermal-deformation welding cycle.

Criteria for estimation of structure of welded joints are as follows:

- macroparameters of structural perfection (retention of the single-crystal nature and crystallographic orientation of the base metal, deviation of crystallographic orientation of the weld metal from the respective characteristics of the initial base metal);
- parameters of structure at a meso-level (density of dislocations, uniformity of their distribution, scatter of the most probable crystalline orientation of the weld metal).

Investigations were performed on single crystals of tungsten, molybdenum and niobium. This eliminated the effect of multiplicity of crystallographic orientations within the melting zone on structural perfection of the weld, as in polycrystals and even heavily textured metals this factor has a substantial effect on accuracy of the investigation results.

One-component textured polycrystals always contain part of grains with the orientation other than the basic one, which affects both mechanism of inheritance of structure and its perfection. Moreover, investigations of single crystals, owing to the accuracy of determination of crystallographic orientation of welded (melted) surfaces, can provide much more conspicuous results on the effect of this characteristic on structural perfection of the weld metal. In addition, the choice of single crystals as the investigation object makes it possible to study characteristics of formation of different dislocation distributions under the effect of welding conditions and parameters with specific crystallographic orientations of the single crystals welded.

The choice of refractory metals for the investigations was based on the necessity to have the possibility to widely vary thermal fields during welding. Besides, owing to the isomorphic nature of refractory metals less distortions are brought into structure during solidification and cooling, thus providing a more accurate answer to the questions posed. Initial refractory metals are characterised by a low content of impurities, which also allowed us to raise the accuracy of results and avoid the probability of a non-uniform nucleation of the solidification centres. According to the certificate data on the initial single crystals grown by the zone melting method, the metals investigated had the following compositions, wt.%:

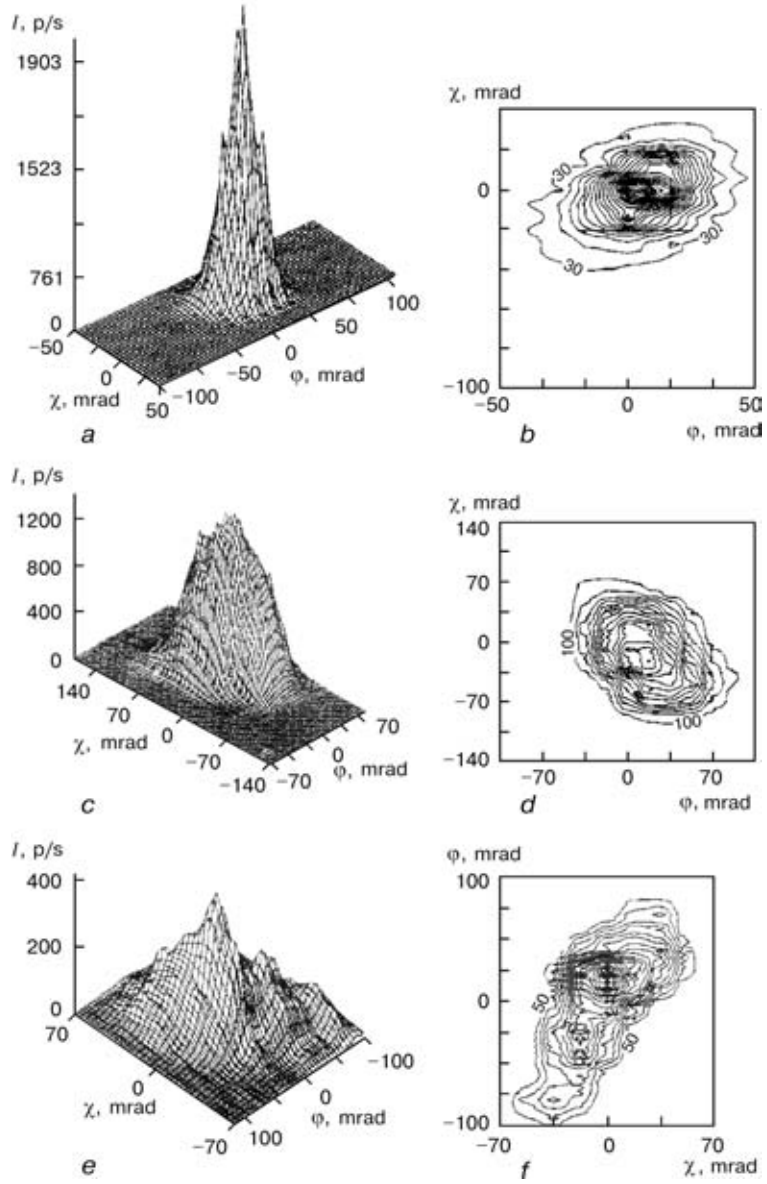


**Figure 1.** Spatial distribution of intensity $I$ (*a, c, e*) and iso-intensive lines (*b, d, f*) of scattered X-ray radiation in azimuthal plane $I_{q\perp}$ for different zones of a welded joint in tungsten single crystals: *a, b* — base metal; *c, d* — fusion line; *e, f* — central part of the weld (melting surface (111), welding direction [110], reflex (222), welding speed 28 mm/s)

**W** — 99.99; [C] — $1 \cdot 10^{-3}$–$1 \cdot 10^{-5}$;
[O] — $1 \cdot 10^{-3}$–$1 \cdot 10^{-5}$; [H] — $(5–8) \cdot 10^{-5}$;
**Mo** — 99.99; [C] — $1 \cdot 10^{-3}$–$1 \cdot 10^{-4}$;
[O] — $1 \cdot 10^{-3}$–$1 \cdot 10^{-4}$; [H] — $1 \cdot 10^{-4}$–$1 \cdot 10^{-5}$;
**Nb** — 99.99; [C] — $1 \cdot 10^{-2}$–$1 \cdot 10^{-3}$;
[O] — $1 \cdot 10^{-2}$–$1 \cdot 10^{-3}$; [H] — $1 \cdot 10^{-4}$–$1 \cdot 10^{-5}$.

The base (initial) metal is characterised by a uniform distribution of dislocations, a small number of low-angle boundaries and disorientation of elements of a substructure in an irradiated volume of 1 mm$^2$ equal to 10–20 mrad (Figure 1, *a, b*).

Samples for welding experiments were cut from single-crystal rods 20–36 mm in diameter grown by zone melting. The rods used had a different crystalline orientation of the axis: <110>, <111>, <112> and <100>. This allowed us to vary crystallographic orientations of fusion surfaces and welding directions, the top surface being kept unchanged — (110). The accuracy of orientation of the single-crystal rods, according to the certificate data, is approximately 35 mrad. Welding of the samples cut from different rods may lead to a substantial disorientation in the joint. Special arrangements were made to avoid the negative effect of such disorientation: firstly, the samples for welding were taken from one rod; and, secondly, the flat plates were cut from the rods, which were then cut lengthwise. The plates were abutted for welding along the cut. This provided the same crystallographic orientation of the fusion surfaces and welding directions and avoided a distorting effect of inaccuracies of cutting and assembly of the plates for welding. As a result, the relative disorientation of the samples in a butt was not in excess of 35 mrad (accuracy of determination of orientation by the Laue method). The samples were cut by the electric-spark method. A defective surface layer was removed by

machining followed by electric polishing. Immediately before assembly for welding, the surfaces of the samples were cleaned by chemicals, degreased and dried. Thickness of the samples welded was from 0.5 to 2.0 mm.

The top surface, end and specially made oblique sections were used for microstructural and X-ray examinations. The special surface was provided as a result of cutting the welded samples at an angle of 90 mrad to the welding direction and normal to the top surface. The purpose of preparation of special examination surfaces was to increase accuracy of estimation of characteristics of different zones in welded joints through enlarging the examination area.

The welding experiments were performed using a highly concentrated precision electron beam in vacuum in order to accurately reproduce results on comparatively small (about $20 \times 60$ mm) samples, ensure mobility and locality of heating, vary the thermal welding cycles over wide ranges and eliminate contamination of the weld metal. The standard electron beam welding equipment was utilised.

As it was necessary to study peculiarities of solidification and structure allowing for the possible process variants, the experiments were conducted within a wide range of welding conditions and parameters, including with electron beam preheating and postweld heating. Heat removal was regulated by using the process fixture. The welding speed was varied from 1 to 40 mm/s, and the preheating temperature was varied from 200 to 800 °C. The welded joint was of the butt type with through penetration.

It should be noted that a consistent through penetration is an imperative condition of producing the quality single-crystal welded joint. Violation of stability of welding conditions, weld geometry and homogeneity of the temperature field may cause formation of high-angle grain boundaries and extra defects of the crystalline structure. Welding parameters were selected on this basis. Table 1 gives typical conditions and parameters of welding tungsten single crystals of a differing thickness. For molybdenum and niobium the beam current was decreased 1.5 and 2 times, respectively, compared with tungsten.

Metallographic examinations were carried out using optical microscopes «MIM-7» and «Neophot 32» at a magnification of 10 to 500 power. The density of chaotically distributed dislocations was determined from the etching pits by using the calculation method suggested in [12]. This method has an insufficient accuracy and sensitivity, and is employed mostly for express-estimation of the state of structure. Retaining of a single-crystal nature and absence of high-angle boundaries were estimated by the express-method from the presence of regions of a differing etchability. It should be noted that the metallography method is very rapid, but it gives only qualitative estimates.

Values of microhardness are an indirect measure of defectiveness of single crystals and their welded joints. Microhardness was measured using the LECO hardness meter M-400 with an automatic indenter drive under a load of 0.5–1.0 N and holding for 15 s.

X-ray examinations by the Laue method and the rocking crystal method were used to study crystallographic orientation and relative disorientation of elements of a substructure of both base metal and welds. The Laue method of backward take was employed to estimate the degree of single-crystallinity and deviation of crystallographic orientation of the weld metal from the base metal. Positions of reflexes in diagrams, their distortion and directions of prefered smears, compared with the reference ones, served as the characteristics. The method of the backward take of a rocking single crystal was employed for quantitative estimation of the dislocation substructure parameters and determination of uniformity of distribution of elements of the dislocation ensemble. When using a single-crystal sample, one should take into account the quantitative relationship between width $\delta_{q\perp}$ and shape $I_{q\perp}$ of distribution of the X-ray reflex intensity and parameters of the dislocation ensemble [13, 14]. Criteria for estimation of the substructure elements were position, general angle broadening and shape of distribution of the reflex intensity, while in formation of the intensity peaks in distribution $I_{q\perp}$ the criteria were their quantity, angle broadening of individual peaks and level of the intensity drop between them. This allowed us to estimate the density of dislocations, their distribution, as well as general, mean and local angles of disorientation of elements of the dislocation ensemble. Examinations were performed with the URS-2.0 unit and the DRON-3M diffractometer using copper radiation.

Distributions of the intensity of X-ray reflections in azimuthal directions of reflexes, such as {110}, {200}, {310}, {321}, {222} and {211}, constituting the angle of less than 785 mrad with one of the examination planes were studied. The appropriate corrections were made in the intensity values at an inclined position of a sample.

Therefore, the qualitative and quantitative characteristics (metallographic methods) complemented with the quantitative parameters of structure (X-ray methods) allow the many-aspect characterisation of the initial metal, as well as variations caused by its melting and solidification during the welding process, with a high degree of accuracy and reliability.

To make investigations more convenient, the basic factors determining formation of structure within the welded joint zone were subdivided into characteristics of the welding conditions and parameters and parameters of the initial structure.

Investigations of welded joints in niobium and tungsten single crystals, produced at a speed ranging from 3 to 30 mm/s, revealed the following structural-orientation peculiarities of metal of these joints depending upon the welding conditions and parameters (primarily the welding speed).

First of all, X-ray (Figures 1–3) and metallographic examinations showed the possibility of re-

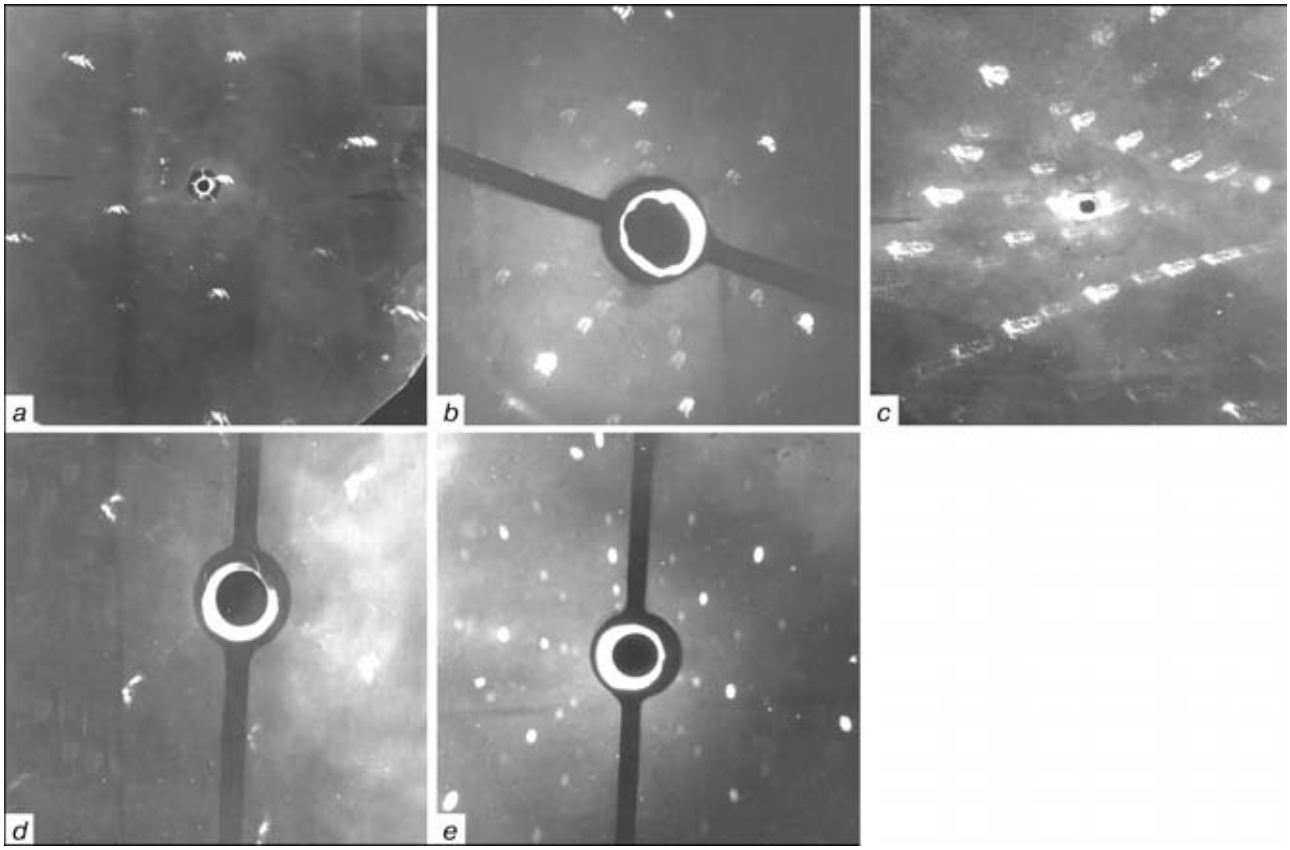


**Figure 2.** Diagrams of the EB weld metal on tungsten single crystals produced at a speed of 28 mm/s with the following initial orientations of fusion surfaces: *a* — [110]; *b* — [100]; *c* — [111]; *d* — [112]; *e* — base metal {110}

taining of a single-crystalline structure of welded joints in single crystals of a differing crystallographic orientation, produced within the above speed range. The weld metal inherited the base metal crystallographic orientation with each of the considered combinations of welding conditions, orientations of the fusion surface and welding directions (Figure 1). However, the diagrams of different zones of a welded joint fixed deviations of the orientation relative to that of the base metal from 35 to 175 mrad. The disorientation angle depends primarily upon the initial orientation of the weld edges, as well as upon the

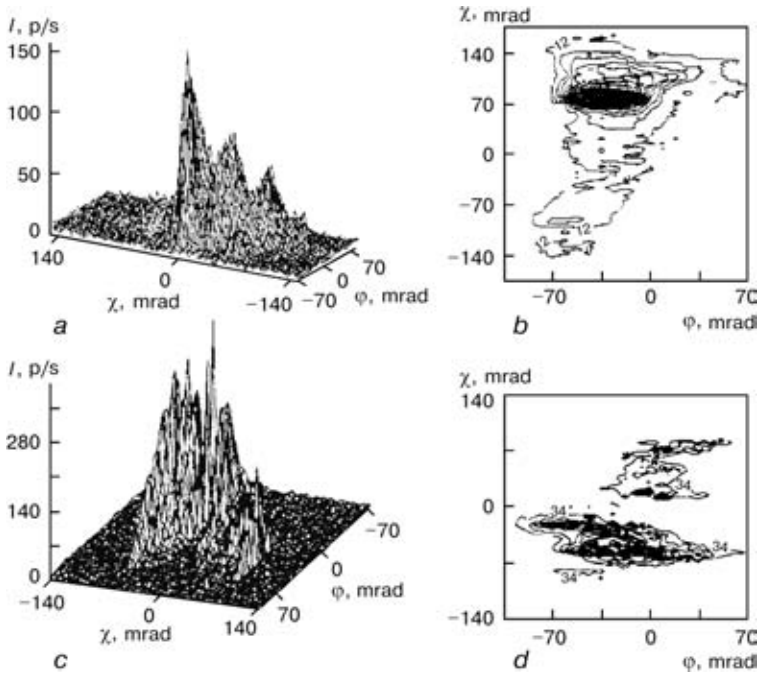


**Figure 3.** Spatial distribution of intensity (*a*, *c*) and iso-intensive lines (*b*, *d*) of scattered X-ray radiation in azimuthal plane $I_{q^{\perp}}$ for the central part of the weld: *a*, *b* — molybdenum; *c*, *d* — tungsten (fusion surface (211), welding direction [110], reflex (211), welding speed 3 mm/s)

**Table 1.** Typical conditions of EBW of tungsten single crystals

| *Thickness of metal welded, mm* | *Beam current, mA* | *Welding speed, mm/s* |
|---|---|---|
| 1.0 | 110 | 5 |
| 1.0 | 150 | 22 |
| 1.5 | 190 | 22 |
| 2.0 | 230 | 22 |

*Notes.* 1. Preheating conditions were selected on the basis of alloy welded, sample size and fixture type. 2. Accelerating voltage in all cases was 30 V. 3. Pressure inside the chamber amounted to 6.7 MPa.

**Table 2.** Estimates of dislocation structure of metal in the zone along the weld axis* resulting from calculation of the actual physical broadening of radial distribution of the intensity of scattering of X-ray radiation

| *Welding speed, mm/s* | *Actual broadening, mrad* | *Density of chaotically distributed dislocations, $cm^{-2}$* | *Mean distance between walls $\times 10^{-3}$, nm* | *Density of distribution of dislocations on walls, $cm^{-2}$* | *Angle of local disorientation of subgrains, mrad* |
|---|---|---|---|---|---|
| 2.8 | 5.061<br>8.372 | $8 \cdot 10^8$ | 3.9 | $2 \cdot 10^9$ | 1–5 |
| 28 | 16.24<br>20.32 | $0.2 \cdot 10^7$ | 1.2 | $3 \cdot 10^{10}$ | 5–10 |

*Initial orientation of the melting surface [111].
**Values of actual broadening are given for reflexes (110) and (220).

welding conditions and parameters. Values of variations in the crystallographic orientation across the section, obtained by the Laue method, are 35–175 mrad. As the measurement error of 35 mrad and inaccuracy of cutting and assembly of the samples equal to 35–50 mrad are commensurable with the values obtained, deriving of the exact numerical dependencies of variations in crystallographic orientation of the weld metal upon the welding conditions and parameters involves problems. Nevertheless, it is possible to distinguish the main trends in inheritance of the crystallographic orientation depending upon the welding conditions and parameters. These trends are identical for the molybdenum, tungsten and niobium single crystals. However, there are also some differences not of a principal importance. Exact peaks of the intensity of reflection of the weld metal (tungsten) are indicative of a more developed polygonisation process (Figure 3).

Main peculiarities of variations in structure of the welded joints in a direction from the base metal to the weld centre are as follows: spots in the diagrams and patterns of the intensity of scattered X-ray radiation gradually increase in width and split into individual maxima (Figures 1–3). This is indicative of variations in density and distribution of dislocation defects in different parts of the weld.

Consider generalised results of investigation of the welds made by penetration of a solid plate, resulting in minimisation of the effect of the error of positioning and preparation of samples. Table 2 gives the data of investigation of welded joints with the fusion surface orientation of (111) (welding direction <112>). As seen from the Table, the welding speed has a substantial effect on perfection of structure of the weld metal (the first and second groups of structure parameters characterising inheritance of the base metal structure), i.e. on the accuracy of inheritance of the base metal structure. The best results were obtained at a fusion surface of (111) and welding direction of [100] and [110], and the worst results — at a welding direction of [111]. Good inheritance of perfection of the single-crystal structure with a fusion surface of (111) for all welding directions was fixed at low welding speeds (2.8 mm/s) (disorientation of substructure was equal to 20–30 mrad, deviation of orientation of the weld in its central part was 35–50 mrad). Further decrease in the welding speed (to 1 mm/s) aggravates the trend to decrease in disorientation of the substructure elements and dislocation density with the welding speed decreased to this orientation of the fusion surface. However, low welding speeds may cause problems of a technology character (increase in the weld width, burns-through etc.).

Similar examinations of butt welded samples reveal the effect of disturbances associated with assembly and preparation of fusion surfaces (Table 3, Figure 4). Disorientation of the substructure elements at the weld centre for the best welding variants is 40–50 mrad. For a fusion surface of (001) [100], disorientation of the substructure elements at the central part of the weld produced at a speed of 2.8 mm/s amounts to 110–140 mrad. Increasing the welding speed to 30 mm/s leads to decrease in disorientation to 30–40 mrad. With further increase in the welding speed (to 40 mm/s) the trend to further improvement of perfection of the weld structure was fixed, but, like at low welding speeds, this results in a techno-

**Table 3.** Disorientation of the substructure elements within the zone of the weld axis in tungsten butt welded joints made at different welding speeds on samples with a different crystallographic orientation

| *Surface orientation* | *Welding speed, mm/s* | *Maximum disorientation, mrad* | |
|---|---|---|---|
| | | $v_{w\perp}$ | $v_{w\parallel}$ |
| [100] | 2.8 | 100–160 | 60–70 |
| | 22.0 | 40–60 | 15–30 |
| | 28.0 | 35–40 | 15–20 |
| [110] | 2.8 | 110–190 | 35–55 |
| | 22.0 | 45–55 | 18–25 |
| | 28.0 | 30–35 | 5–10 |
| [111] | 2.8 | 30–40 | 15–25 |
| | 22.0 | 65–100 | 35–160 |
| | 28.0 | 50–60 | 30–40 |
| [112] | 2.8 | 120–175 | 40–55 |
| | 22.0 | 50–65 | 50–60 |
| | 28.0 | 35–40 | 25–30 |

*Note.* Orientation of the sample surface — [110]; $v_{w\perp}$ — normal to the welding direction; $v_{w\parallel}$ — parallel to the welding direction.

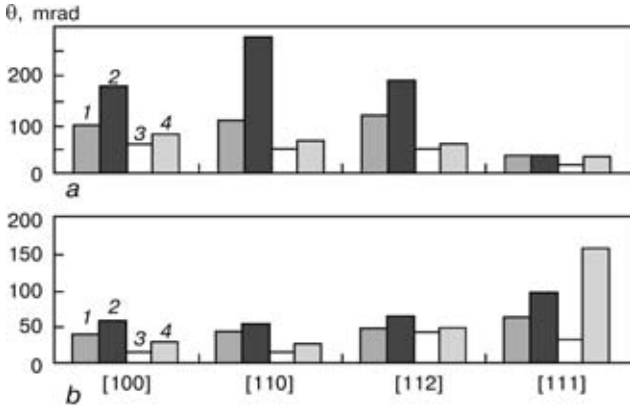


**Figure 4.** Histograms of disorientation (*1, 3* — minimum; *2, 4* — maximum) of substructure elements of the weld produced by EBW at different speeds: *a* — 2.8; *b* — 28 mm/s; *1, 2* — normal to the welding direction; *3, 4* — parallel to the welding direction (θ — angular width)

logical problem of formation of sound welds (undercuts, recesses etc.).

As seen from Tables 1–3 and Figures 2 and 4, the effect of the welding speed on perfection of the weld metal structure is closely related to the initial orientation of the base metal. Examinations of samples of other crystallographic orientations, welded under different conditions (speeds), show that, along with the welding conditions and parameters, an even higher effect on formation of the weld metal structure is exerted by orientation of the initial melting surface (Figures 2, 4, 5), as the fusion surface serves as a primer (substrate) for solidification. The degree of inheritance of the substrate structure determines perfection of the weld metal structure.

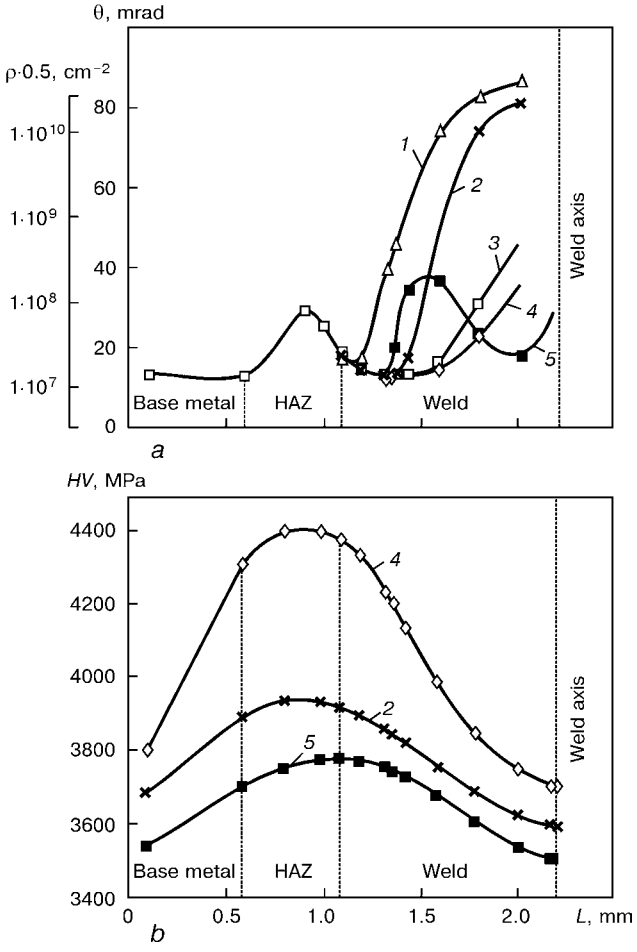


**Figure 5.** Variation in characteristics of substructure in a cross section of welded joints in tungsten single crystals of a differing orientation: *a* — disorientation of substructure elements, total dislocation density; *b* — microhardness: *1* — [111]; *2* — [112]; *3* — [100]; *4* — [110]; *5* — [100] (polycrystalline structure along the axis)

Analysis of the above data showed that the best results could be obtained for samples with a melting surface of {100} and {110} at increased welding speeds, while for samples with a melting surface of {111} the best results were obtained at low welding speeds, and the less perfect single-crystal welds were produced at a melting surface of {112}. Increasing the welding speed for surface orientations of [111] and [112] leads to some decrease in maximum values of disorientation of the substructure elements. However, reflexes with clearly defined heterogeneous asterism were revealed in the X-ray patterns (see Figure 2), which is indicative of the presence of redundant, non-uniformly distributed dislocations with different Burgers vectors. This distribution of dislocations forms regions of local overstresses susceptible to recrystallisation. For a fusion surface orientation of {112} we failed to produce welds with a structure close to that of the base metal.

Therefore, it can be concluded that each initial crystallographic orientation has its own optimal welding conditions and parameters providing a more perfect structure.

Results of estimation of the total dislocation density in the weld structure coincide with earlier established dependencies of perfection of the weld metal structure upon the crystallographic orientation of the initial metal, as well as welding conditions and parameters. As disorientation of the substructure elements increases, the dislocation density grows from about $1 \cdot 10^6$–$1 \cdot 10^7$ to $1 \cdot 10^8$–$1 \cdot 10^9$ cm$^{-2}$. In regions where the total dislocation density grows more than 10 times, the density of chaotically located dislocations falls (see Table 2) because of their re-grouping and formation of sub-boundaries. The total dislocation density of the entire dislocation ensemble increases due to variations in the concentration and disorientation of sub-boundaries.

Values of microhardness in different parts of the weld are shown in Figure 5. Microhardness grows in the HAZ and decreases in the zone of the weld axis. Decrease in microhardness of metal in the central part of the weld may be related to the polygonisation processes (decrease in the density of chaotically located dislocations and formation of sub-boundaries). Redistribution of dislocations leads to changes in distribution of interstitial impurities. Increase in the concentration and angle of disorientation of the dislocation walls is accompanied by growth of the concentration of impurities, i.e. «cleaning» of the material matrix.

The revealed structural orientation peculiarities can be explained as follows. Crystallographic orientation of metal and perfection of structure in growth

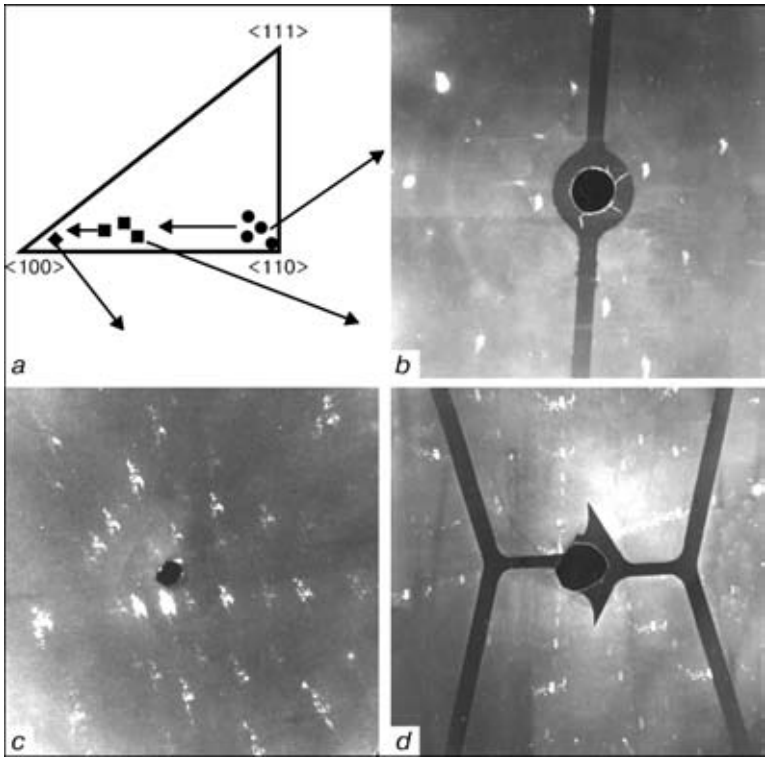


**Figure 6.** Stereographic projection (*a*) and diagrams (*b–d*) of orientations of niobium crystals demonstrating variations in the direction of their growth depending upon the speed of displacement of the molten pool: *b* — 2.8; *c* — 3.6; *d* — 5.6 mm/s

of crystals depend to a substantial degree upon the parameters, the solidification rate in particular [6, 15–17]. Apparently, each specific range of the solidification rates has its own, most favourable crystallographic directions, the so-called crystallographic planes of the priority growth.

We conducted experiments intended to verify validity of this postulate and specify it for the EBW conditions. The samples were locally and successively remelted with electron beam by overlapping the penetrated zone to a distance more than half the weld width. Figure 6 shows results of X-ray examinations of these samples. It follows from them that variations in both orientation of growth and perfection of structure of the remeled weld metal depend upon the speed of displacement of the molten zone. Thus, at a speed of 2.8 mm/s (Figure 6, *b*) solidification occurs in a direction close to [110]. Diffraction spots in the diagrams have the form of reflexes of a regular shape with a slightly developed internal structure, which is indicative of an insignificant disorientation of blocks and a high perfection of material. Increasing the speed to 3.6 mm/s (Figure 6, *c*) leads to growth of crystals in the [310] direction, i.e. the orientation gradually shifts to the [001] direction. The diffraction spots are more smeared and have an internal structure. At a speed of displacement equal to 5.6 mm/s (Figure 6, *d*) the direction of a preferred growth is [001].

If the solidification direction and substrate orientation coincide with the direction of a preferred growth, the solidification process to occur requires the least overcooling, it takes place under more equilibrium conditions, and metal structure is more perfect.

Therefore, the decisive factors in formation of structure of a welded joint are perfection and initial crystallographic orientation of the fusion surface, as the latter serves as a foundation on which the «bricks» of a solidifying metal are arranged, inheriting its orientation and perfection. Effect of the solidification rate is more pronounced in the case of non-coincidence of initial orientation and direction of a preferred growth, which prevents inheritance of the initial structure. Manifestation of this phenomenon is growth of the dislocation density, causing redistribution of dislocations, thus leading to formation of overstressed centres in the case of unfavourable welding conditions and parameters. The stronger the deviation of the welding parameters from the favourable ones for a given crystallographic orientation, the higher the defectiveness of a structure. This can explain difference in the dislocation density and disorientation of the substructure elements in metal of the welds produced at different welding speeds (see Figures 4 and 5, Tables 2 and 3).

As the solidification rate is different across the section of the weld (almost equal to zero near the fusion line, and maximum, almost equal to the welding speed along the weld axis [1, 18]), the effect of conditions of growth of single crystals on their perfection can be traced in one weld (see Figures 1 and 5).

X-ray reflexes for the base metal had a smooth distribution of the intensity with a width of about 10–20 mrad. In the HAZ the width of this distribution grows, but its shape remains smooth. The clearly defined peaks in the intensity distribution appear in the central part of the weld. These peaks characterise a well-formed sub-grain structure.

The dislocation density in the weld metal may grow almost by an order of magnitude even with the best variants of relationships between the initial crystallographic orientations and welding speed, while in other less successful experiments it may grow to a much higher value (see Figure 5, *a*).

Values of microhardness (see Figure 5, *b*) correlate with the above results of X-ray examinations. Regions with the highest density of chaotically located dislocations have a maximum hardness, and regions in which the dislocations are arranged into walls and the sub-boundaries are formed have a minimum hardness.

It can be concluded here that variations in the welding speed are capable of substantially (by orders of magnitude) changing the dislocation density in the weld metal, thus determining inheritance of structure of the initial base metal by the weld metal. Increase in the speed of welding of the samples, in which the densely packed crystallographic planes of the [100] and [110] type prevail, leads to formation of the least distorted structure of the weld metal. For surfaces with the less densely packed crystallographic planes of the type of [111] and close to them, the similar results can be obtained with decrease in the welding speed.

It should be emphasised that the results obtained should not be allowed for separately, and the effect of the crystallographic orientation should not be separated from the effect of welding conditions and parameters. And it is the last factor that the scatter of the data obtained is associated with. Variations in the welding conditions and parameters, most different from the optimal ones, may lead to a substantial scatter of the data and degree of dependence of structural perfection upon these parameters. Each particular case requires specification of solidification conditions, especially the speed, and even to a high degree — the initial crystallographic orientation at the moment of nucleation of a crystal (the initial stage of solidification).

Results of the investigations performed helped to determine the ways of producing welded joints in both single crystals and textured and polycrystalline metals with a minimum distortion of the initial structure and required properties.

Therefore, X-ray and metallography examinations proved that in fusion welding the weld metal inherited the structural state of the base metal.

The degree of inheritance of the initial structural state, determining the level of mechanical properties of a welded joint, can be estimated not only by deviation of crystallographic orientation of the weld metal from the base one, but also by disorientation of the substructure elements, density and distribution of dislocations.

The degree of inheritance is determined by the initial crystallographic orientation, as well as welding conditions and parameters. With their favourable combination the deviation of the crystallographic orientation of the weld metal from the initial one is not in excess of 90 mrad, and disorientation of the substructure elements is 30–40 mrad at 10–20 mrad for the base metal. Growth of the dislocation density (by an order of magnitude and more) in the weld metal and differing distribution of dislocations were fixed in all the variants of the investigated crystallographic orientation and welding conditions.

The revealed peculiarities of inheritance are attributable to correspondence of the solidification rate and speed of preferred growth for a certain crystallographic orientation. Variations in the inheritance characteristics across the section of the welds is caused by variations in the solidification rate.

Each crystallographic orientation of the weld edges has specific welding conditions and parameters characterised by a minimum distortion of the initial structural state. Lower welding speed and preheating are required for a satisfactory inheritance of structure of the weld edges by the weld metal, in the texture of which the less densely packed crystallographic planes of the type of (111) and (112) prevail. And vice versa, for the densely packed planes (100) and (110) of the fusion surface the best results can be obtained at increased welding speeds.


1. Petrov, G.L., Tumarev, A.S. (1977) *Theory of welding processes*. Moscow: Vysshaya Shkola.
2. (1982) *Metallurgy and technology of welding of refractory metals and alloys on their base*. Ed. by S.M. Gurevich. Kyiv: Naukova Dumka.
3. Trefilov, V.I., Milman, Yu.V., Firstov, S.A. (1975) *Physical principles of refractory metals strength*. Kyiv: Naukova Dumka.
4. Vayngard, D. (1967) I*ntroduction to physics of metal solidification*. Moscow: Mir.
5. Chalmers, B. (1968) *Theory of solidification*. Moscow: Metallurgiya.
6. Savitsky, E.M., Burkhanov, G.S. (1972) *Single crystals of refractory and rare metals and alloys*. Moscow: Nauka.
7. (1988) *Theory of welding processes*. Ed. by V.V. Frolov. Moscow: Vysshaya Shkola.
8. Savage, W.F., Aronson, A.H. (1966) Preferred orientation in the weld fusion zone. *Welding J.*, **2**, 85–89.
9. Matsuda, F., Hashimoto, T., Senda, T. (1969) Fundamental investigation of solidification structure in weld metal. *Transact. of NKJM*, **1**, 43–49.
10. Nerodenko, M.M., Polishchuk, E.P., Rabkina, M.D. et al. (1979) Peculiarities of solidification and fracture of welded joints of thin sheet molybdenum and niobium alloys. *Avtomatich. Svarka*, **11**, 14–18.
11. Nerodenko, M.M., Polishchuk, E.P., Milman, Yu.V. et al. (1978) Relationship between crystallographic textures of base and weld metals in low-alloy molybdenum alloys. *Ibid.*, **12**, 12–16.
12. Pshenichnikov, Yu.P. (1974) *Revealins the fine structure of crystals*. Moscow: Metallurgiya.
13. Barabash, R.I., Karasevskaya, O.P., Kononenko, V.A. (1977) Examination of metal dislocation structure by the rocking crystal method. In: *Physics of metals*. Issue 70.
14. Krivoglaz, M.A. (1983) *Diffraction of X-rays and neurons in irregular crystals*. Kyiv: Naukova Dumka.
15. (1972) *Growth of and defects in metal crystals*. Ed. by D.E. Ovsienko. Kyiv: Naukova Dumka.
16. Esin, V.O. (1965) Direction of preferred growth of crystals with cubic lattice. *Fizika Metallov i Metallovedenie*, **20**, 226–230.
17. Pikunov, M.V., Shishkov, V.V., Strigina, N.I. et al. (1973) Preferred direction of growth of refractory metals under conditions of floating-zone melting. *Izv. Vuzov, Tsvetn. Metallurgiya*, **5**, 110–112.
18. Prokhorov, N.N. (1968) *Physical processes in metals during welding*. Moscow: Metallurgiya.

# ADDITIONAL APPROACHES TO THE EVALUATION OF SUSCEPTIBILITY OF LOW-CARBON AND LOW-ALLOY STEELS TO LAMELLAR-TOUGH AND LAMELLAR-BRITTLE FRACTURES

**A.V. BERNATSKY**
E.O. Paton Electric Welding Institute, NASU, Kyiv, Ukraine

The paper sets forth the possibilities for determination of reduction in area $\varphi_z$ and $KCV_z$ based on the results of testing standard samples cut out across the direction of rolling on the sheet plane. An additional notion of lamellar cracking coefficient is introduced, which is the $KCV_z^{max}$: $KCV^{max}$ ratio in the entire range of transition temperature.

***Keywords:*** *low-carbon and low-alloy steels, anisotropy of mechanical properties, reduction in area, impact strength, lamellar-tough and lamellar-brittle fracture*

It was established from the results of expert evaluation of fractured welded joints, connections and structures, and from the laboratory investigations made at the E.O. Paton Electric Welding Institute, that the anisotropy of characteristics of toughness and ductility of rolled metal influences greatly not only the technological strength of welded joints, but also service reliability and life of welded structures due to formation of lamellar-tough and lamellar-brittle cracks [1–3].

Absence in the domestic practice (until the end of the 1990s) of the methods of testing the rolled metal in the direction of thickness did not make it possible to judge even approximately of its suitability for the defect-free manufacture and service of welded structures, and also limited the output of steels with standardized characteristics of reduction in area $\varphi_z$, that predetermined the working out of GOST 28879–90.

The main problem consisted in the necessity of creation of a separate document on regulation of allowable anisotropy of characteristics of ductility and crack resistance of rolled metal, including the impact strength to provide the resistance of welded joints not only to lamellar-tough fractures in welding, but also to lamellar-brittle fractures in service.

The important criterion of evaluation of susceptibility of rolled metal to lamellar-tough fractures is the reduction in area $\varphi_z$ [4–6].

From the data of foreign and domestic researchers, the lamellar cracks in welding metal structures occur at $\varphi_z < 15$ % and almost eliminated at $\varphi_z > 25$ % [7, 8].

German researchers have developed the system of estimates for the evaluation of different factors for establishing required values $\varphi_z$ of rolled metal, which, in the opinion of authors of the present article, include some not quite correct positions, and also statements of a discussing nature. The approach proper, defining more precisely the estimation of contribution of different factors to the resistance of connections and welded joints to the lamellar fractures from the engineering point of view represents an undoubted interest. At the same time the requirements of the consumer to the supplied rolled metal should have, probably, the more definite nature.

In accordance with the earlier developed GOST 28870–90 «Steel. Methods of Tensile Testing of Thick-Sheet Rolled Metal in the Direction of Thickness» depending on reduction in area $\varphi_z$, the sheet rolled metal is classified into groups of quality, designated as Z15, Z25, Z35 (Table 1).

Group of quality Z15 is lowest, and steels, included into it, are not suitable for use in structures or connections where the occurrence of tensile forces in the direction of sheet thickness are possible. It is considered that in structures manufactured from the sheet rolled metal of the group of quality Z35 the lamellar-tough cracks cannot occur. Steels used in critical welded connections and structures refer to an intermediate group of quality Z25.

It is recommended to record the ultimate resistance $\sigma_t^z$ and yield strength $\sigma_y^z$ in cases of limited values of reduction in are $\varphi_z$ between the groups of quality Z15 and Z25 (Figure 1).

It was alluring from the engineering point of view to develop the mechanism of determination of reduction of area $\varphi_z$ from the results of testing standard samples located in the sheet plane $\varphi$. Using the results of testing low-carbon and low-alloy steels, carried out at PWI, it is possible to plot the graphical dependence of $\varphi_{min}$ on $\varphi_{z\,min}$ (Figure 2).

**Table 1.** Classification of sheet rolled metal depending on reduction in area

| *Group of quality* | *Value of reduction in area $\varphi_z$, not less than, %* | |
|---|---|---|
| | *Mean values from results of testing three samples* | *Separate* |
| Z15 | 15 | 10 |
| Z25 | 25 | 15 |
| Z35 | 35 | 25 |

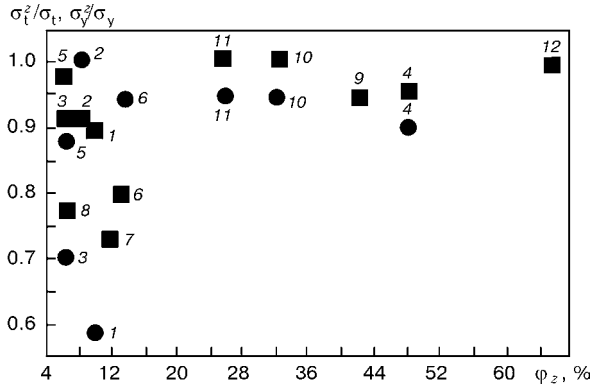


**Figure 1.** Dependence of ratio of strength characteristics of test specimens ($\sigma_t^z/\sigma_t$ and $\sigma_y^z/\sigma_y$) on reduction in area $\varphi_z$ in the direction of thickness (mean value): *1* — St.3, 70 mm thickness; *2* — 16G2AF, 20 mm; *3* — 16G2AF, 40 mm; *4* — 14G2AF, 40 mm; *5* — 14G2AF, 40 mm; *6* — 14G2AF, 36 mm; *7* — 14G2AF, 36 mm; *8* — 16G2AF, 40 mm; *9* — 16G2AF-Sh, 40 mm; *10* — 09G2S, 15 mm; *11* — 14G2AF, 50 mm; *12* — 12KhGDAF, 50 mm; ● — $\sigma_t^z/\sigma_t$; ■ — $\sigma_y^z/\sigma_y$

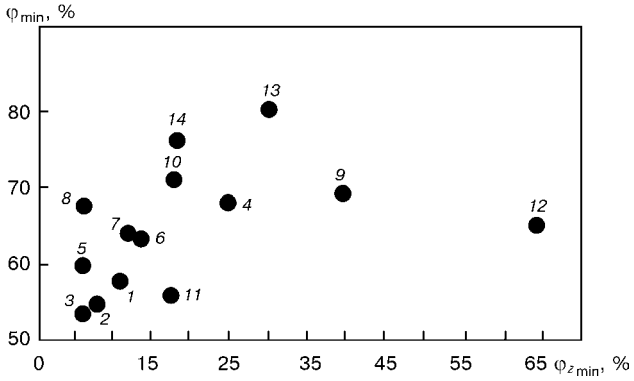


**Figure 2.** Dependence of reduction in area in the direction of thickness $\varphi_z^{min}$ on reduction in area in the rolling area $\varphi_{min}$. Designations of *1–12* here and in Figure 4 are similar to Figure 1; *13* — 09G2S-Sh, 50 mm; *14* — 09G2S, 35 mm

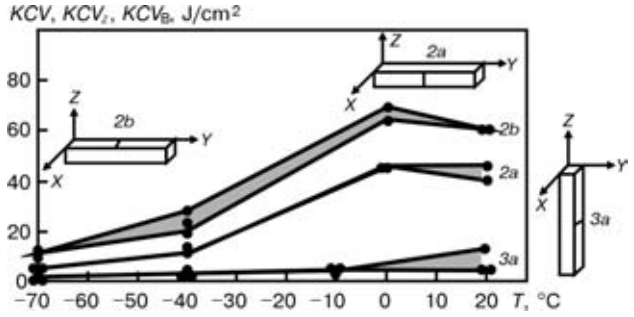


**Figure 3.** Dependence of impact strength $KCV$, $KCV_z$, $KCV_B$ on temperature for specimens *2a, 2b* and *3a* of 09G2S grade of steel

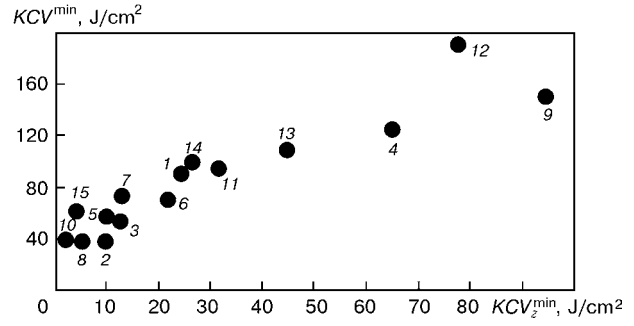


**Figure 4.** Dependence of impact strength in the direction of thickness $KCV_z^{min}$ on impact strength $KCV^{min}$ in rolling plane: *13* — 09G2S-Sh, 50 mm; *14* — 09G2S, 35 mm; *15* — 17G1S, 15 mm

**Table 2.** Results of mechanical tensile tests of 15 mm thick steel of 09G2S grade

| *Location of specimens* | $\sigma_y$, *MPa* | $\sigma_t$, *MPa* | $\delta$, *%* | $\varphi$, *%* |
|---|---|---|---|---|
| Across direction of rolling | 352–360 / 356 | 482–509 / 495.5 | 34–40 / 36 | 71–75 / 73 |
| Direction *Z* | 359–381 / 370 | 465–475 / 470 | 18–33 / 25.5 | 24–40 / 32 |

*Note.* Here and in Tables 3, 4 the numerator includes ranges of values, while the denominator includes the mean values.

Using the dependence obtained it is possible to determine by reduction in area $\varphi < 60$ % the belonging of steel grade tested to the group of quality Z15 (Table 1) and in some case to Z25 and Z35 ($\varphi > 60$ %).

In other words, from results of acceptance tensile tests in the conditions of mass production of structural steels it is possible to evaluate approximately the susceptibility of a steel sheet and its welded joints to lamellar-tough fractures.

As is outlined in [3], the determination of $\varphi_z$ is necessary, but not sufficient condition for the evaluation of susceptibility of the sheet or welded joint to lamellar-tough and, in particular, to lamellar-brittle fractures. Thus, in some cases, the satisfactory value $\varphi_z$ does not always correspond to the required level of metal crack resistance in tough and, in particular, in brittle state.

Tables 2 and 3 and Figure 3 give results of tensile and impact bend tests of 15 mm thick steel of 09G2S grade.

In spite of preliminary predictions, based on values of reduction in area in the thickness direction $\varphi_z$ = = 24–40 %, the impact strength $KCV_z$ (Figure 3, curve *3a*) occurred to be inadmissibly low within the entire range of temperatures. It should be noted that impact strength specimens with a notch, located in the thickness direction (*2a*) and «from sheet surface» (*2b*), also showed very low values of the impact strength that indicates the possibility of initiation of fractures, including those from the sheet surface. Further, this characteristic (conditionally $KCV_B$) can be used for obtaining the additional information.

**Table 3.** Results of mechanical impact bend tests of 15 mm thick steel of 09G2S grade

| *Location of specimens and notches* | *Impact bend tests, J/cm², at T, °C* | | | |
|---|---|---|---|---|
| | *−70* | *−40* | *0* | *+20* |
| *2a*, $KCV$ | 4 | 10–11 / 10.5 | 45 | 41–45 / 43 |
| *2b*, $KCV_B$ | 9–10 / 10.5 | 20–27 / 23.5 | 65–69 / 67 | 60 |
| *3a*, $KCV_z$ | 1–2 / 1.3 | 2.5–4.0 / 3 | 3–4 / 3.6 | 4–12 / 6.6 |

*Note.* Location of specimens relative to rolling direction is shown in Figure 3.

**Table 4.** Results of mechanical tensile tests of 24 mm thick steel of X57 type

| *Location of specimens* | $\sigma_y$, *MPa* | $\sigma_t$, *MPa* | $\delta$, % | $\varphi$, % |
|---|---|---|---|---|
| Across rolling direction | 471.5–457.7 / 462.3 | 574.2–579.7 / 576.6 | 25.3–29.3 / 26.6 | 62.0–64.0 / 63.3 |
| Direction *Z* | 452.1–457.2 / 453.8 | 566.0–571.1 / 568.6 | 21.0–23.3 / 21.7 | 50.0–57.0 / 52.3 |

**Table 5.** Results of mechanical impact bend test of 24 mm thick steel of X57 type

| *Location of specimens and notches* | *Impact bend test, J/cm², at T, °C* | | | | | |
|---|---|---|---|---|---|---|
| | *–70* | *–40* | *–20* | *0* | *+20* | *+50* |
| *2a*, *KCV* | 55.0–61.0 / 54.5 | 91.0–105.0 / 96.6 | – | 111.0–114.0 / 112.3 | 325.0–124.0 / 189.0 | – |
| *3a*, $KCV_z$ | – | 5.0–10.0 / 7.3 | 4–10 / 6 | – | 20.0–9.0 / 15.5 | 42.0–55.0 / 48.5 |

The use of test specimens for impact strength of rolled metal in the thickness direction (*3a*) was re-commended in the standard draft. This was met with objections from the side of representatives of the metallurgical industry because of the impossibility to manufacture the welded cruciform specimens in the conditions of a mass production at the metallurgical plants and difficulties to provide a sufficient impact strength in the direction *Z*. By these reasons the impact strength tests were not included into GOST 28870–90. This decision does not provide a direct evaluation of resistance of steels to the lamellar-brittle fractures. An attempt was made to evaluate the susceptibility of steels to the formation of lamellar-tough and lamellar-brittle fractures, in particular, from the results of impact bend tests of standard specimens located across the rolling direction in the sheet plane (*2a*).

The main idea, confirmed by numerous tests, consists in the fact that there is no almost anisotropy of the transition temperature in steels having a slightly-expressed crystallographic texture of rolling. In other words, $KCV_z$ value is reduced with respect to values of *KCV* at the upper «shelf» of temperature relationship of the impact strength that predetermines its appropriate decrease in the range of the transition temperatures. In this case the transition temperature, determined by a fraction of a tough component in fractures, remains similar in both cases.

Figure 4 shows the relationship between the minimum values of $KCV_z$ and *KCV* for steel grades investigated at the «upper shelf».

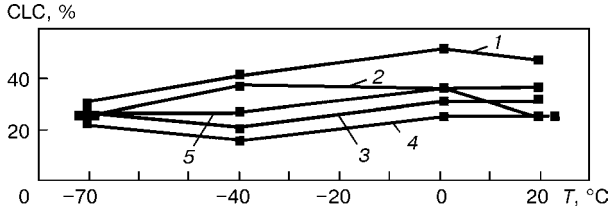


**Figure 5.** Dependence of CLC for steels with a slightly-developed crystallographic texture on temperature: *1* — 14G2AF, 40 mm; *2* — 14G2AF, 35 mm; *3* — 09G2S-Sh, 50 mm; *4* — 14G2AF, 35 mm; *5* — 16G2AF, 20 mm

Using the impact strength *KCV*, determined from the results of testing standard specimens, located across the rolling direction in the sheet plane, it is possible to evaluate only approximately the minimum values of $KCV_z$ in the conditions of a tough state of the metal.

Figure 5 shows the coefficient of a lamellar cracking (CLC) representing the $KCV_z^{max}/KCV^{max}$ ratio in the entire range of transition temperatures for some steels investigated.

Values CLC, confirming the absence of the clearly expressed anisotropy of transition temperatures for steels supplied in hot-rolled condition are shown in Figure 5.

It was established (Tables 4 and 5) in investigation of mechanical properties of 24 mm thick steel of a controllable rolling (X57) that steel is characterized by the isotropy of ductility characteristics in the rolling plane and direction *Z* (reduction in area $\varphi_z$ = = 50–57 % is comparable almost with reduction in area $\varphi$ = 62–64 %).

Other characteristics of strength and ductility obtained in testing specimens cut out in the direction *Z*, also correspond almost to similar characteristics obtained in testing specimens cut out in the sheet plane.

At the same time the steel of X57 grade is characterized by an increased susceptibility to lamellar-

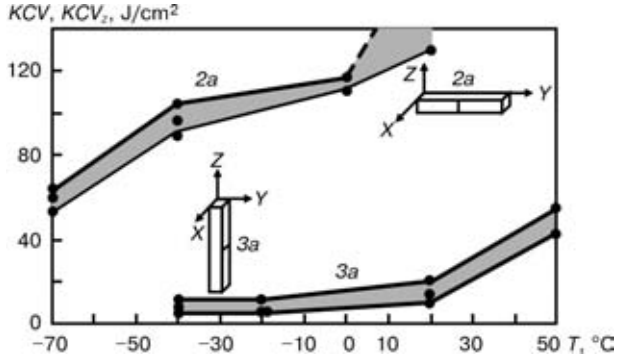


**Figure 6.** Dependence of impact strength *KCV* and $KCV_z$ for specimens *2a* and *3a* of X57 type steel on temperature

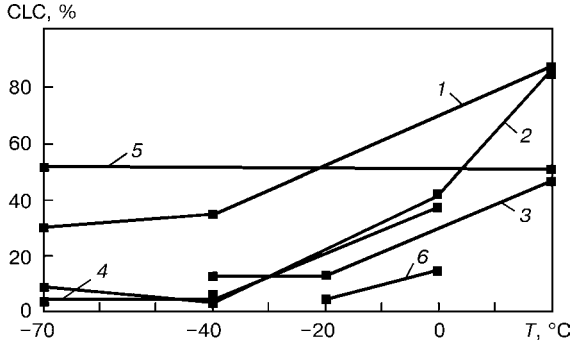


**Figure 7.** Dependence of CLC for steels of a controllable rolling with a developed crystallographic texture on temperature: *1–4* — 09G2S with different temperature of rolling end; *5* — X70 type; *6* — X57 type

brittle fractures even at positive temperatures (Figure 6). Thus, at $T = 20$ °C the values $KCV_z$ are equal to 9–20, and at negative test temperatures — to 4–10 J/cm$^2$.

Unlike steels with a slightly-developed crystallographic texture, steels of a controllable rolling have highly-differed values CLC (Figure 7) that proves the presence of anisotropy of transition temperatures.

It is impossible in the latter case to judge of susceptibility of rolled metal to lamellar-brittle fractures from values $KCV$.

Thus, the steels of a controllable rolling require direct tests to determine the $KCV_z$ values during service under the conditions of a minimum temperature.

## CONCLUSIONS

1. It was established that it is possible to evaluate the susceptibility of some low-carbon and low-alloy steels with a slightly-developed crystallographic texture to the initiation of lamellar-tough cracks from the results of tests of standard tensile specimens located across the rolling direction in the sheet plane φ.

2. It is possible to determine approximately the values $KCV_z^{max}$ and temperature of metal transition to the brittle state from the results of impact bent tests $KCV^{max}$ of standard specimens located across the rolling direction in the sheet plane.

3. Direct tests of specimens, located in the direction of sheet thickness, are necessary for impact bend $KCV_z$ to evaluate the susceptibility of steels of a controllable rolling to lamellar-tough and lamellar-brittle fractures.

1. Girenko, V.S., Bernatsky, A.V., Rabkina, M.D. (1987) Lamellar, lamellar-brittle and lamellar-tough fracture of welded joints. *Problemy Prochnosti*, **3**, 70–76.
2. Girenko, V.S., Bernatsky, A.V., Kozachek, V.M. et al. (1990) Static strength of cruciform welded joints at low temperatures. *Avtomatich. Svarka*, **2**, 28–32.
3. Bernatsky, A.V. (2000) Influence of anisotropy of the rolled stock mechanical properties on initiation and development of tough and lamellar-tough fractures. *The Paton Welding J.*, **7**, 31–37.
4. Novikov, V.I., Girenko, V.S., Bernatsky, A.V. (1985) Anisotropy of the properties of rolled metal and performance of welded structures. *Avtomatich. Svarka*, **12**, 13–19.
5. Granstrom, A. (1976) The relevance of test methods for lamellar tearing of steel structures. *IIW Doc. IX-948–76*.
6. Schonheer, W. (1979) Metallurgical and constructional measures for the prevention of lamellar tearing in welded structures. *IIW Doc. IX-II 42–79*.
7. Lombardini, J. (1979) Evaluation of lamellar tearing in the structural steel. *IIW Doc. IV-1138–79*.
8. Schonheer, W. (1978) ψ-value as criterion for judging the lamellar tearing tendency of steel structures. *IIW Doc. IX-1080–78*.

# REDISTRIBUTION OF RESIDUAL WELDING STRESSES UNDER THE EFFECT OF NORMAL INCIDENT SHOCK WAVE

**V.G. PETUSHKOV**
E.O. Paton Electric Welding Institute, NASU, Kyiv, Ukraine

Interaction of normal incident shock wave with the field of internal stresses in metal is considered. It is shown that under rational conditions of loading of structural steels this correction is about 5 % of the wave amplitude. Therefore, it can be ignored in practical calculations.

***Keywords:*** *residual stress, explosion treatment, stress relief, shock wave, dynamic yield stress, elasto-plastic strain*

Explosion treatment using captive strip or cord explosive charges has received currently a wide acceptance for relieving residual stresses in welded joints. A number of studies [1–4 etc.] have been dedicated to practical and physical aspects of this phenomenon. For example, study [1] considered symmetric case of initial stresses $\sigma_{y0} = \sigma_{z0}$ and $\sigma_{x0} = 0$ to investigate the path of a point representing the stress-strain state of a material in the space of principal stresses during explosion loading and unloading. The plane of front of the shock wave in this case is located in parallel to the surface of metal, axes $\sigma_y$ and $\sigma_z$ are in the plane of the surface of a plate treated, and axis $\sigma_x$ is normal to it. It is assumed that behaviour of metal corresponds to the model of an elasto-plastic medium. In the case under consideration, whatever the initial stresses are within the elasticity limits, the straight line of an elastic stress propagates to the yield surface at points which belong to a certain straight line, the projection of which to plane $\sigma_x$, $\sigma_y$ is straight line $QQ$ shown in Figure 1 (in the case of the elasticity waves this is straight line $PP$). $0D = 0E = 0F = 0G = \sigma_s$ (here $\sigma_s$ is the dynamic yield stress), section $0S$ is the projection of a hydrostatic axis. During further loading the representative point moves along straight line $QQ$.

In a characteristic case the path of loading is more complex for the majority of the types of welded joints at $\sigma_{y0} \neq \sigma_{z0}$. As shown below, these paths in the plastic region are a family of curves that have as an asymptote at high values of $\sigma_s$ the straight lines the projections of which to plane $\sigma_x$, $\sigma_y$ are $PP$ and $QQ$.

The purpose of this study was to determine the above paths and, on this basis, boundaries of the region of applicability of the diagram shown in Figure 1 for a case of asymmetry of initial stresses. It should be noted here that there are physical theories of the processes of interaction of shock waves with stressed metal which are based on more sophisticated models of a medium, including those which allow for non-unidimensionality of loading (see, e.g. [5, 6]). Nevertheless, it is of interest to analyse how high the correction to calculations, allowing for asymmetry of initial residual stresses, may be. The input data for the consideration using the diagram suggested are residual stresses $\sigma_y$ and $\sigma_z$ in metal welded and values of stresses $\sigma_{xk}$ caused by external loading.

If we use the associated yield law for a material that follows the Saint Venan–von Mises yield criterion (the case of ideal plasticity) in the form [7, 8]:

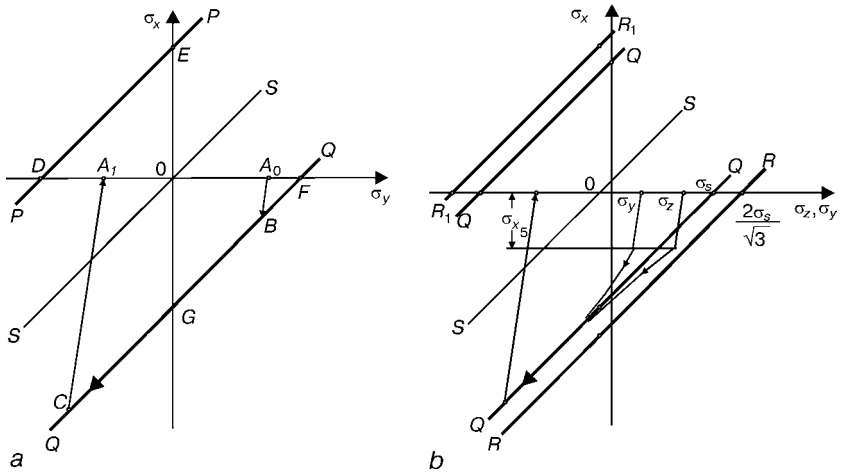


**Figure 1.** Paths of a representative point in plane of principal stresses for a case of «approximated» (*a*) and «refined» (*b*) theory

| $\Delta\sigma_0$ | $S_{x1} = -1/3\sqrt{4\sigma_s^2 - 3\Delta\sigma_0^2}$ | $\beta = \frac{2\sigma_s - 3S_{x1}}{2\sigma_s + 3S_{x1}}$ | *Number of curve in Figure 2, b* |
|---|---|---|---|
| 0 (broken) | $\frac{2\sigma_s}{3}$ | $\infty$ | – |
| $\frac{\sigma_{YS}}{2}$ | $0.660\sigma_s$ | 190.0 | *5* |
| $\frac{2\sigma_{YS}}{3}$ | $0.654\sigma_s$ | 106.0 | *4* |
| $\frac{3\sigma_{YS}}{4}$ | $0.651\sigma_s$ | 83.3 | *3* |
| $\sigma_{YS}$ | $0.638\sigma_s$ | 46.0 | *2* |
| $2\sigma_{YS}/\sqrt{3} \approx 1.15\sigma_{YS}$ | $0.629\delta_s$ | 34.0 | *1* |

$$\frac{d\varepsilon_{xp}}{S_x} = \frac{d\varepsilon_{yp}}{S_y} = \frac{d\varepsilon_{zp}}{S_z} = \frac{|d\varepsilon_p|}{|S_i|}, \quad (1)$$

where $\varepsilon_i$ is the strain and $S_i$ are the stress tensor components, we can derive the following system of equations:

$$\frac{4}{3}Gd\varepsilon_x = \frac{dS_x}{1 - \left(\frac{3S_x}{2\sigma_s}\right)^2};$$
$$-\frac{2}{3}Gd\varepsilon_x = \frac{dS_y}{1 - \frac{9S_x S_y}{2\sigma_s^2}} = \frac{dS_z}{1 - \frac{9S_x S_z}{2\sigma_s^2}} \quad (2)$$

(here $G$ is the deviator component of the stress tensor), which will make it possible to find the loading parameter dependence of $\sigma_x$, $\sigma_y$ and $\sigma_z$. Figure 1, *b* shows on the combined coordinate planes $\sigma_x$, $\sigma_y$ and $\sigma_x$, $\sigma_z$ the probable paths of loading in the elastic and plastic regions corresponding to solutions of system (2). Here the region confined by straight lines $RR$ and $R_1R_1$ is the projection of a yield cylinder, straight line $QQ$ is the asymptote of the paths at $\sigma_x \to \infty$, and $\sigma_{x1}$ corresponds to the beginning of plastic flow. It is more convenient to consider the process on coordinates $\sigma_x$, $\sigma_m$, where $\sigma_m = 1/2(\sigma_y + \sigma_x)$. The corresponding paths are shown in Figure 2, *a*.

The loading process can be described as follows.

1. The initial point belongs to section $AD$, $\sigma_{m0} = 1/2(\sigma_{y0} + \sigma_{z0})$. Different values of $\Delta\sigma_0 = \sigma_{y0} + \sigma_{z0}$: $|\Delta\sigma| < 2/3\sqrt{\sigma_{YS}^2 - \sigma_{m0}}$, $|\sigma_{m0}| < \sigma_{YS}$, where $\sigma_{YS}$ is the static yield stress, may correspond to one initial point. It was assumed in the calculations that $\sigma_s = 3\sigma_{YS}$.

2. Elastic loading occurs along straight line

$$\sigma_x = \frac{1 - \nu}{\nu}(\sigma_m - \sigma_{m0}) \text{ at } \nu = \frac{1}{3}\ \sigma_x = 2(\sigma_m - \sigma_{m0}). \quad (3)$$

3. The point of yield going to the surface is characterised by value

$$\sigma_{x1} = \frac{1 - \nu}{1 - 2\nu}\left(\frac{2}{3}S_x + \sigma_{m0}\right), \quad (4)$$

where $S_{x1} = -1/3\sqrt{4\sigma_s^2 - 3\Delta\sigma_0^2}$.

At $\nu = 1/3$ $\sigma_{x1} = 3S_{x1} + 2\sigma_{m0}$.

4. Further loading can be described by the following parametric equations derived from solving system (2):

$$\begin{cases} \frac{\Delta\sigma_x}{\sigma_s} = -\frac{2}{3}\left(\frac{\beta e^t - 1}{\beta e^t + 1} + t\right) - \frac{S_{x1}}{\sigma_s}, \\ \frac{\Delta\sigma_m}{\sigma_s} = \frac{1}{3}\left(\frac{\beta e^t - 1}{\beta e^t + 1} - 2t\right) + \frac{S_{x1}}{2\sigma_s}, \end{cases} \quad (5)$$

where $\beta = \frac{2\sigma_s - 3S_{x1}}{2\sigma_s + 3S_{x1}}$; $t > 0$; $\Delta\sigma_x = \sigma_{xk} - \sigma_{x1}$; $\Delta\sigma_m = \sigma_{mk} - \sigma_{xk}$ is the wave amplitude; $\sigma_{mk}$ is the value of $\sigma_m$ corresponding to $\sigma_{xk}$; and $\sigma_{m1}$ is that corresponding to $\sigma_{x1}$.

Asymptotic relationship between $\sigma_{xk}$ and $\sigma_{mk}$ at large amplitudes of $\sigma_{xk}$ can be derived from formulae (5) and relationships (3) and (4): $\sigma_{xk} \to \sigma_{mk} - \sigma_s$. Therefore, the paths of loading in the plastic region on coordinates $\sigma_x - \sigma_m$ have the form of curve $NR$ shown in Figure 2, *a*.

Consideration of loading using the simplified diagram suggests replacement of the path of broken line $KNR$ and $\Delta\sigma$ equal to zero. Point $P$ corresponds to an approximated unloading value of $\delta'_{m2}$, point $T$ corresponds to the precise value of $\sigma_{m2}$. Designate correction $PT$ as $\sigma_p$ ($\sigma_p > 0$).

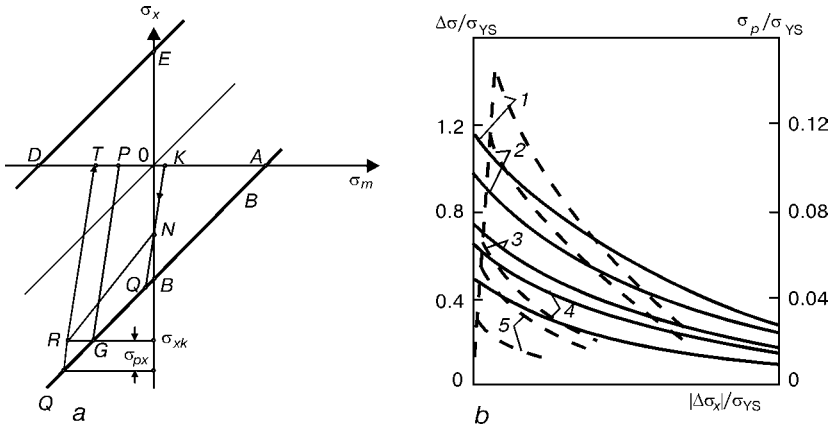


**Figure 2.** Plots in plane of principal stresses illustrating algorithms and results of application of the «refined» theory: $\sigma_m = 1/2(\sigma_y + \sigma_z)$ (see *a*, *b* and the rest of the designations in the text)

To determine the stressed state after unloading, it is necessary to know the values of $\sigma_{m2}$, $\sigma_p$ and difference of stresses after unloading $\Delta\sigma_2 = \sigma_{y2} - \sigma_{z2}$. The $\Delta\sigma_x$ dependencies of $\Delta\sigma$ and $\sigma_p$ at $\nu = 1/3$, obtained by transformation of system (5), have the following form in the parametric representation:

$$\frac{\Delta\sigma}{\sigma_{YS}} = \pm 4\sqrt{3\beta}\,\frac{\exp(t/2)}{\beta e^t + 1}, \quad \frac{\sigma_p}{\sigma_{YS}} = \frac{6}{\beta e^t + 1},$$

where sign in the first formula coincides with that of $\Delta\sigma_0$.

Figure 2, *b* shows the calculation corrections to parameters given in the Table. Dashed lines correspond to the $\sigma_p$ value, and solid lines correspond to $\Delta\sigma$.

The algorithm of using the simplified diagram with corrections is as follows. The following calculations are made, proceeding from initial stresses $\sigma_{y0}$ and $\sigma_{z0}$:

$$\sigma_{m0} = 1/2(\sigma_{y0} - \sigma_{z0}),\ \Delta\sigma_0 = \sigma_{y0} - \sigma_{z0}.$$

Then, allowing for the known wave amplitude $\sigma_{xk}$, the approximated broken line of loading and unloading of the type of *KQGP* is plotted, and the approximated unloading value of $\sigma'_{m2}$ (point *P* in Figure 2, *a*) is determined. Then the $\Delta\sigma_x$ value is found. The values of $\Delta\sigma_p$ and $\Delta\sigma_0$ can be determined from the value of $\Delta\sigma_x = \sigma_{xk} - \sigma_{x|}$ using plots shown in Figure 2, *b*; and then $\sigma_{y2}$ and $\sigma_{z2}$ are found from formulae

$$\sigma_{y2} = \sigma'_{m2} + \frac{\Delta\sigma_2}{2} - \sigma_p, \quad \sigma_{z2} = \sigma'_{m2} - \frac{\Delta\sigma_2}{2} - \sigma_p.$$

It can be seen from Figure 2, *b*, that the $\Delta\sigma$ correction is most substantial, and the value of $\sigma_p$ at $\Delta\sigma_x < -\sigma_s$ can be ignored.

If $\sigma_{m2} < -\sigma_{YS}$, point *T* starts drifting (see Figure 2, *a*) to increase in the $\sigma_m$ values after the shock-wave process. The calculation made on the basis of the associated yield law (1) and condition of the $\varepsilon_y = \varepsilon_z = 0$ uniaxial strain showed that the final state of $\sigma_{m3}$ and $\Delta\sigma_3$ could be determined from the following system of equations:

$$\sigma_{m3}^2 + \frac{3}{4}\Delta\sigma_3^2 = \sigma_{YS}^2, \quad \frac{\Delta\sigma_3}{\Delta\sigma_2} = \left(\frac{\sigma_{m3}}{\sigma_{m2}}\right)^{\gamma},$$

where $\gamma = \dfrac{3(1-\nu)}{1+\nu}$; at $\nu = \dfrac{1}{3}$ $\gamma = 3/2$.

It can be assumed in the first approximation that $\sigma_{m3} = -\sigma_{YS}$ and $\Delta\sigma_3 = \Delta\sigma_2 - (\sigma_{YS}/\sigma_{m2})^{3/2}$.

It is important to know also correction $\sigma_{px}$ (see Figure 2, *a*) for a practical use of the above calculations. This correction is a difference between the «precise» and approximated wave amplitude needed to determine the certain final state $\sigma_{m2}$ characterised by point *T*.

The value of $\sigma_{px}$ can be determined from the following transcendental equation:

$$\frac{\sigma_{px}}{\sigma_s} = \frac{4}{1 + \beta\exp(\alpha - \sigma_{px}/\sigma_s)},$$

where $\alpha = 2 + (3/\sigma_s)(S_{x|} + \sigma_{m0} - \sigma_{m2})$ and $\sigma_{m2} < \sigma_{m0}$.

The calculation made at $\sigma_{m2} = 0$ showed that at $\sigma_s = 3\sigma_{YS}$ $\max(\sigma_{px}/\sigma_s) = 0.114$, which is less than 6 % of the wave amplitude $\sigma_{xk}$ equal in this case to $\sigma_s$. Therefore, this correction can be also ignored in practical calculations. This results from the fact that an insignificant relative variation in the wave amplitude $\sigma_{xk}$ leads to more pronounced variations in the final state of $\sigma_{m2}/\sigma_{YS}$, as usually $\sigma_{xk} \cong 6\sigma_{YS}$.

We should dwell now on peculiarities of the dynamic shock-wave process allowed for in this study in comparison with the quasi-static loading and unloading conditions. For example, as shown in [9, 10], the actual high-rate picture of deformation of a tough elasto-plastic material can be described using the elasto-plastic quasi-static process characterised by some efficient dynamic yield stress, which depends upon the strain rate and toughness of the material.

At an actual strain rate achieved in the process of relieving residual stresses by explosion treatment of such materials as steel St.3, the dynamic yield stress is 3–5 times as high as the static one. These data generated from experiments on high-rate tension and compression of rods are given in [11]. In addition, peculiarity of the dynamic character of deformation should be allowed for by adding to the process considered the drift of the point which represents the stressed state of a material with respect to the static yield stress.


1. Petushkov, V.G., Fadeenko, Yu.I. (1980) On explosion treatment of welded joints. *Fizika Goreniya i Vzryva*, **5**, 64–68.
2. Kudinov, V.M., Trufyakov, V.I., Petushkov, V.G. et al. (1976) Parameters of explosive charges used to relieve residual stresses in butt welded joints. *Avtomatich. Svarka*, **1**, 46–49, 61.
3. Petushkov, V.G., Fadeenko, Yu.I. (1999) *Welding stresses relief by explosion treatment*. N.-Y.: Backbone.
4. Kudinov, V.M., Petushkov, V.G. (1986) Technology of explosion treatment of welded metal structures. In: *Annual of Big Soviet Encyclopedia*. Issue 13. Moscow: Sov. Entsikl.
5. Petushkov, V.G., Grishaenko, A.I. (1997) Calculation of stress-strain state of a solid body subjected to local explosion loading. *Fizika Goreniya i Vzryva*, **6**, 92–101.
6. Petushkov, V.G., Titov, V.A. (2001) Parameters of shock-wave loading used to relieve residual welding stresses by explosion treatment. *The Paton Welding J.*, **4**, 56–58.
7. Kachanov, L.M. (1969) *Principles of plasticity theory*. Moscow: Nauka.
8. Sedov, L.I. (1984) *Mechanics of continuum*. Moscow: Fizmatgiz.
9. Stepanov, G.V. (1981) *Elasto-plastic strain of materials under pulsed loads*. Kyiv: Naukova Dumka.
10. Rakhmatulin, Kh.A., Demianov, Yu.A. (1961) *Strength under intensive short-time loads*. Moscow: Fizmatgiz.
11. Pisarenko, G.S., Petushkov, V.G. (1970) Mechanical properties of some materials in high-rate tension. *Problemy Prochnosti*, **7**, 3–8.

# METHOD OF EVALUATION OF THE EFFECTIVENESS OF MULTIFACTORIAL CONTROL OF THE WELDING PROCESS

**I.A. TARARYCHKIN**
East-Ukrainian National University, Lugansk, Ukraine

The paper suggests a method to evaluate the effectiveness of preventive measures, aimed at improvement of the accuracy of the multifactorial process. Criteria are defined, which allow determination of the nature of the change in the accuracy and stability of the process being controlled. The possibilities of the method are considered in the case of narrow-gap arc welding of a circumferential weld on a thick-walled cylindrical shell.

***Keywords:*** *narrow-gap arc welding, process control, statistical regulation, product quality, preventive measures, accuracy criteria*

Method of statistical regulation, described in [1], allows controlling the condition of a uni-dimensional technological process by a pre-established accuracy characteristic. The actual welding processes, as a rule, are multidimensional, and their current condition is determined by a combination of a large number of factors (mode parameters). Control of multifactorial technological processes is associated with the need to control their condition and periodically taking preventive measures, aimed at increasing the accuracy of the process being controlled [2–4].

Analysis of the accuracy of multifactorial systems is made difficult by the absence of procedures, allowing objective estimation of their condition. Performance of such analysis is related to the need to assess the effectiveness of the preventive measures.

The difficulties, arising in this case, are related to the fact that purposeful change of the process condition by one or several accuracy characteristics may lead to change of the value of other characteristics, because of the presence of an implicit or explicit correlation. In this case a situation may arise, when an attempt to change the process condition, in order to improve its accuracy will lead to a reverse result.

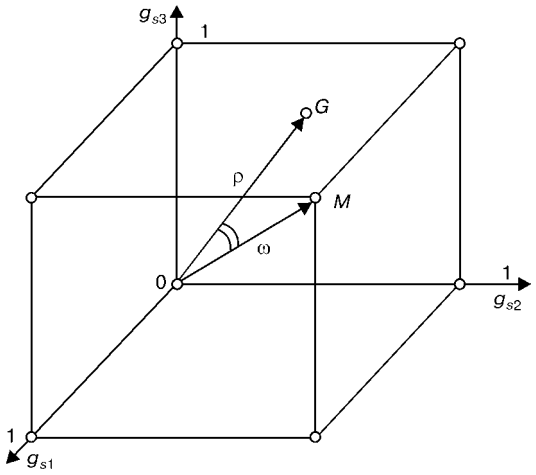


**Figure 1.** Schematic of relative location of vectors **G** and **M** in $g_{s1}\ g_{s2}\ g_{s3}$ system of coordinates

If before taking the preventive measures, the condition of an $n$-dimensional process was described by vector $\mathbf{G}^*$ with coordinates $g^*_{s1}$, $g^*_{s2}$, ..., $g^*_{sn}$, and after the measures were taken it was characterized by vector $\mathbf{G}^{**}$ with coordinates $g^{**}_{s1}$, $g^{**}_{s2}$, ..., $g^{**}_{sn}$, it necessary to determine, whether the registered change of the process condition indeed corresponds to the case of improvement of its accuracy.

Let us assume that before the start and after completion of preventive measures, the accuracy of an $n$-dimensional process was ensured, i.e. conditions $g^*_{si} < 1$ and $g^{**}_{si} < 1$ ($i$ = 1, 2, ..., $n$) were satisfied, and the purpose of taking these measures was improvement of accuracy. For the case of three variables, the process condition can be described in the system of co-ordinates $g_{s1}\ g_{s2}\ g_{s3}$ (Figure 1). The boundary of the limit state is the surface of a unit cube. An arbitrary point **G**, located inside the cube, has co-ordinates $g_{s1}$, $g_{s2}$, $g_{s3}$. In this case the smaller is angle ω between vector **G** and cube diagonal (vector **M**), the higher the accuracy of the process, as with increase of ω vector **G** approaches the boundary of the limit state. In addition, the latter occurs also with the increase of the length of radius-vector ρ.

In keeping with the described approach, evaluation of the effectiveness of the preventive measures should be performed as follows. If the initial position of vector $\mathbf{G}^*$ is characterized by a set of values $\rho^*$ and $\omega^*$, and after taking such measures values $\rho^{**}$ and $\omega^{**}$ correspond to vector $\mathbf{G}^{**}$, the accuracy of the process is improved, provided the following condition is satisfied:

$$\begin{cases}\Delta\rho = \rho^* - \rho^{**} > 0;\\ \Delta\omega = \omega^* - \omega^{**} > 0.\end{cases} \quad (1)$$

The process accuracy will not change, if

$$\begin{cases}\Delta\rho = 0;\\ \Delta\omega = 0,\end{cases} \quad (2)$$

and will decrease at

$$\begin{cases}\Delta\rho < 0; \\ \Delta\omega < 0. \end{cases} \quad (3)$$

Now, if parameters $\Delta\rho$ and $\Delta\omega$ are of different signs, i.e. one of the following conditions holds:

$$\begin{cases}\Delta\rho < 0; \\ \Delta\omega > 0, \end{cases} \quad \begin{cases}\Delta\rho > 0; \\ \Delta\omega < 0, \end{cases} \quad (4)$$

it is impossible to make an unambiguous conclusion about the nature of the change of process condition.

Implementation of the proposed algorithm of evaluation of the effectiveness of preventive measures is related to the need to determine the following parameters:

• angle $\omega^*$ between vectors $\mathbf{G}^*$ and $\mathbf{M}$ in $n$-dimensional space of factors $g_{si}$ [5]

$$\omega^* = \arccos\left(\sum_{i=1}^{n} g_{si}^* \Big/ \sqrt{n\sum_{i=1}^{n} g_{si}^{*2}}\right);$$

• angle $\omega^{**}$ between vectors $\mathbf{G}^{**}$ and $\mathbf{M}$

$$\omega^{**} = \arccos \frac{\sum_{i=1}^{n} g_{si}^{**}}{\sqrt{n\sum_{i=1}^{n} g_{si}^{**2}}};$$

• increment of angle $\Delta\omega$

$$\Delta\omega = \arccos \frac{\sum_{i=1}^{n} g_{si}^{*}}{\sqrt{n\sum_{i=1}^{n} g_{si}^{*2}}} - \arccos \frac{\sum_{i=1}^{n} g_{si}^{**}}{\sqrt{n\sum_{i=1}^{n} g_{si}^{**2}}}; \quad (5)$$

• modulus of vector $\mathbf{G}^*$

$$\rho^* = \sqrt{\sum_{i=1}^{n} g_{si}^{*2}};$$

• modulus of vector $\mathbf{G}^{**}$

$$\rho^{**} = \sqrt{\sum_{i=1}^{n} g_{si}^{**2}};$$

• increment of modulus $\Delta\rho$

$$\Delta\rho = \sqrt{\sum_{i=1}^{n} g_{si}^{*2}} - \sqrt{\sum_{i=1}^{n} g_{si}^{**2}}. \quad (6)$$

Effectiveness of preventive measures is evaluated, depending on the sign of $\Delta\omega$ and $\Delta\rho$ criteria in keeping with the established inequalities (1)–(4).

Let us consider the possibilities of the proposed method in the case of filling of a V-shaped groove with a multilayer weld by the following schematic: one layer per pass. In order to ensure the edge penetration the torch, directed along the gap center, makes transverse oscillatory motions. The conditions for implementation of the welding process may change with time, due to random and systematic causes. So, as the groove is filled, its current width will increase, which may cause lacks-of-penetration at the walls. During welding the oscillation amplitude may change, which may also be accompanied by appearance of lacks-of-penetration. Analyzing the condition of a two-dimensional process, with monitoring by the current width of the gap $2B$ (accuracy criterion $g_{s1}$) and amplitude of torch oscillations $A_t$ (accuracy criterion $g_{s2}$), it should be noted that point $A$ (Figure 2), characterizing the limit condition of the process, corresponds to the case of possible formation of lacks-of-penetration at further increase of the current width of the groove. In this case, $g_{s2} = 0$ is taken, i.e. it is assumed that the amplitude of torch oscillations corresponds to the nominal value, while oscillations occur in parallel to the axis, coinciding with the groove center.

Point $B$ (Figure 2) corresponds to a limit condition of the process, in which further reduction of the amplitude of torch oscillations is accompanied by formation of lacks-of-penetration. In this case it is assumed that there are no deviations of the geometrical dimensions of edge preparation ($g_{s1} = 0$).

Thus, in terms of the possible formation of lacks-of-penetration, the condition of the welding process for points $A$ and $B$ (Figure 2) turns out to be equivalent, despite the differences in the conditions of its implementation.

If we use the proposed procedure, and define the process condition in point $A$ by a set of values $g_{s1}^* = 1$, $g_{s2}^* = 0$, and in point $B$ by $g_{s1}^{**} = 1$, $g_{s2}^{**} = 0$, respectively, then $\Delta\omega = 0$ and $\Delta\rho = 0$. This means, that in terms of the possible formation of lacks-of-penetration, the above conditions of the process should be recognized to be equivalent.

The considered example demonstrates, that when the proposed procedure is used, the controlled parameters of process accuracy should be selected, proceeding from the condition of a significant influence on product quality characteristics, and the parameters proper should have the same or close status, determined by the recommendations, given in Table 1.

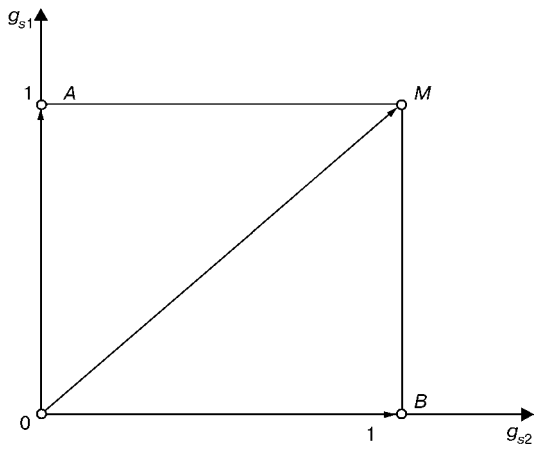


**Figure 2.** Schematic for determination of the condition of a two-dimensional welding process, using complex accuracy criteria $g_{s1}$ and $g_{s2}$

**Table 1.** Status of the controlled parameters of welding process accuracy

| *Status of the controlled parameter of process accuracy* | *Anticipated consequences of lowering the process accuracy by the parameter* | *Recommendations on control and documentation of the process condition* |
|---|---|---|
| Critical | It will certainly lead to formation of difficult-to-detect defects, requiring subsequent repair | Control, using systems of statistical regulation by a combined schematic [2]. Documenting, using control cards [6] and condition control cards [1] |
| Important | High probability of formation of defects, part of which will require further repair | Control, using the first or second regulation sequence [2]. Documenting, using control cards or condition control cards |
| Significant | May lead to formation of defects, detection and correction of which will not create any serious problems | Control, using $g_{si}$ criteria and documenting the current condition in those cases, when an unsatisfactory accuracy of the process is found |
| Insignificant | Formation of defects, which may require subsequent repair, is not anticipated | Control by current indices of measuring instruments. No documenting is done |

**Table 2.** Tolerance ranges, established for the controlled parameters of the process

| *Controlled parameter of the welding process* | *Nominal value of the parameter* | *Tolerance range limit, mm* | | *Designation of the appropriate complex accuracy criteria* |
|---|---|---|---|---|
| | | *Upper* | *Lower* | |
| $2B$, mm | Assumed to be equal to average value $2B_{av}$ for the current width of gap $2B$ in welding of an individual layer | $2B_{av} + 2$ | $2B_{av} - 2$ | $g_{s1}$ |
| $A_t$, mm | $0.5(2B_{av} - 10)$ | $0.5(2B_{av} - 10) + 1$ | $0.5(2B_{av} - 10) - 1$ | $g_{s2}$ |
| $U_a$, V | 30 | 32 | 28 | $g_{s3}$ |
| $v_w$, cm/s | 0.52 | 0.54 | 0.50 | $g_{s4}$ |
| $I_w$, A | 320 | 330 | 310 | $g_{s5}$ |

Let us analyze the possibility of evaluation of the effectiveness of preventive measures, when controlling the condition of a multifactorial process of narrow-gap arc welding of a circumferential weld of a shell with 75 mm wall thickness. The angle of opening of a one-sided groove is 5°. Unsatisfactory accuracy of the multifactorial welding process may lead to formation of lacks-of-penetration of the side walls. Subsequent detection and repair of such defects, lying in thick metal at a great depth, runs into serious technical problems.

Possible formation of lacks-of-penetration is influenced by a number of factors such as the current width of the gap $2B$, amplitude of torch oscillations $A_t$, as well as arc voltage $U_a$. During the groove filling with the circumferential weld, the welding speed $v_w$ is gradually increased (as a result of vertical displacement of the torch from the axis of rotation), which is accompanied by a decrease of the heat input and may lead to formation of lacks-of-penetration. Welding current $I_w$ is another parameter, influencing the heat input. Therefore, it should be taken into account, when controlling the process condition.

Thus, as the controlled five-dimensional process approaches the boundary of the limit state, corrective measures should be taken, which are related to lowering of welding speed (angular speed of the shell rotation) and increase of the amplitude of torch oscillations. Such corrections of process condition will result in a total change of accuracy characteristics, because of a presence of correlation links between mode parameters. The taken corrective measures, aimed at prevention of lacks-of-penetration, should be accompanied by an actual, not anticipated process accuracy.

In order to ensure the possibility of evaluation of the accuracy of a multifactorial welding process, it is necessary to first set the nominal values and admissible range of variation of the controlled characteristics (define design tolerance). Nominal values and design tolerance range for such characteristics may be established, proceeding from the available production experience, by welding a test batch of samples at the stage of technology optimization, by the results of analysis of publications, taking into account the experts' opinion, etc.

For the considered case of welding the circumferential weld, the specified tolerance ranges for the

**Table 3.** Values of complex accuracy criteria of narrow-gap arc welding

| *Controlled parameter of welding process* | *Values of accuracy criteria, when taking preventive measures* | |
|---|---|---|
| | *Before* | *After* |
| $2B$, mm | $g^*_{s1} = 0.57$ | $g^{**}_{s1} = 0.62$ |
| $A_t$, mm | $g^*_{s2} = 0.83$ | $g^{**}_{s2} = 0.64$ |
| $U_a$, V | $g^*_{s3} = 0.77$ | $g^{**}_{s3} = 0.83$ |
| $v_w$, cm/s | $g^*_{s4} = 0.81$ | $g^{**}_{s4} = 0.71$ |
| $I_w$, A | $g^*_{s5} = 0.66$ | $g^{**}_{s5} = 0.70$ |

controlled characteristics of process accuracy are given in Table 2.

Table 3 gives the values of complex criteria of accuracy, designed in keeping with the procedure of [1], before and after taking the preventive measures, related to correction of the angular speed of rotation of the shell and amplitude of oscillations of the welding torch. Values of $\Delta\omega$ and $\Delta\rho$ were found during processing the data in Table 3, using dependencies (5) and (6):

$$\begin{cases}\Delta\rho = 0.069;\\ \Delta\omega = 0.03.\end{cases}$$

Positive values of the calculated criteria $\Delta\rho$ and $\Delta\omega$ indicate that taking preventive measures increases the accuracy of the controlled welding process. This means that the above measures are highly effective.

Thus, it is rational to use the proposed method to evaluate the effectiveness of the preventive actions in those cases, when higher requirements are made of the accuracy of the controlled multifactorial welding process and quality of welded joints.


1. Tararychkin, I.A. (2001) Statistic regulation of welding technological processes using the method of construction of charts of condition control. *The Paton Welding J.*, **10**, 28–31.
2. Tararychkin, I.A. (2002) *Statistical methods of quality assurance of welded products*. Lugansk: V. Dal EUNU.
3. *ISO 9001–2001*. Quality management systems. Requirements. Introd. 01.01.01.
4. *ISO/TO 10017–99*. Recommended practices for selection of statistical methods as applied to ISO 9001:1994. Introd. 01.01.99.
5. Korn, G., Korn, T. (1973) *Reference book on mathematics for researchers and engineers*. Moscow: Nauka.
6. Hawler, L., Howell, J., Gold, B. et al. (1984) *Statistical methods of quality control of products*. Moscow: Standart.


# CALCULATION OF VISCOSITY OF SLAG SYSTEMS OF FLUX-CORED WIRES


**V.N. SHLEPAKOV** and **S.M. NAUMEJKO**
E.O. Paton Electric Welding Institute, NASU, Kyiv, Ukraine



Van-Laar theory and Melvin-Hughs methods were the basis to develop the procedure of evaluation of dynamic viscosity of three-component salt-oxide systems. The possibility of preliminary theoretical investigation of the viscosity of slag systems is demonstrated.



***Keywords:*** *viscosity, multicomponent slag systems, flux-cored wires, Van-Laar theory, Melvin-Hughs method, slag viscosity, non-associated liquids*


In arc welding the viscosity of slag melts has a dominating importance in formation of weld and its quality. The conception about the relation between conditions of weld producing and main physical-chemical properties of slags is reflected in some works [1–5]. It was established that in vertical and overhead positions and in welding circumferential welds it is rational to use the short slags with an increased viscosity where the slag is solidified quickly and prevents reliably the weld pool from its spreading. Otherwise, slag during welding is flowing out, thus resulting in the formation of poorly formed hummocky welds with metal overlaps, undercuts and other defects. At the same time, the slags, having relatively low values of viscosity at temperature of steel melting (slag has a time for spreading over the surface), and quickly-solidified short slags at temperature decrease to 1200–1300 °C are necessary in flat welding for producing a smooth surface of the weld. Thus, knowing the temperature relationship of the slag viscosity it is possible to predict the welding-technological properties of flux-cored wires by the indices of covering capability of the slag and weld formation in vertical plane.

Experimental determination of viscosity is rather labour-intensive, a practical aspect of slag selection does not often take into account the change in some properties. One of the alternative methods is the construction of mathematical models to predict the temperature relationships of viscosity of the slag systems. Many known mathematical models are complicated and based on a large number of experimental data [6–8]. In the present article a method of calculation of viscosity of three-component systems on the basis of Van-Laar theory and Melvin-Hughs method is offered [9].

Van-Laar theory considers alloys consisting of molecules of almost similar sizes, mixed chaotically and interacting one with another in a certain way. This method leads to rather complex equations, which show that energy in interexchange depends on a coordination number and energy of interaction $Q_{ij}$, typical of different pairs of molecules. Theory in its interpreted form takes into account only the interaction of the nearest neighbors and makes no allowances for attraction to molecules locating beyond the first coordination layer. Equations describing the change in viscosity are suitable only for non-associated liquids, i.e. for salt-oxide slag systems, having an ion nature.

According to the Van-Laar theory and Melvin-Hughs method [9], the coefficient of viscosity in binary regular melts with allowance for the ion nature of the systems has a form

$$\eta = \frac{x_1 x_2}{x_1 + x_2}\left(\frac{1}{6\pi r_1 D}\frac{\partial \mu_1}{\partial l} - \frac{1}{6\pi r_2 D}\frac{\partial \mu_2}{\partial l}\right)\frac{\partial l}{\partial x_1}, \qquad (1)$$

where $x_1$, $x_2$ are the molar fractions of components 1 and 2 in the melt respectively; $r_1$, $r_2$ are the radius of molecules of components 1 and 2, nm; $D$ is the coefficient of diffusion; $\mu_1$, $\mu_2$ are the chemical potentials of components 1 and 2 in the melt; $l$ is the distance between molecules, measured in the direction normal to the movement direction.

The Van-Laar theory for the two-component system will be used for three-component systems. Then the viscosity can be expressed in the form

$$\eta = \frac{x_1 x_2}{x_1 + x_2 + x_3}\left(\frac{1}{6\pi r_1 D}\frac{\partial \mu_1}{\partial l} - \frac{1}{6\pi r_2 D}\frac{\partial \mu_2}{\partial l}\right)\frac{\partial l}{\partial x_1} + \frac{x_1 x_3}{x_1 + x_2 + x_3}\left(\frac{1}{6\pi r_1 D}\frac{\partial \mu_1}{\partial l} - \frac{1}{6\pi r_3 D}\frac{\partial \mu_3}{\partial l}\right)\frac{\partial l}{\partial x_1} + \frac{x_2 x_3}{x_1 + x_2 + x_3}\left(\frac{1}{6\pi r_2 D}\frac{\partial \mu_2}{\partial l} - \frac{1}{6\pi r_3 D}\frac{\partial \mu_3}{\partial l}\right)\frac{\partial l}{\partial x_1}. \qquad (2)$$

Definite dependences of viscosity coefficient on composition can be obtained according to equation (2), if chemical potentials of yielding units are known. Expressions of chemical potentials for the three-component system were obtained on the basis of data for two-component systems in the approximation of a complicated model of the theory of regular solutions:

$$\mu_\kappa = \mu_\kappa^0 + RT\ln x_\kappa - \sum_{j=1}^{K}(x_i x_j Q'_{ij} + 2x_i x_j^2 Q''_{ij}) + \sum_{j=1}^{k-1}(x_i Q'_{ik} + 2x_i x_k Q''_{ik}) + \sum_{j=k+1}^{n}(x_j Q'_{kj} + x_j^2 Q''_{kj}), \qquad (3)$$

where $\mu_k$ is the chemical potential of «k» component in the melt; $\mu_k^0$ is the chemical potential of a pure liquid component «k»; $x_k$, $x_i$, $x_j$ are the molar fractions of components; $Q'_{ij}$, $Q_{ij}$, $Q'_{ik}$, $Q''_{ik}$, $Q'_{kj}$, $Q''_{kj}$ are the energies of interparticle interaction determined from state diagrams of binary melts, J; $R$ is the universal gas constant; $T$ is the slag temperature, K.

Chemical potentials of components 1, 2 and 3 in the melt have the following form:

$$\mu_1 = kT\ln x_1 + (x_2^2 + x_2x_3)\,Q'_{12} + (x_2^3 + x_2^2x_3 - x_1x_2^2)\,Q''_{12} + (x_2x_3 + x_3^2)\,Q'_{13} + (x_2x_3^2 + x_3^3 - x_1x_3^2)\,Q''_{13} - x_2x_3Q'_{23} - 2x_2x_3^2Q''_{23}; \qquad (4)$$

$$\mu_2 = kT\ln x_2 + (x_1^2 + x_1x_3)\,Q'_{12} + (2x_1^2x_2 + 2x_1x_2x_3)\,Q''_{12} - x_1x_3Q'_{13} - 2x_1x_3^2Q''_{13} + (x_1x_3 + x_3^2)\,Q'_{23} + (x_1x_3^2 + x_3^3 - x_2x_3^2)\,Q''_{23}; \qquad (5)$$

$$\mu_3 = kT\ln x_3 - x_1x_2Q'_{12} - 2x_1x_2^2Q''_{12} + (x_1^2 + x_1x_2)\,Q'_{13} + (2x_1^2x_3 + 2x_1x_2x_3)\,Q''_{13} + (x_1x_2 + x_2^2)\,Q'_{23} + (2x_1x_2x_3 + 2x_2^2x_3)\,Q''_{23}, \qquad (6)$$

where $k$ is the Boltzmann's constant equal to $1.38\cdot10^{-24}$ J/K.

Differentiating expressions (4)–(6) by $l$

$$\frac{\partial \mu_1}{\partial l} = \frac{\partial \mu_1}{\partial x_1} - \frac{\partial \mu_1}{\partial x_2} - \frac{\partial \mu_1}{\partial x_3} = kT \times \left(\begin{array}{l}\frac{1}{x_1} - (3x_2 + x_3)\frac{Q'_{12}}{RT} + (2x_1x_2 - 2x_2x_3 - 5x_3^2)\frac{Q''_{12}}{RT} + (x_3 + x_2)\frac{Q'_{23}}{RT} + \\ +2x_3(x_3 + 2x_2)\frac{Q''_{23}}{RT} - (3x_3 + x_2)\frac{Q'_{13}}{RT} + (2x_1x_3 - 2x_2x_3 - 5x_3^2)\frac{Q''_{13}}{RT}\end{array}\right)\frac{\partial x_1}{\partial l}, \qquad (7)$$

$$\frac{\partial \mu_2}{\partial l} = \frac{\partial \mu_2}{\partial x_2} - \frac{\partial \mu_2}{\partial x_1} - \frac{\partial \mu_2}{\partial x_3} = kT \times \left(\begin{array}{l}\frac{1}{x_2} - (3x_1 + x_3)\frac{Q'_{12}}{RT} + 2(x_1^2 + x_1x_3 - x_2x_3 - 3x_1x_2)\frac{Q''_{12}}{RT} - \\ - (3x_3 + x_1)\frac{Q'_{23}}{RT} + (2x_2x_3 - 5x_3^2 - 2x_1x_3)\frac{Q''_{23}}{RT} + (x_1 + x_3)\frac{Q'_{13}}{RT} + \\ + 2(x_3^3 + 3x_1x_3^2)\frac{Q''_{13}}{RT}\end{array}\right)\frac{\partial x_2}{\partial l}, \qquad (8)$$

$$\frac{\partial \mu_3}{\partial l} = \frac{\partial \mu_3}{\partial x_3} - \frac{\partial \mu_3}{\partial x_1} - \frac{\partial \mu_3}{\partial x_2} = kT \times \left(\begin{array}{l}\frac{1}{x_3} + (x_1 + x_2)\frac{Q'_{12}}{RT} + 2(x_2^2 + 2x_1x_2)\frac{Q''_{12}}{RT} - (x_1 + 3x_2)\frac{Q'_{23}}{RT} + \\ + 2(x_2^2 + x_1x_2 + x_1x_3 - 3x_2x_3)\frac{Q''_{23}}{RT} - (3x_1 + x_2)\frac{Q''_{13}}{RT} + \\ + 2(x_1^2 + x_1x_2 - x_2x_3 - 3x_1x_3)\frac{Q''_{13}}{RT}\end{array}\right)\frac{\partial x_3}{\partial l}. \qquad (9)$$

At the condition $x_1 + x_2 + x_3 = \text{const}$ and $r_1 \approx r_2 \approx r_3$ the viscosity of pure components is

$$\eta_1^0 = \frac{kT}{6\pi r_2 D},\ \eta_2^0 = \frac{kT}{6\pi r_3 D},\ \eta_3^0 = \frac{kT}{6\pi r_1 D}. \qquad (10)$$

Substituting values of derivatives (7)–(9) to formula (2) and taking into account (10) it is possible to describe the viscosity of melts whose yielding units are either not changed or undergo negligible changes.

Let us consider the salt-oxide system $CaO–CaF_2–Al_2O_3$. Volume and radius of holes, occurring in melting slags (compositions of slags are indicated in Table 1), can be evaluated using equation [10]:

$$V_h = 0.68\left(\frac{kT}{\sigma}\right)^{3/2} = \frac{4}{3}\pi r_h^3, \qquad (11)$$

where $\sigma$ is the surface tension of slags, N/m; $r_h$ is the radius of holes, having a form

$$r_h^3 = \frac{3\cdot0.68(kT/\sigma)^{3/2}}{4\pi}\ \text{(m)}. \qquad (12)$$

The surface tension of slags is $\sigma_1 = 0.35$, $\sigma_2 = 0.42$, $\sigma_3 = 0.34$ N/m at temperature 1873 K [4]. Thus, from the experimental data of surface tension and formula (12) we shall find the radius of holes $r_h$ necessary for a tough yielding (Table 1).

In all compositions of slags the value of radius of holes is occurred to be close ($r_h$ = 0.135–0.150 nm) to the sizes of oxygen ion ($r$ = 0.132 nm), single-atom

**Table 1.** Composition of slags and radius of holes occurring in melting slags

| *No. of composition* | *Element content, wt.%* | $r_h$, *nm* |
|---|---|---|
| 1 | $60CaF_2–7CaO–33Al_2O_3$ | 0.148 |
| 2 | $20CaF_2–55CaO–25Al_2O_3$ | 0.135 |
| 3 | $65CaF_2–10CaO–25Al_2O_3$ | 0.150 |

**Table 2.** Experimental and calculated data of viscosity of $CaO–CaF_2–Al_2O_3$ system slags

| *Composition, mass fraction of elements, %* | *Temperature, °C* | *Viscosity, Pa·s* | |
|---|---|---|---|
| | | *Calculated* | *Experimental* |
| $60CaF_2–7CaO–33Al_2O_3$ (ANF-6) | 1400 | 0.0945 | 0.40 [11] |
| | 1500 | 0.0299 | 0.033 [11] |
| | 1600 | 0.0121 | 0.031 [11] |
| $20CaF_2–55CaO–25Al_2O_3$ | 1400 | 0.285 | 0.15 [4] |
| | 1500 | 0.056 | 0.08 [4] |
| | 1600 | 0.0216 | 0.08 [4] |
| $65CaF_2–10CaO–25Al_2O_3$ (ANF-23) | 1400 | 0.045 | 0.10 [11] |
| | 1500 | 0.0307 | 0.03 [11] |
| | 1600 | 0.0205 | 0.03 [11] |

ions are the units of tough yielding, i.e. these slags refer to non-associated liquids and the Van-Laar theory can be applied to them.

As the theoretical units of the tough yielding are unchanged at all the temperatures, the relationship between the coefficients of viscosity of fluoride and oxides can be obtained by extrapolation of polytherms of viscosity of pure components plotted in the system of coordinates $\lg \eta = f(1/T)$.

The values obtained by extrapolation

$$\lg \eta^0_{CaO} = \frac{7050}{T} - 5.22; \quad (13)$$

$$\lg \eta^0_{Al_2O_3} = \frac{14030}{T} - 8.78; \quad (14)$$

$$\lg \eta^0_{CaF_2} = \frac{3850}{T} - 3.62 \quad (15)$$

represent coefficients of viscosity of hypothetic oxides and fluorides capable to form the liquid solutions within the whole interval of compositions at temperatures being lower than the temperature of melting of real oxides. In spite of this, their use provides the necessary values of coefficients of viscosity of melts at temperatures being lower than those of melting of pure components.

Parameters of interaction for binary systems were determined from state diagrams by equations:

$$RT\ln\frac{x_1'}{x_1} + [(x_2')^2 - (x_2'')^2]\,(Q_{ij}' - Q_{ij}'') + [(x_2')^3 - (x_2'')^3]\,2Q_{ij}'' = 0; \quad (16)$$

$$RT\frac{x_2''}{x_2} + [(x_1'')^2 - (x_1')^2]\,(Q_{ij}' + 2Q_{ij}'') - [(x_1'')^3 - (x_1')^3]\,2Q_{ij}'' = 0, \quad (17)$$

where $x_1' + x_2' = 1$; $x_1'' + x_2'' = 1$; $x_1'$ and $x_2''$ are the molar fractions of components (upper index — phase number, lower index — number of component).

Table 2 gives the experimental and calculated data of viscosity of slags of $CaO–CaF_2–Al_2O_3$ system. Deviation of calculated polytherms of viscosity of ANF-6 and ANF-23 slags from experimental data is also caused by the fact that real slags ANF-6 and ANF-23 contain up to 3 % $SiO_2$ in its composition which is not taken into account in calculations. Thus, it is possible to describe the viscosity of oxide-fluoride melts with the help

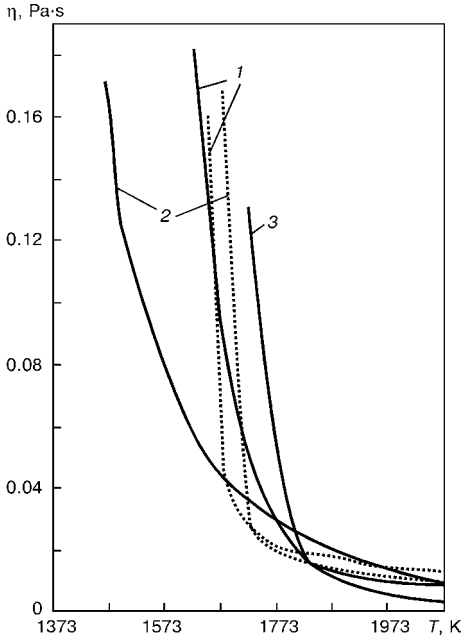


Temperature relations of dynamic viscosity η of welding slags of $CaO–CaF_2–Al_2O_3$ system for flux of composition ANF-6 (*1*), ANF-23 (*2*) and $20CaF_2–55\ CaO–25Al_2O_3$ (*3*) (solid curves — calculated data from formula (2), point curves — experiment by [11])

of theoretical formulae. It is evident, that the viscosity of melt depends both on the size and shape of separate molecules and complexes formed by them, and also on strength of intermolecular bonds, and, in case of formation of complexes, also on the ratio of strength of bonds between the molecules inside and outside the complex. It can be assumed for the $CaO–CaF_2–Al_2O_3$ system investigated from the data of viscosity that there is no formation of complexes in the selected points of the system.

It should be noted in conclusion that the theory of Van-Laar and Melvin-Hughs method make it possible to evaluate the dynamic viscosity of three-component salt-oxide systems. Comparative evaluation of calculated and experimental data proves the suitability of use of the developed procedure for the preliminary theoretical investigation of viscosity of the slag systems.


1. Popel, S.I. (1971) *Theory of metallurgical processes*. Moscow: VINITI.
2. Popel, S.I., Pavlov, V.V. (1965) Thermodynamic calculation of surface tension of solutions. In: *Surface phenomena in melts and solid phases formed from them*. Nalchik.
3. Kuzmenko, V.G., Galinich, V.I., Tokarev, V.S. et al. (1999) Investigation of properties of slag melts as applied to validation of welding fluxes composition. Part 1. Structure. *Avtomatich. Svarka*, **11**, 38–41.
4. Podgaetsky, V.V., Kuzmenko, V.G. (1988) *Welding slags*. Kyiv: Naukova Dumka.
5. Sokolov, L.N., Bajdov, V.V., Kunin, L.L. (1974) About peculiarities of structure of surface layer of slag melts. *Teoriya Metallurg. Protsessov*, **2**, 87–90.
6. Lyubimov, A.P., Gvozdeva, L.I. (2000) Theory of free volume. *Zhurnal Fiz. Khimii*, **2**, 247–250.
7. Glesston, S., Leidler, C., Eiring, G. (1948) *Theory of absolute reaction rate*. Moscow: Inostr. Literatura.
8. McAllister, R.A. (1960) Application of Eiring's theory for evaluation of kinematic viscosity of binary systems. *J. Analytic Chemistry*, **3**, 427.
9. Melvin-Huhgs, E.A. (1962) *Physical chemistry*. Book 2. Moscow: Inostr. Literatura.
10. Esin, O.A., Geld, P.V. (1966) *Physical chemistry of pyrometallurgical processes*. Part 2. Interaction with participation of melts. Moscow: Metallurgiya.
11. Zhmojdin, G.I., Moldavsky, O.D. (1970) Viscosity of fluorine-containing melts. *Izv. AN SSSR, Series Metally*, **1**, 70–73.

# SPARSELY-ALLOYED HIGH-STRENGTH STEELS FOR WELDED STRUCTURES

L.I. MIKHODUJ[1], V.I. KIRIAN[1], V.D. POZNYAKOV[1], P.A. STRIZHAK[1] and V.V. SNISARENKO[2]
[1]E.O. Paton Electric Welding Institute, NASU, Kyiv, Ukraine
[2]Company «Ukrstalkonstruktsiya», Kyiv, Ukraine

Results of analysis of properties and weldability of sparsely-alloyed high-strength steels of 06G2B and 09G2SYuch ($\sigma_y \geq$ $\geq$ 440 MPa) are given. Prospects of their use in manufacture of unique and reliable engineering structures of different purpose (bridges, towers, pressure vessels, tanks) are estimated.

***Keywords:*** *high-strength steels, weldability, strength properties, cold resistance, delayed fracture*

Rational use of advanced microalloyed materials with high characteristics of mechanical properties makes it possible to reduce effectively the metal and energy consumption, to increase the reliability and life, to widen the technical capabilities of engineering structures and to solve the new tasks without technical modification of the production. In industrialized countries the new generation of steels with 600–800 MPa yield strength is used now for this purpose [1, 2] and the problem of application of the stronger materials is under the consideration [3]. These steels contain mainly up to 0.12 % of carbon and the limited amount of manganese, molybdenum, niobium, titanium and boron. To attain the required complex of their properties, both the heat and also thermomechanical treatment (controllable rolling) are used. In some cases nickel, chromium, copper and other elements (up to 2–3 % in total) are added to these steels.

Undoubted advantage of these structural steels is their high reliability, cold resistance, good weldability, reached as a result of more economic alloying as compared with known materials. At the same time, due to a latter circumstance, these steels represent a specific group of materials, as the resistance of welded joints to a delayed and brittle fractures [4] can be decreased in the process of technological treatments in fabrication of metal structures.

Unfortunately, in domestic practice the low-alloy steels with up to 350 MPa yield strength are used until now in fabrication of unique and large engineering structures [5]. Taking into account the foreign experience, it can be expected that in the nearest future they will be not competitive in separate cases not only in the far and near foreign countries, but also in our country. This is mainly promoted by the fact that only separate attempts are outlined in Ukraine for the creation and mastering of production of new, stronger and promising structural steels.

The aim of the present work was to analyze comprehensively the properties and weldability of two domestic sparsely-alloyed high-strength grades of steels (Nb-containing 06G2B and microalloyed 09G2SYuch with $\sigma_y \geq 440$ MPa) as regards to their promising application in fabrication of unique and reliable engineering structures of different purpose (bridges, towers, pressure vessels, tanks).

**Composition and properties of steels.** Requirements to the composition and properties of steels investigated, according to technical specifications, are given in Table 1. The Table includes also data about widely known steels of grades 10KhSND and 16G2AF (with $\geq$ 390 and $\geq$ 440 MPa yield strength) for comparison.

In accordance with TSU 14-16-150–99 the Nb-containing steels of 06GB and 06G2B grades (developed by Mariupol Institute of Structural Materials «Prometej») of strength classes C 355–C 490 are supplied in sheets of 8–50 mm thickness. Here, the producing of four levels of strength properties ($\sigma_y \geq$ $\geq$ 355, 390, 440 and 490 MPa; $\sigma_t \geq$ 450, 490, 540 and 590 MPa) is regulated by varying heat treatment conditions at almost similar characteristics of ductility and impact toughness. Steels can be supplied with a guaranteed values of reduction in area in axis $Z$ and discontinuity (class 0). In the present investigations the steel of strength class C 440, 40 mm thickness was used, $\sigma_y \geq$ 440 MPA of discontinuity class 0.

Steel of 09G2SYuch grade can be supplied according to TSU 322-16-127–97 in sheets of 8–40 mm thickness. In this case the different level of rolled metal properties can be provided depending on thickness and methods of heat treatment: $\sigma_y$ = 325–450 MPa, $\sigma_t$ = 480–570 MPa, $\sigma \geq$ 19 %, $KCU \geq$ 29 and $KCV \geq$ $\geq$ 29 J/cm$^2$ at temperature −40 – −70 °C. Steel of 09G2SYuch of 18 mm thickness and $\sigma_y \geq$ 450 MPa was basic for investigations.

Carbon equivalent $C_{eq}$, whose calculated formula was suggested by the International Institute of Welding (IIW) serves as an approximate index of weldability of steels. Among steels, given in Table 1, steel 16G2AF has the highest value of $C_{eq}$. By this reason, the welding of the above steel is connected with certain difficulties. Experience of fabrication of structures from this steel confirms completely the data of [6, 7]. Therefore, steel of 10KhSND ($C_{eq}$ = 0.35–= 0.52 %), recommended for use in fabrication of widely-spread heavy-loaded structures, was used as a basic steel in our investigations for comparison. Among the steels investigated, steel 06G2B of strength classes C 440 and C 490 had the lowest values of carbon equivalent ($C_{eq}$ = 0.33–0.43 %). Index $C_{eq}$ of steel 09G2SYuch is somewhat higher (0.41–

**Table 1.** Composition and properties of steels of increased and high strength

| Steel grade | Elements, wt.% | | | | | | | | | |
|---|---|---|---|---|---|---|---|---|---|---|
| | C | Si | Mn | Cr | Ni | Mo | Cu | Al | Ti | Nb |
| 06G2B | 0.04–0.08 | 0.15–0.35 | 1.3–1.6 | – | – | 0.05–0.08 | 0.15–0.30 | 0.02–0.05 | < 0.02 | 0.03–0.05 |
| 09G2SYuch | 0.08–0.11 | 0.3–0.6 | 1.9–2.2 | – | – | – | 0.3–0.6 | 0.035–0.065 | – | – |
| 10KhSND | ≤ 0.12 | 0.8–1.1 | 0.5–0.8 | 0.6–0.9 | 0.5–0.8 | – | 0.40–0.65 | – | – | – |
| 16G2AF | 0.14–0.20 | 0.3–0.6 | 1.3–1.7 | ≤ 0.4 | ≤ 0.3 | – | 0.15–0.30 | – | – | – |

**Table 1** (cont.)

| Steel grade | Elements, wt.% | | | | | $C_{eq}$, % | $\sigma_y$ | $\sigma_t$ | $\delta_{5,\%}$ | $KCU_{-70}$ | $KCV_{-70}$ |
|---|---|---|---|---|---|---|---|---|---|---|---|
| | V | Ce | $N_2$ | S | P | | MPa | | | J/cm² | |
| 06G2B | – | – | < 0.012 | < 0.010 | < 0.02 | 0.33–0.43 | 440 | 540 | 22 | – | 59 |
| 09G2SYuch | – | 0.002–0.005 | – | < 0.015 | < 0.02 | 0.41–0.51 | 450 | 570 | 19 | 29 | 29 |
| 10KhSND | – | – | – | < 0.035 | < 0.035 | 0.35–0.52 | 390 | 530–660 | 19 | 29 | – |
| 16G2AF | 0.08–0.14 | – | 0.015–0.025 | < 0.035 | < 0.035 | 0.40–0.62 | 440 | 590 | 20 | 29 | – |

0.51 %) and coincides completely by its level with that of steel 10KhSND.

Chemical composition and mechanical properties of the basic steel and steels investigated are given in Tables 2 and 3. Significant increase in standardized indices of ductility $\delta_5$, $\psi$ and impact toughness $KCV$ in the steels investigated is noticeable. This is typical of the modern microalloyed steels due to a high grain refining and reduction in content of harmful impurities (sulphur, phosphorus).

Both these steels possess a good adaptability to fabrication of metal structures (they allow use of all the types of mechanical treatment and technological operations, associated with a plastic deformation, such as bending, rolling, stamping and so on).

**Effect of welding thermal cycles on HAZ metal properties.** In the HAZ of sparsely-alloyed steels a formation of bainitic-martensitic structures containing a high amount of a ferritic component is possible at delayed rates of cooling ($w_{6/5}$ < 3–5 °C/s) [4, 5, 8]. Unfavorable ratios of these components of microstructure can lead to the reduction in strength and ductility of both HAZ and the welded joint metal, as a whole.

Therefore, it seemed rational to carry out special investigations for the selection of optimum conditions of cooling HAZ metal of the steels investigated. For this, specimens-simulators of 13 × 13 × 150 mm size, which were subjected to treatment in MSR-75 unit [9] according to different thermal cycles of welding (TCW), were used. Standard specimens for tensile and impact bend tests were manufactured from these simulators.

During investigations the conditions of treatment were selected for simulators so that to simulate the conditions of metal formation in HAZ of welded joints, namely heating to 1300–1350 °C temperatures and subsequent cooling at different rates $w_{6/5}$ = 2.5–25 °C/s (in 600–500 °C temperature range).

Results of carried out investigations provided feasibility to establish the optimum conditions for different methods of welding and conditions of conductance of works. Minimum rates of cooling were determined for all the steels investigated, at which there were no significant reduction in level of cold resistance, yield strength and HAZ metal ductility. It was outlined that the degree of TCW effect on each of steels investigated is different.

The yield strength of HAZ metal in Nb-containing 06G2B and low-alloy 10KhSND steels at delayed rates of cooling can reduce to 8–10 % as compared with similar characteristics of the parent metal. In steel 09G2SYuch in this case the reduction in $\sigma_y$ is much higher (to 26–28 %). At delayed rates of cooling the tendency to deterioration of ductility (reduction in area) of HAZ metal was observed in steels 09G2SYuch and 10KhSND. In this case the TCW does not almost influence the ultimate resistance $\sigma_t$ of the above-mentioned materials. In general, the investigations could

**Table 2.** Chemical composition of steels investigated

| Steel grade | Elements, wt.% | | | | | | |
|---|---|---|---|---|---|---|---|
| | C | Si | Mn | Cr | Ni | Mo | Cu |
| 06G2B | 0.080 | 0.27 | 1.5 | – | – | 0.19 | 0.23 |
| 09G2SYuch | 0.097 | 0.36 | 1.9 | – | – | – | 0.39 |
| 10KhSND | 0.091 | 0.98 | 0.7 | 0.77 | 0.8 | – | 0.37 |

**Table 2** (cont.)

| Steel grade | Elements, wt.% | | | | | | |
|---|---|---|---|---|---|---|---|
| | Al | Ti | Nb | $N_2$ | Ce | S | P |
| 06G2B | 0.04 | 0.013 | 0.047 | 0.008 | – | 0.006 | 0.011 |
| 09G2SYuch | 0.06 | – | – | N/D | 0.004 | 0.010 | 0.015 |
| 10KhSND | – | – | – | Same | – | 0.018 | 0.012 |

**Table 3.** Mechanical properties of steels investigated

| Steel grade | $\sigma_y$ | $\sigma_t$ | $\delta_5$ | $\psi$ | $KCV$, J/cm$^2$, at $T_{test}$, °C | | |
|---|---|---|---|---|---|---|---|
| | MPa | | % | | +20 | −40 | −70 |
| 06G2B | 458 | 582 | 34 | 84 | > 300 | > 300 | > 300 |
| 09G2SYuch | 468 | 593 | 31 | 79 | 210–260 / 234 | 170–216 / 196 | 146–179 / 160 |
| 10KhSND | 408 | 580 | 26 | 75 | 30–43 / 39 | 18–23 / 21 | 10–16 / 13 |

*Note.* Numerator gives ranges, while dominator gives mean value.

establish the optimum range of cooling rates, at which the values of strength and ductility of HAZ metal remain stable in steels investigated.

As a rule, a significant deterioration of cold resistance of HAZ metal of the sparsely-alloyed steels as compared with similar characteristics of the parent metal is occurred under the effect of TCW [10].

It should be noted that steels of grades 09G2SYuch and 06G2B are differed negligibly as to the level of cold resistance of HAZ metal ($KCV_{-40} \geq 27$ and $\geq 35$ J/cm$^2$).

Steel 10KhSND is inferior by the characteristics of HAZ metal cold resistance to both sparsely-alloyed steels investigated ($KCV_{-40} \geq 15$ J/cm$^2$). It should be outlined that this steel has low values of impact toughness at negative temperatures and in initial state (Table 3).

More complete idea about the cold resistance of welded joints from sparsely-alloyed steels investigated can be obtained from the results of investigations of large-sized specimens, made in accordance with recommended technologies and criteria of fracture mechanics.

**Resistance of steels investigated to a delayed fracture.** The delayed fracture of welded joints is usually a hazardous defect of structures made from steels of increased or high strength. Their formation is caused by the following factors: martensitic and bainitic components in microstructure of HAZ metal; diffusion hydrogen; residual welding stresses of the I kind.

The most complete idea about the role of the first two factors and third partially at the a delayed fracture of structural steel welded joints can be obtained using the implant test, the use of which was recommended by IIW [11].

Specimens-implants of 6 mm diameter and 200 × × 300 mm plates were prepared from steels 06G2B, 09G2SYuch and 10KhSND. The UONI-13/55 grade electrodes of 4 mm diameter were used as basic electrodes. The control of conditions of their storage and baking allowed us to reproduce such limits of content of diffusive hydrogen in the deposited metal which are most often observed in welding structures in real conditions: $[H]_{diff}$ = 5–16 ml/100 g (at analysis of its content by a chromatographic method). Welding conditions of specimens were also varied, with the help of which the rate of cooling HAZ metal of implant samples was adjusted within the wide enough ranges ($w_{6/5}$ = 8–26 °C/s). Critical tensile stress $\sigma_{cr}$ of a definite technological variant, at which the HAZ metal is resisted against cold crack formation, was taken as an index of crack resistance. In each case a maximum tensile stress $\sigma_{cr\ max}$ from external load $P$ was also served as a criterion, at which the cracks in implant samples were not initiated during 20 h. Optimum conditions of welding of a definite technological variant were selected according to the condition at which $\sigma_{cr\ max} > (0.75–0.80)\sigma_{0.2}$ of the parent metal.

Investigations showed that steel of 06G2B grade is characterized by a high enough resistance to a delayed fracture. Even at unfavourable conditions of tests ($w_{6/5} \approx 26$ °C/s, $[H]_{diff} \approx 16$ ml/100 g) the implant samples from this steel were not fractured during 20 h at $\sigma_{cr}$ = 360 MPa, that is $\approx 0.77\sigma_{0.2}$.

Resistance to a delayed fracture of other two steels depends on the diffusive hydrogen content in the deposited metal. If the concentration of $[H]_{diff}$ was limited by 5–7 ml/100 g, the implant samples of 09G2SYuch and 10KhSND steels were not fractured at loads $\sigma_{cr} > 0.7$ of yield strength of appropriate steels. With increase in hydrogen concentration above this level the values $\sigma_{cr}$ in both steels are decreased. This refers greatly to steel 10KhSND that proves its high susceptibility to a delayed fracture as compared with steel 09G2SYuch.

Results of tests of implant samples from these steels at most intensive cooling of HAZ metal ($w_{6/5}$ = = 25–25 °C/s) are given in Figure 1.

The generalized results about the effect of rate of cooling HAZ metal of 09G2SYuch and 10KhSND steels at different concentration of diffusive hydrogen in the deposited metal on $\sigma_{cr}$ of implant samples are given in Figure 2. Results of investigations indicate that as to a delayed fracture the sparsely-alloyed high-strength steels of 06G2B and 09G2SYuch grades at comparable conditions of fabrication of structures are superior to a well-known steel of increased strength of 10KhSND grade. Here, the conditions of their use should be, probably, selected in such a way that content of diffusive hydrogen did not exceed 8–9 ml/100 g, and the rate of cooling of HAZ metal was < 30 °C/s.

**Resistance of steels to lamellar fracture.** Anisotropy of ductility and toughness is typical of sheet rolled metal of structural steels. It is expressed in a noticeable deterioration of these properties in the transition from longitudinal direction to transverse and in an abrupt their deterioration in the direction of thickness (direction $Z$) that is usually associated with the presence of non-metallic inclusions in steel, elongated thin sulphides in particular. Low values of ductility and toughness in combination with occurring forces in the direction $Z$ in welded connections of metal structures, mainly with T-, fillet and overlap joints, are the main cause of formation of lamellar cracks.

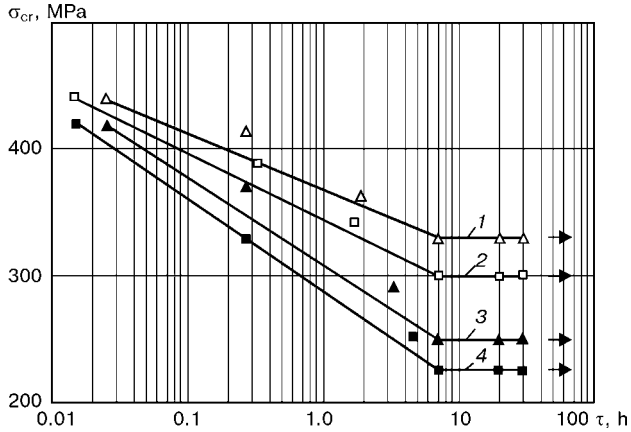


**Figure 1.** Effect of weld metal saturation with hydrogen at intensive rate of cooling on susceptibility to a delayed fracture of implant samples from steels 09G2SYuch (*1, 3*) and 10KhSND (*2, 4*): *1, 2* — $[H]_{diff}$ = 10; *3, 4* — 16 ml/100 g

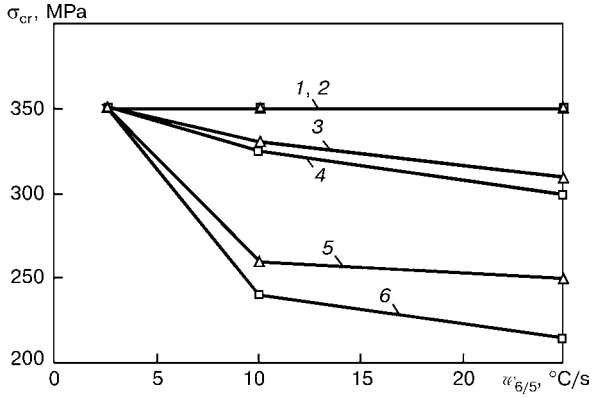


**Figure 2.** Effect of cooling rate on $\sigma_{cr}$ of implant samples from steels 09G2SYuch (*1, 3, 5*) and 10KhSND (*2, 4, 6*) at different content of diffusion hydrogen: *1, 2* — $[H]_{diff}$ = 5–7; *3, 4* — 9–10; *5, 6* — 15–16 ml/100 g

However, the new generation of steels in the process of production are more often subjected to different types of refining treatment and contain, as a rule, a large amount of sulphur. Therefore, their role in a lamellar fracture can be decreased. Probably, when analyzing lamellar fractures of these steels it is rational to make allowance for a possible role of nitride needle-shaped inclusions in this process. Structural steels of the new generation contain often nitrogen and nitride-forming elements (aluminium, vanadium, niobium, titanium, etc.). Specifics of their production process can also contribute to the formation of nitride inclusions. The required complex of properties in them is formed in cooling or heat treatment of metals [12, 13]. Therefore, it is desirable to provide obligatory the technical specifications on production of the mentioned steels, and also certificates of quality with information about the reduction in area, that was included into TSU 14-16-150–99 and TSU 322-16-127–97.

During conductance of the present investigations special butt joints were made from all three steels in accordance with GOST 28870–90 and then cylindrical specimens were cut from them for tensile tests. Results of investigations showed that steel 10KhSND has unsatisfactory resistance to the formation of lamellar cracks, as its reduction in area is very low ($\psi_z \approx 9$–10 %). The sparsely-alloyed steels 06G2B and 09G2SYuch are characterized by the high resistance to formation of lamellar cracks ($\psi_z$ = 27–37 %). By this characteristic they are much superior to steel of 10KhSND grade.

Thus, the results of carried out investigations showed that the sparsely-alloyed steels of 06G2B and 09G2SYuch grades ($\sigma_y$ = 440–450 MPa) provide high values of cold resistance at temperatures down to –70 °C on Charpy V-notched samples and by some characteristics of weldability (effect of TCW on properties of HAZ metal, resistance to delayed and lamellar fracture) are much superior to structural steel of 10KhSND grade ($\sigma_y$ = 390 MPa).

## CONCLUSIONS

1. As to their service properties the sparsely-alloyed steels of 06G2B and 09G2SYuch grades meet completely the requirements specified to steels of the level of strength $\sigma_y \geq 440$ MPa and European standards. In addition, their high cold resistance at temperatures –40 – –70 °C on Charpy V-notched samples ($KCV$ = = 150–300 J/cm$^2$) should be noted.

2. In optimum range of rates of cooling the HAZ metal of steels investigated provides the required strength properties and cold resistance ($KCV \geq 27$ and $\geq 35$ J/cm$^2$ at temperatures down to –40 °C for steels 09G2SYuch and 06G2B, respectively). It is assumed that these investigations will be added in future with tests of welded joints of a full thickness using approaches and criteria of fracture mechanics.

3. To decrease the probability of a delayed fracture of joints of 06G2B and 09G2SYuch steels it is necessary to limit the content of diffusive hydrogen in the deposited metal and rate of HAZ metal cooling.

4. The investigated batches of steels 06G2B and 09G2SYuch provide rather high values of reduction in area in the direction of thickness ($\psi_z$ = 27–37 %), that creates premises for their high resistance to a lamellar fracture.


1. Fischer, J.W., Dexter, R.J. (1994) High-performance steel for America's bridges. *Welding J.*, **1**, 35–43.
2. Tani, S., Kaneko, V., Ishiguro, M. et al. (1996) Recently developed structure steel for use in civil engineering and construction. *NKK Technical Rev.*, **74**, 17–25.
3. Herold, E.H., Zinke, M., Zwickert, H. et al. (1999) Neues in der Schweißtechnik 1998. *Schweißen und Schneiden*, **5**, 266–288.
4. Lundin, C.D., Gill, T.P.S., Qino, C.Y.P. et al. (1990) Weldability of low-carbon micro-alloyed steels for marine structures. *WRS Bull.*, **359**, 100.
5. (1993) *Welded engineering structures*. Vol. 1. Principles of structure design. Ed. by L.M. Lobanov. Kyiv: Naukova Dumka.
6. Zhiznyakov, S.N., Konopatov, V.S., Lyalin, K.V. (1988) Causes of defect formation in welded joints of metal structures of Magnitogorsk Metallurgical Plant production. In: *Series Manufacture of metal and erection-building structures*. Issue 11.
7. Tishaev, S.I., Odessky, P.D. (2001) New generation of low-alloy steels for metal structures. *Metally*, **7**, 56–64.
8. Demchenko, Yu.V., Asnis, A.E., Ivashchenko, G.A. et al. (1986) Influence of thermal welding cycle on structure and toughness of HAZ metal of heat-hardened steel 09G2S. *Avtomatich. Svarka*, **11**, 10–13.
9. Sidoruk, V.A., Dudko, D.A., Gorbenko, N.V. et al. (1985) Simulation of thermal welding cycle in heat-affected zone during electroslag welding with modulated current. *Ibid.*, **7**, 12–15.
10. Brozda, J., Zeman, M. (2000) Weldability evaluation of a modern TMCR steel by using simulation techniques. *Acta Metallurgica Sinica*, **1**, 103–111.
11. (1973) Recommendation for the use of implant test as a complementary information test on the cold cracking susceptibility during the welding of steel. *IIW Doc. IX-830–73*.
12. Yavojsky, V.I., Rubenchik, Yu.I., Okenko, A.P. (1980) *Non-metallic inclusions and properties of steel*. Moscow: Metallurgiya.
13. Hrivnyak, I. (1984) *Weldability of steels*. Moscow: Mashinostroenie.

# PRODUCING WELDED JOINTS EQUIVALENT IN STRENGTH ON QUENCHING STEELS WITHOUT PREHEATING AND HEAT TREATMENT

**A.T. NAZARCHUK, V.V. SNISAR** and **E.L. DEMCHENKO**
E.O. Paton Electric Welding Institute, NASU, Kyiv, Ukraine

The paper deals with the possibility of producing equivalent joints on high-strength quenching steels by arc welding without preheating and heat treatment. Good prospects for application of austenitic-martensitic consumables in welding of high-strength steels without preheating and heat treatment with the level of weld metal strength of 1150–1200 MPa.

***Keywords:*** *welding, quenching steels, high-strength steels, multilayer welds, high-strength welds, welded joints, delayed fracture, process strength, cold cracks*

It is known [1–5] that the high level of mechanical properties of high-strength steels, as well as their quenching susceptibility lead to a number of specific difficulties arising in welding. These difficulties and methods to overcome them have been studied for many years. However, they remain to be urgent problems even now. This primarily is prevention of initiation of cold cracks in the HAZ and weld metal, as well as solidification cracks in weld metal and hot cracks in the HAZ, and the need to produce the metal of the weld, HAZ and joint as a whole with mechanical properties, equivalent or close to those of base metal [1–3].

Particular difficulties arise in those cases, when heat treatment of welded joints in high-strength steels is impossible (for instance, welded joints in hulls, vessels, large constructions), as well as when just annealing is to be used instead of the required quenching with subsequent annealing [2, 3].

Of all the above difficulties, arising in welding of high-strength steels, the most serious and specific are those, related to the problem of provision of the required technological strength of welded joints, in particular their cold cracking resistance [1–5], and producing joints, equivalent in strength to base metal.

Over many years considerable scope of data has been accumulated on integrated evaluation of technological strength of joints in quenching steels with application of qualitative (technological sample) and quantitative (instrumental) testing methods [1–6]. At some time special attention was given to the quenching hypothesis of cold crack formation. The adverse influence of hydrogen (hydrogen hypothesis) on resistance of welded joints to cracking was taken into account.

Various aspects of the influence of quenching phenomena [7–10, 11], as well as hydrogen content [12–14] on cold cracking resistance of welded joints in quenching steels are considered.

Proceeding from the current concepts, the main technological methods to prevent cold cracking in welded joints of high-strength quenching steels [1–3] are as follows: rational selection of steels for welded structures; regulation of the thermal cycle of welding and its control; different kinds of preheating in welding; regulation of time stresses in welding; application of austenitic welding consumables; reduction of hydrogen content in the base metal and weld metal. Prior cladding of the edges, peening of welded joints etc. are used much more seldom. The considered methods of prevention of cold cracks are mostly used simultaneously.

Application of the main technological methods of prevention of cold cracks in joints of quenching steels is possible in two areas: welding with consumables, matching the base metal, and with high-alloyed austenitic consumables. This work is devoted to analysis of these directions and possibility to produce welded joints equivalent in strength.

It is known [2, 3, 15] that performance of multilayer welds, where the metal is similar to base metal, runs into great difficulties in prevention of transverse cold cracks, both in the HAZ and base metal.

On the whole, the technological features of making multilayer welds with the metal, similar to the base metal, in joining high-strength steels, depend on the required level of mechanical properties of these joints and their technological strength.

An integrated approach to evaluation of cracking susceptibility of such joints was used, based on analysis of welded joints with multilayer welds [16, 17]. Quenching phenomena and extremely high importance of hydrogen influence on the technological strength of the joints was taken into account.

This approach is based on the following statements. Testing results should provide an objective idea of the joint resistance to both longitudinal and transverse cold cracks. During testing performance it is necessary to take into account the influence of the change of stresses in welding, arising from a change of metal volume due to thermal impact and phase transformations.

The possibility is established of using the procedure [16, 17] of composite samples not only for evaluation of weld metal, but also of the welded joint as

**Table 1.** Mechanical properties of some alloyed quenching steels at room temperature*

| *Steel grade* | $\sigma_t$, *MPa* | $\sigma_y$, *MPa* | $\delta$, % | $\psi$, % | *KCU*, $J/cm^2$ |
|---|---|---|---|---|---|
| 14KhN4MDA | 960–1020 | 850–880 | 15–16 | 52–60 | 165–185 |
| 15Kh2N4MDA | 950–980 | 800–820 | 25–30 | 55–60 | 210–220 |
| 30Kh2N2M | 1100–1120 | 950–1010 | 10–12 | 40–45 | 100–125 |

*Material in as-welded and as-quenched condition.

a whole. This procedure allows evaluation of the mutual influence of weld metal on HAZ metal, and vice versa. Obtained results are in good agreement with the results of large-sized technological samples [17].

For similar welded joints it is important to control the quenching phenomena in the welding zone by selection and purpose-oriented implementation of an optimal thermal cycle of welding in the HAZ. Issues of self-heating and self-heat treatment of the metal in the welding zone in performance of multilayer welds, including optimization of grove filling in narrow-gap welding [18] also become important.

An effective method of improvement of the technological strength and mechanical characteristics of welded joints is control of weld metal solidification and thermodeformational welding cycle, due to periodical heat input, portion formation of weld metal and its solidification [19, 20]. Main regularities of solving these problems are as follows: refinement of primary crystallites in weld metal solidification; change of orientation of the front of weld metal crystallites meeting and their disorientation; elimination of «weakness» in the weld middle; change of the nature of growth of weld metal crystallites; intermittent nature of their growth from layer to layer; refinement of secondary structure both in weld metal and in the HAZ of welded joints; additional control of the thermal cycle of welding. Work [20] shows the ability to control the rate of metal cooling in the welding zone in the lower subcritical temperature range due to an optimal combination of the duration of arcing and duration of the pause between the adjacent periods of arcing. These parameters, as well as the welding current and weld formation rate [20] have a decisive influence on the resistance of welded joints both to cold and hot cracks in portioned formation of the welds.

In view of the above concepts, producing joints of high-strength steels of 14KhN4MDA, 15Kh2N4MDA, 30Kh2N2M type (Table 1) by fusion arc welding without preheating and heat treatment, making the welds to have metal close in its composition to the base metal, is limited by the following conditions: metal thickness of not more than 80–100 mm; thermal cycle of welding should ensure in the HAZ metal decomposition of overcooled austenite with formation of structures, which are characterized by sufficient cold cracking resistance; if development of structures, promoting formation of cold cracks cannot be prevented, it is necessary to envisage self-heat treatment of the welded joint directly from the heat of welding; for additional control of the thermal cycle of welding it is rational to perform self-preheating, portion formation of welds or use their combined action; diffusible hydrogen concentration in the molten metal should not exceed 1.0–1.5 $cm^2$ per 100 g of metal.

Methods of self-preheating and self-heat treatment are based on optimizing the impact of heat, consumed in deposition of the previous and subsequent layers of a multilayer weld. In the case of mechanized welding large-sized products, it appears that it is possible to use only two such processes, namely welding with reciprocal motion of the arc and two-arc welding into separate pools with a strictly specified arc spacing.

In the case of welding bodies of revolution (performance of circumferential welds) of 400 to 500 mm diameter, self-preheating and self-heat treatment do not create any difficulties, as the process proper features a periodic impact of heat, evolved in deposition of subsequent layers. With decrease of the items diameter, it is sometimes necessary to take measures to limit the self-heating temperature.

Welding with reciprocal motion of the arc yields good results. Unfortunately, however, the issues, relating to the technology of conducting the process and its automation, are yet unsolved. Eventually, in arc welding of high-strength steels with welds with the metal, matching the base metal, without preheating and heat treatment the set of measures and methods to prevent cracking is greatly limited.

Right now in arc welding of large-sized structures of high-strength steels, resulting in performance of welds with the metal, similar to the base metal in its composition, the following technological solutions can be recommended:

- narrow-gap consumable-electrode arc welding with optimization of the thermal cycle of welding by a rational selection of the gap width and use of transverse oscillations of the electrode;
- consumable-electrode arc welding with portion formation of welds to control metal solidification and thermal cycle of welding [19, 20];
- twin-arc welding with the specified arc spacing to provide self-heating and self-heat treatment of welded joints [21];
- combination of portion formation of welds with self-heating in one- and two-arc welding [20];
- optimization of the process of arc welding by a rational filling of the groove (process is characterized by a periodical deposition of multiple layers directly in the groove in down- or uphill welding [18], which

**Table 2.** Mechanical properties of weld metal, produced in welding 15Kh2N4MDA steel

| *Welding consumable* | *Welding process* | $\sigma_{0.2}$, *MPa* | $\sigma_t$, *MPa* | $\delta$, % | $\psi$, % | $KCU_{20}$, *J/cm²* | $KCV_{-60}$, *J/cm²* |
|---|---|---|---|---|---|---|---|
| ANVP-60 | Manual | 600–700 | 1000–1100 | 15–18 | 40–50 | 105–110 | 60–80 |
| ANVP-80 | Same | 780–850 | 1050–1150 | 15–18 | 40–50 | 100–110 | 60–80 |
| ANVP-100 | » | 950–1050 | 1150–1200 | 12–16 | 25–35 | 70–90 | 50–70 |
| PPANVP-80 | Mechanized $CO_2$ welding | 750–900 | 1000–1200 | 14–16 | 30–40 | 60–70 | 45–50 |
| EK-17VI | SAW | 840–910 | 1150–1190 | 18–22 | 45–50 | 65–75 | 50–55 |
| PPANVP-80 | Same | 750–800 | 900–1000 | 18–25 | 35–40 | 65–75 | 50–55 |

can be effectively implemented in narrow-gap welding);

• twin-arc welding with an optimal distance between the arcs, using high-strength wires of different compositions.

The above solutions separately or with their combined action, as a rule, allow ensuring the required technological strength of joints in high-strength steel in their welding without preheating and producing weld metal, close in its composition to the base metal. However, making such welds and joints, as a whole, in welding of high-strength steels without a complete postweld heat treatment may create difficulties in terms of provision of equivalent strength. In welding of steels, for instance, 14KhN4MDA and 30Kh2N2M the weld metal strength was equal to 750–850 MPa at base metal strength of up to 900–1050 MPa.

In terms of improvement of the strength of weld metal, close to the base metal in its composition, welding with two-arcs, using high-strength wires of various compositions, is of interest. Particularly favourable is the process, in which the first arc runs in a shielding gas, and the second under a layer of flux. Such a decision allows using wires for the second arc of a composition, similar to that of the base metal. This opens up the possibilities for making multilayer composite welds, where the metal in each layer has different properties.

Results of studying the influence of the proportion of layers with different properties on the mechanical characteristics of a two-layer metal, are given in [22]. Strength characteristics of two-layer samples, for instance, with 30 % of the hard (high-strength) and 70 % of the soft (less strong) component, are on the level of strength of base metal (30Kh2N2M steel). In this case, ductility and impact toughness are higher than similar characteristics of a stronger structural component [22]. Integrated assessment shows that such a composite metal of a weld, consisting of layers with different properties, has higher mechanical characteristics than its individual components.

The second area of producing welded joints on high-strength steels with a high resistance to cracking, is arc welding of high-strength steels without preheating and postweld heat treatment with application of welding consumables, providing an austenitic weld metal. However, in view of the low level of strength of the austenitic weld metal, the welds should be made to have a large reinforcement, in order to provide an equivalent strength of welded joints. This signifi-

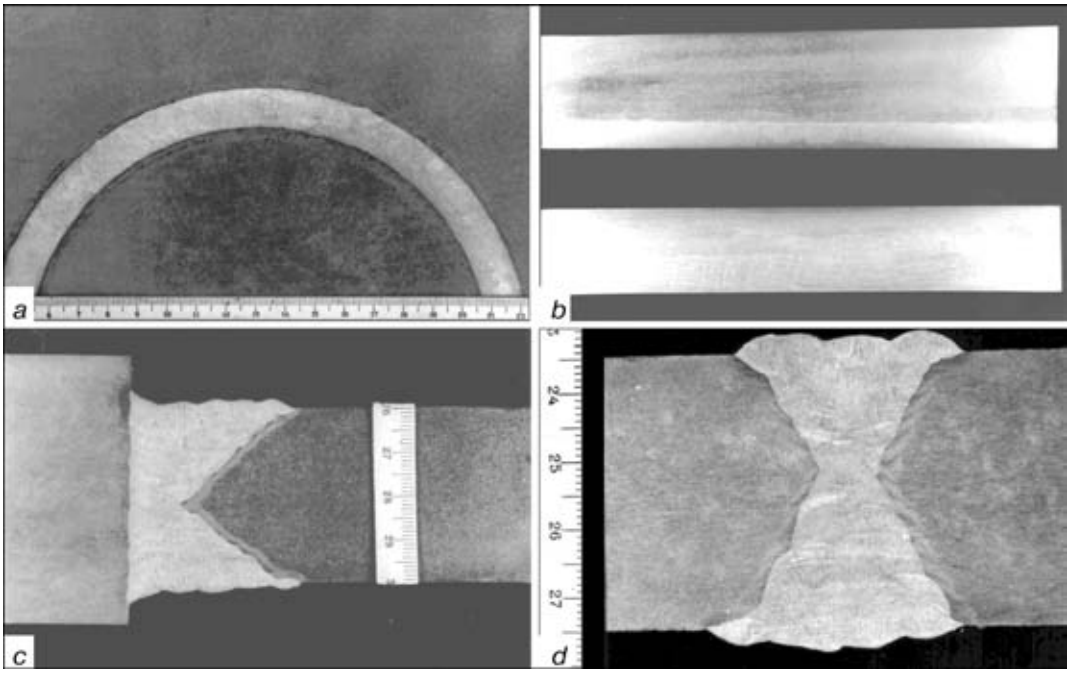


**Figure 1.** Characteristic view of longitudinal (*a*, *b*) and transverse (*c*, *d*) macrosections, cut out of rigid technological samples of welded joints in steel 15Kh2N4MDA. Welding was performed without preheating and heat treatment with ANVP-80 electrodes

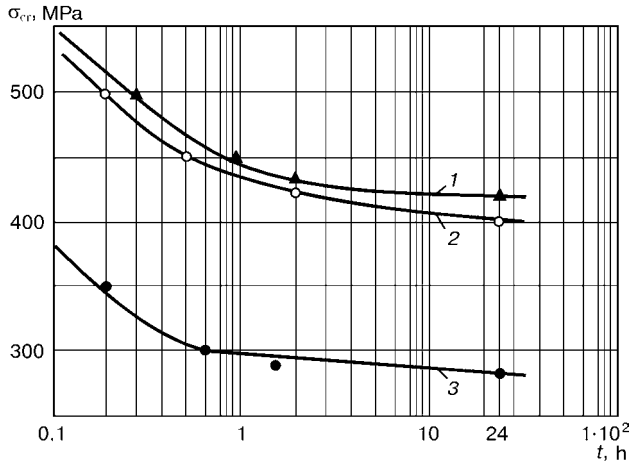


**Figure 2.** Delayed cracking resistance of welded joints in 30Kh2N2M steel, made without preheating and heat treatment with electrodes LO-1 (*1*), UONI 13/45 (*2*) and ANVP-80 (*3*) ($\sigma_{cr}$ — critical stress at delayed fracture)

cantly increases the scope of welding operations and consumption of expensive welding consumables. More over, excess reinforcement of the weld induces a stress concentration, which in a number of cases impairs the welded joint performance.

PWI proposed a new process for welding high-strength quenching steels [23], which consists in application of welding consumables, providing formation in the weld metal of a structure with austenite decomposition at temperature below 200 °C and of decomposition products, promoting production of weld metal with high strength characteristics at a good level of ductility and toughness. This welding process is based on a positive influence of austenitic weld metal on the kinetics of phase transformations in the HAZ of high-strength steel and change of the nature of distribution of stresses in a welded joint. Its application allows conducting welding of high-strength quenching steels without preheating and postweld heat treatment of items (as in the case of making an austenitic weld), while producing welded joints, equivalent to the base metal in strength. One of the variants of practical implementation of the proposed process is application of high-strength welding consumables, providing weld metal with the composition and structure of low-carbon martensite or austentic-martensitic steel.

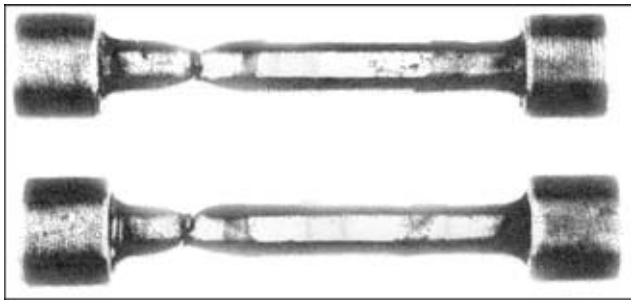

**Figure 3.** Appearance of samples of a welded joint in 15Kh2N4MDA steel, made with ANVP-80 electrodes, after testing by static tension at the temperature of 20 °C

PWI developed technologies and consumables for manual and mechanized welding [24–27]. Technology of manual electron beam welding envisages use of advanced, developed in PWI electrodes of grades ANVP-60, ANVP-80 and ANVP-100, which provide weld metal with the yield point of 600, 800 and 1000 MPa, respectively. Flux-cored wire PPANVP-80 was developed for mechanized welding in $CO_2$ or a mixture of Ar + $CO_2$. In SAW it is recommended to use ceramic flux, solid wire EK-17VI and flux-cored wire PPANVP-80. In welding of high-strength steel, for instance 15Kh2N4MDA, these consumables ensure producing an austenitic-martensitic weld metal with the hardness on the level of *HV* 3000 MPa. Mechanical properties of weld metal, produced in welding of the above steel, are shown in Table 2. Manufacture of new welding consumables has been mastered by PWI Pilot Production (wire according to TU PWI 77–90 specification; electrodes according to TU PWI 721–89 specification).

It should be noted that steels and welds with the above level of mechanical properties may be susceptible to delayed fracture and cold cracking, particularly at increased concentration of hydrogen. The higher the level of strength properties of the metal, the more pronounced is the adverse influence of hydrogen.

In this connection in development of the above welding consumables, particular attention was given to provision of minimum concentration of hydrogen

**Table 3.** Generalized technological recommendations on welding some high-strength alloyed steels without preheating

| *Steel grade* | *Metal gauge* | *Welding consumables* | *Welding process, main technological recommendations* |
|---|---|---|---|
| 14KhN4MDA | 40 mm thick sheet | Similar to base metal | Gas-shielded consumable electrode two-arc welding; arc spacing of 250–275 mm; heat input of each arc of 24.5–25.5 kJ/cm |
| 15Kh2N4MDA | Same | High-alloyed austenitic-martensitic | Manual electric-arc welding; mechanized welding in $CO_2$ or mixtures; welding using ceramic flux; modes, similar to those used in welding with austenitic consumables |
| 30Kh2N2M | 80 mm thick sheet | Similar to base metal | Two-arc welding; single-arc welding with reciprocal displacements of the electrode with the sequence of 3 layers per pass [18]; arc spacing or length of self-preheating section of 265–285 mm; heat input of 26.0–28.5 kJ/cm |
| 35KhN3M + St.3 | Forging + sheet | Same | Two-arc welding; arc spacing of 275–325 mm; heat input of about 40 kJ/cm |

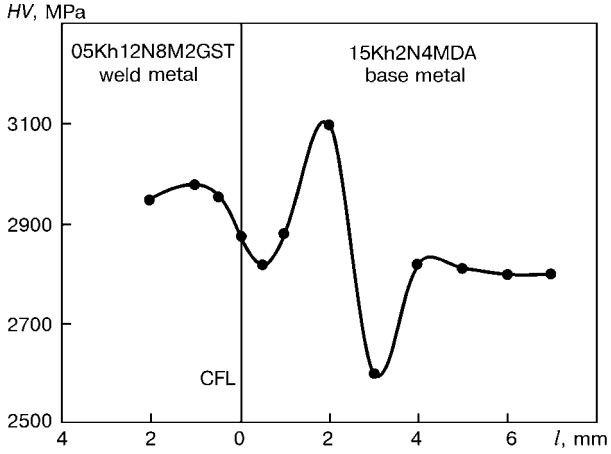


**Figure 4.** Hardness distribution in the fusion zone of an austenitic-martensitic weld on 15Kh2N4MDA steel in welding without preheating and heat treatment with ANVP-80 electrodes (CFL — conditional fusion line, $l$ — distance from CFL)

in weld metal. An optimum combination of components, included into the composition of the ceramic flux, electrode coatings and core of the flux-cored wire, their optimum proportion in combination with a number of technological measures [28] allowed solving the above problem. In welding at DCRP new consumables provide a low concentration of hydrogen in the weld metal: diffusible (determined by chromatography) — on the level of 1.3–2.0 $cm^3/100$ g, residual (determined by the method of reduction melting in a jet of gas carrier) — 0.3–1.0 $cm^3/100$ g, total — not more than 3.0 $cm^3/100$ g. Such a concentration of hydrogen does not have an essential influence on the welded joint resistance to cold cracking.

Evaluation of the resistance of welded joints, made by new technologies to cracking was conducted on sheets of steel 15Kh2N4MDA (see Table 1) of 40 mm thickness, using the known Central R&D Institute for Shipbuilding Technology (TsNIITS) technological samples and «round welded-in patch» [4], as well as delayed cracking tests by the Implant method [29]. Conducted evaluation showed that new consumables allow producing in welding of high-strength steels without preheating and heat treatment the sound welded joints with sufficient cold cracking and delayed fracture resistance, close to the variant of the austenitic weld. In confirmation of this statement, Figure 1 gives a characteristic appearance of longitudinal and transverse macrosections from TsNIITS technological samples and a «round welded-in patch», and Figure 2 shows the curves of delayed fracture (by the Implant method) of welded joints, made with austenitic LO-1, pearlitic UONI-13/45 and austenitic-martensitic ANVP-80 electrodes.

Mechanical properties of welded joints of high-strength 15Kh2N4MDA steel, produced without preheating and subsequent heat treatment, using ANVP-80 electrodes, are characterized by the following indices: cylindrical samples are cut out of the joint across the weld, and at testing for static tension at the temperature of 20 °C fail in the base metal outside

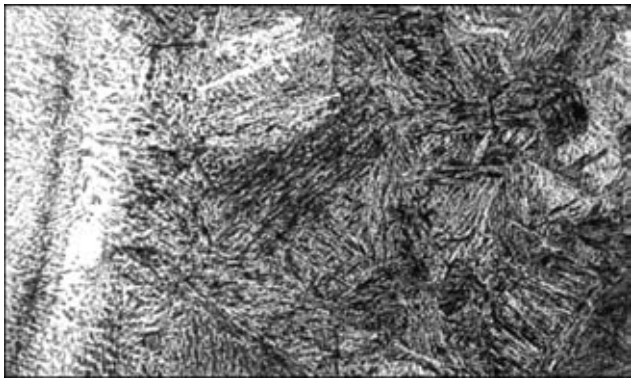

**Figure 5.** Microstructure of HAZ metal of a welded joint on 15Kh2N4MDA steel, made without preheating and heat treatment with ANVP-80 electrode (×500)

the HAZ (Figure 3) with the yield point of 840–930 MPa, impact toughness in testing of Mesnager samples with a semicircular notch along the fusion line is equal to 130–200 $J/cm^2$, that of samples with a notch in the HAZ metal at 1 mm distance from the fusion line is 150–160 $J/cm^2$. Hardness of HAZ metal does not exceed $HV$ 3250 MPa (Figure 4), and its structure is characterized as upper bainite (Figure 5).

Generalized technological recommendations on welding some alloyed steels without preheating are given in Table 3.

Welding of high-strength steels by composite welds, made with austenitic and austenitic-martensitic consumables, appears to be a highly promising approach. As is shown in [22], mechanical properties of composite two-layer samples can largely be controlled by varying the proportion of hard and soft layers. Varying the number of layers in a multilayer weld, made with austentic and austentic-martensitic consumables, it is possible to produce welds with the most optimum proportion of strength and ductility, determined proceeding from the mechanical properties of a specific steel being welded.

## CONCLUSIONS

1. Fulfillment of the above recommendations on welding of high-strength quenching steels without preheating and heat treatment, when making welds matching the base metal, ensures the required resistance of the joints to cold cracking with weld metal strength of up to 850 MPa.

2. Developed austenitic-martensitic consumables allow achieving the level of weld metal strength of up to 1200 MPa in quenching steel welding without preheating and heat treatment, while providing the required technological strength.

3. For further improvement of strength of weld metal in welded joints on high-strength steels, produced without preheating and heat treatment, we may recommend making composite welds, consisting of individual layers of different strength.

1. (1962) *Technology of electric fusion welding*. Ed. by B.E. Paton. Moscow-Kyiv: Mashgiz.
2. (1974) *Technology of electric fusion welding of metals and alloys*. Ed. by B.E. Paton. Moscow: Mashinostroenie.

3. Makara, A.M. (1963) *Investigation of the problems of technology and metals science in welding alloyed structural steels*. Kyiv: PWI.
4. Makarov, E.L. (1981) *Cold cracks in welding*. Moscow: Mashinostroenie.
5. Shorshorov, M.Kh. (1965) *Metals science of steel and titanium welding*. Moscow: Nauka.
6. Kasatkin, S.B., Mikhoduj, L.I., Gordonny, V.G. (1996) Procedural approaches to integrated investigation of delayed and brittle fracture in high-strength low-alloy steels. *Avtomatich. Svarka*, **2**, 58–60.
7. Kasatkin, B.S., Brednev, V.I. (1985) Peculiarities of cold cracking mechanism in welded joints of high-strength steels. *Ibid*., **8**, 1–6, 18.
8. Kasatkin, B.S., Brednev, V.I., Tsaryuk, A.K. et al. (1993) Estimation of resistance of 15Kh2MFA steel welded joints to cold cracking. *Ibid*., **5**, 3–7.
9. Tsaryuk, A.K., Brednev, V.I. (1996) Problems of cold cracking prevention. *Ibid*., **1**, 36–40.
10. Tsaryuk, A.K., Brednev, V.I. (1998) On the nature of cold cracking in welding of quenching steels. *Ibid*., **10**, 9–13.
11. Mikhoduj, L.I., Poznyakov, V.D., Yushchenko, A.K. (2000) Resistance of 12KhGN2MFDRA steel welded joints to a delayed fracture. *The Paton Welding J*., **11**, 4–10.
12. Musiyachenko, V.F., Kasatkin, S.B. (1985) Distribution of hydrogen in alloyed steel welded joint and its influence on cold cracking (Review). *Avtomatich. Svarka*, **9**, 3–8.
13. Pokhodnya, I.K., Shvachko, V.I. (1997) Physical nature of hydrogen induced cold cracks in welded joints of structural steels. *Ibid*., **5**, 3–12.
14. Pokhodnya, I.K., Stepanyuk, S.N., Shvachko, V.I. (2000) Role of temperature in hydrogen-induced cracking of structural steels and welded joints. *The Paton Welding J*., **2**, 2–7.
15. Makara, A.M., Gordonny, V.G., Dibets, A.T. et al. (1971) Cold cracks in low-alloy high-strength welds. *Avtomatich. Svarka*, **11**, 1–4.
16. Nazarchuk, A.T., Sterenbogen, Yu.A., Kosyakov, V.P. (1984) Procedure of evaluation of weld metal susceptibility to formation of transverse cracks. *Ibid*., **12**, 7–10.
17. Nazarchuk, A.T., Sverdel, I.P. (1994) Resistance of quenching steel joints with multilayer welds to crack formation. *Ibid*., **1**, 15–19.
18. Nazarchuk, A.T., Sterenbogen, Yu.A. (1984) About optimisation of arc welding process by efficient groove filling. *Ibid*., **11**, 46–49.
19. Nazarchuk, A.T. (1994) Control of weld metal solidification and thermodeformational cycle in automatic arc welding. *Ibid*., **5/6**, 3–9.
20. Nazarchuk, A.T. (1997) Influence of portion-discrete weld formation on the thermal cycle of fusion arc welding. *Ibid*., **5**, 13–17.
21. Nazarchuk, A.T., Sverdel, I.P., Nikulin, V.A. (1995) Twin-arc welding without phereating of banding of 34KhN1M and 34KhN3M steels to discs of large-sized toothed wheels of St.3 steel. *Ibid*., **1**, 30–34.
22. Nazarchuk, A.T. (1992) Examination of the influence of the proportion of layers with different properties on mechanical characteristics of two-layer steel samples. *Ibid*., **7**, 27–29, 32.
23. Gotalsky, Yu.N., Snisar, V.V., Kuporev, A.L. et al. *Method of arc welding of quenching steels*. USSR author's cert. 880671. Int. Cl. B 23 K 28/00. Publ. 15.11.81.
24. Lipodaev, V.N., Gotalsky, Yu.N., Snisar, V.V. et al. *Electrode for welding of low- and medium-alloy high-strength quenching steels without preheating and heat treatment*. USSR author's cert. 1689007. Int. Cl. B 23 K 35/36. Publ. 08.07.91.
25. Demchenko, E.L., Lyakhovaya, I.V., Snisar, V.V. et al. *Electrode for welding of high-strength steels*. USSR author's cert. 1785860. Int. Cl. B 23 K 35/365. Publ. 08.09.92.
26. Gotalsky, Yu.N., Snisar, V.V., Demchenko, E.L. et al. (1990) Welding of high-strength steels with the yield point above 800 MPa without preheating and heat treatment. *Avtomatich. Svarka*, **10**, 38–40.
27. Snisar, V.V., Demchenko, E.L., Ivanchenko, E.V. (2000) Challenging technologies for high-strength steel welding without preheating and heat treatment. *The Paton Welding J*., **11**, 37–40.
28. Demchenko, E.L., Snisar, V.V., Lipodaev, V.N. et al. (1991) Means of lowering the hydrogen content in weld metal of 03Kh12N8M2GST type during arc welding. *Avtomatich. Svarka*, **10**, 23–27.
29. Snisar, V.V., Demchenko, E.L., Gajvoronsky, A.A. (1993) Influence of weld structure on HAZ properties in 30Kh2N2M steel welded joints. *Ibid*., **9**, 43–45.


# MANUFACTURE OF SIDE WALLS OF CAR BODIES WITH STAINLESS STEEL PANELS

**G.G. BASOV** and **A.N. TKACHENKO**
Holding Company «Luganskteplovoz», Lugansk, Ukraine

A modular design of side walls of diesel and electric train cars is proposed, as well as specialized fixtures for manufacture of parts and welded components, improving the efficiency and labour conditions. Technological features of welding the module are described.

***Keywords:*** *welding, welded components, unit, semi-automatic facility, parts, base and auxiliary materials, welding modes, deformations, stresses*

Blanking-welding production, in particular, in fabrication of cars of diesel and electric trains, continuously faces the task of producing higher quality parts and welded components with minimum labour consumption, as well as improving the productivity and labour conditions.

Semi-beaded sheets of Cr–Mn steel of 10Kh13G18DU grade of 953 × 10000 × 1.5 mm size, supplied by Company «Zaporozhstal» are used in fabrication of the head, trailer and motor cars of diesel and electric trains EPL-2T and EPL-9T for manufacturing the lower row of panels of side wall modules of car bodies (Figure 1). This corrosion-resistant steel is austenitic sparsely-alloyed. Its composition is as follows, wt.%: 0.08–0.12 C; 0.7 Si; 17.0–18.5 Mn; 13.0–14.0 Cr; 0.3–0.6 Cu; ≤ 2.0 Ni; ≤ 0.3 S; ≤ 0.0035 P.

By now the steel has passed a series of tests, which allowed recommending its application for cars of diesel and electric passenger trains. Use of this steel improves their fatigue life, decreases the weight due to smaller thickness of parts, which lowers the load on the axles, while increasing the overall dimensions

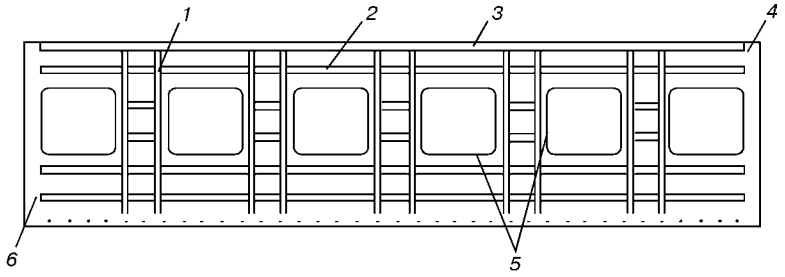


**Figure 1.** Schematic of a side wall module: *1* — post; *2* — beam; *3* — upper beam; *4* — upper row of panels; *5* — window row of panels; *6* — lower row of panels

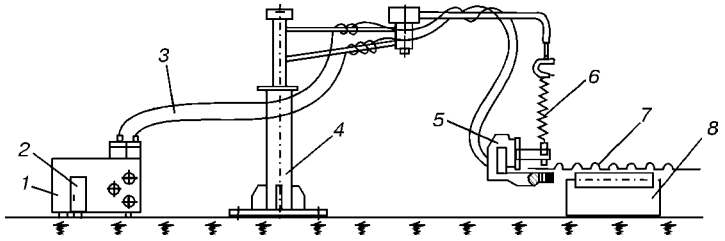


**Figure 2.** Schematic of a specialized unit for hole piercing: *1* — hydraulic plant; *2* — electric cabinet; *3* — high pressure hose; *4* — rotary cantilever; *5* — press-head; *6* — spring suspension; *7* — panel sheet; *8* — roller conveyor

of cars and number of passengers carried, respectively. The steel is characterized by quite high energy properties ($\sigma_t \approx 680$ MPa; $\sigma_{0.2} \approx 350$ MPa) at satisfactory ductility ($\delta > 45$ %).

In order to weld the panels by plug lap joints to the elements of the frame of side wall modules, as well as directly to the binding elements of the main frame of the car body, it was necessary to drill 1396 holes of 8 mm diameter in the sheets for one car. Drilling of such a number of holes increases the labour consumption of sheet fabrication and leads to a longer cycle of fabrication and assembly of the item as a whole.

In order to lower the labour consumption and increase the accuracy of fabrication of this kind of parts, the Works developed the design and technological documentation, as well as manufactured and put into production a specialized unit for piercing holes of 8 mm diameter in the sheets of semi-beaded and window panels. Basic components of the specialized unit for hole piercing are shown in Figure 2.

Panel sheet *7* after forming of the beaded ends in special dies, is placed on roller conveyor *8*, using electric bridge crane. The liquid is fed by hydraulic plant *2* along high-pressure hoses *3* into press-head *5*. Hole piercing force is calculated by the following formula:

$$P_{max} = LS\tau_{sh}k, \qquad (1)$$

where $L$ is the perimeter of part piercing contour, mm; $S$ is the material thickness, mm; $\tau_{sh}$ is the ultimate shear strength of the material, Pa; $k$ is the safety factor ($k$ = 1.1–1.3).

Assuming that $L$ = 25.12 mm, $S$ = 1.5 mm, $k$ = = 1.25 and $\tau_{sh}$ = 550 Pa, we obtain piercing force $P_{max} = 26.10^3$ N. Pressure, induced in the cylinder by the hydraulic plant, is found from the following formula:

$$p = \frac{P_{max}}{(\pi d^2/4)\eta}, \qquad (2)$$

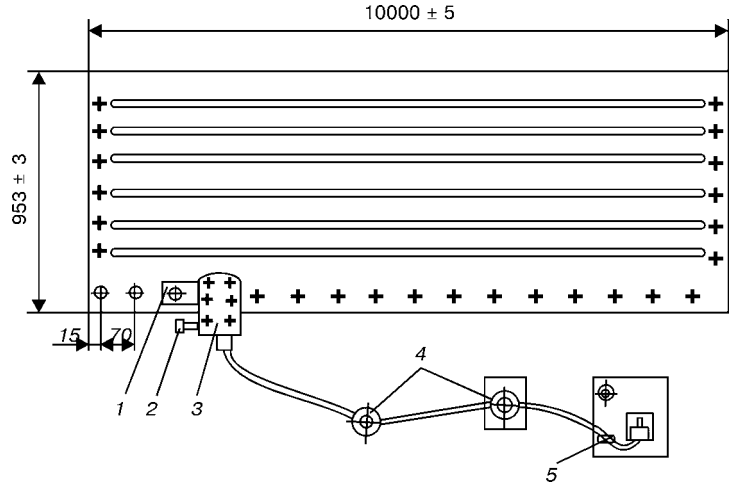


**Figure 3.** Schematic of location of the press-head in hole piercing: *1* — rest; *2* — handle; *3* — press-head; *4* — hinge-type console; *5* — hydraulic distribution system

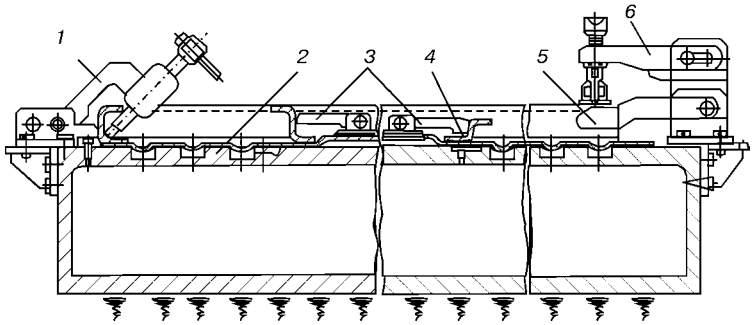


**Figure 4.** Schematic of a facility for assembly and welding of side wall modules (for designations see the text)

Modes of arc welding of sheet steel 10Kh13G18DU and 12Kh18N10T

| *Joint type* | *Wire diameter, mm* | $I_w$, *A* | $U_a$, *V* | $v_w$, *m/h* | *Wire extension, mm* | *Gas flow rate, l/min* |
|---|---|---|---|---|---|---|
| Square butt | 1.0–1.2 | 80–90 | 17–18 | 35–40 | 6–8 | 10–12 |
| Overlap | 1.0–1.2 | 80–90 | 17–18 | 35–40 | 6–8 | 10–12 |
| Tee | 1.0–1.2 | 70–90 | 19–20 | 35–40 | 6–8 | 10–12 |

where $D$ is the cylinder diameter, mm (approximately equal to 8 mm); $\eta$ is the efficiency of the motor, equal to 0.8.

When the hydraulic plant operates on the cylinder of the press-head (Figure 3), the die, fastened on the press-head, pierces the first hole in the panel sheets. Piercing of subsequent holes with a spacing of 70 mm is performed in a similar way after mounting the press-head into the earlier pierced hole.

Hinge type cantilever *4* allows the operator to perform piercing of all the holes on the sheet boards without any readjustment or rotation of the sheet, laid on the roller conveyor. After that the panel sheets and frame elements are fed to the work place for assembly and welding of side wall modules for cars of diesel and electric trains into an assembly-welding facility, specially developed for this purpose (Figure 4). The latter consists of cast iron plates *2* of 1250 × 3500 × 200 mm size, which along their entire length have dressed slots for laying the beaded panels, base rests *3* for fastening the sheets and frame elements, as well as special clamps *1, 5, 6*. The facility, in the area of welding the panel girths, is fitted with special copper elements *4*, which allow ensuring the heat sink in performance of welding operations and reducing welding stresses and strains, respectively.

As different steels are used in the structure of the side wall module (frame elements are made of carbon low-alloyed steels 09G2S (GOST 17066–80), the panel sheets are made of Cr–Mn (stainless) steels 10Kh13G18DU (DI-61U) (TUU 14-15-315–93) and 12Kh18N10T), in the technological process optimal welding modes were selected and applied, both for similar steels (welding of frame elements and panel sheets separately), and for dissimilar materials (welding of frame elements to panel sheets).

Welding of panel elements, as well as its welding to frame elements is performed with a semi-automatic welding machine A-547 in argon at DCRP, using welding wire of 1.0–1.2 mm diameter of Sv-08Kh20N9G7T grade. Modes of arc welding of 10Kh13G18DU and 12Kh18N10T steel (1.5 mm thick) are given in the Table.

In assembly and welding of side wall modules of diesel and electric train cars, it is not possible to completely avoid development of residual welding deformations. In a number of cases they go beyond the admissible limits, envisaged by design documentation, and in some places reach more than 2 mm per 1 m of the item.

The following technological measures were used to lower the level of welding deformations in the item: increasing the rigidity of the sheets of window row of the panels; replacement of steel 10Kh13G18DU by steel 12Kh18N10T in the extreme sheets of window panels of the module, which allowed a considerable lowering of internal stress accumulation in the parts after stamping. Elimination of buckling, formed during welding operations performance, was achieved by applying dummy weld beads on the surface of the panels with their subsequent cleaning and appropriate straightening of the sheets and the item as a whole.

Thus, the following has been developed for the first time and introduced in the enterprise:

- modular structure of side walls, designed for bodies of cars for various purposes with application of sheet panels of Cr–Mn steels and frame elements of carbon steel;
- technology and fixture for assembly of side wall modules of the above steels and their welding.

Gained experience of application of the combined joints in fabrication of cars may be recommended for wide introduction in car-making factories, which will allow lowering the loads on side walls, reducing by 5–6 times the labour-consumption in fabrication of sheet parts from them, improving their quality, and shortening the cycle of assembly of the side wall modules.

# FILLER WIRE FOR NARROW-GAP WELDING OF TITANIUM ALLOY VT23

**V.Yu. BELOUS, V.N. ZAMKOV, I.K. PETRICHENKO** and **V.F. TOPOLSKY**
E.O. Paton Electric Welding Institute, NASU, Kyiv, Ukraine

Experience of practical application of narrow-gap welding of titanium and titanium alloy structures has been analyzed, and advantages of this new technology are demonstrated. Good prospects for application of magnetic processes of welding arc control is noted.

***Keywords:*** *argon-arc welding, narrow-gap welding, titanium alloys, narrow-gap edge preparation, magnetically impelled arc, mechanical properties*

Effectiveness of application of $(\alpha+\beta)$-titanium alloys in welded structures depends primarily on how close are the indices of mechanical and service properties of welded joints and base metal. Since most of welding operations in fabrication of titanium structures are performed by tungsten electrode argon-arc welding, joining elements more than 3 mm thick is performed with edge preparation [1], which requires application of filler wire. The latter is used in argon-arc welding to resolve two problems [2]: technological (groove filling and producing a full-sized weld) and metallurgical (adjustment of chemical and phase composition of weld metal).

Properties of welded joint metal largely depend on correct selection of filler wire, which is particularly important in welding thick metal, when the weld consists predominantly of filler wire material.

This paper considers the influence of filler wire composition on the mechanical properties of welded joints in alloy VT23, produced by tungsten electrode narrow-gap welding in argon by a magnetically impelled arc [3].

According to the data of [4], it is recommended to use wire of grade SP15 [5] for welding plate alloy VT23. Later research, however, demonstrated [2] that optimal results in welding of this alloy are obtained with application of wire of grade VT203 (Table 1). Strength of welded joints made with this wire (after annealing at 750 °C for 30 min) and strength of the alloy proper are practically the same at a satisfactory impact toughness *KCU* of weld metal ($\sigma_t$ = 1100–1200 MPa, $a_n$ = 30–35 J/cm$^2$), and fatigue life of welded joints to fracture (at maximum cycle stress of 570 MPa) is equal to $(5–6)\cdot10^4$ cycles.

In [2] it is emphasized that these results were obtained in welding of plates 20 mm thick, weight fractions being 70 % of base metal and 30 % of filler wire metal in the weld metal. Unfortunately, neither the groove shape, nor the welding process are mentioned. On the other hand, it should noted that such a proportion of the amount of base and filler metal in the weld is a particular case, and may only be obtained with a quite definite groove shape, welding method and mode. Therefore, recommendations of [2] are not the common ones for alloy VT23 and should be determined more precisely.

The task was to compare the properties of welded joints made (at other conditions being equal), using filler wires VT203 and SP15, and select the wire, which will provide higher indices of welded joint properties. Samples of alloy VT23 8 and 20 mm thick were welded in order to evaluate the quality of welds with different weight fractions of filler and base metals in them.

Samples 8 mm thick were square butt welded in one pass by a tungsten electrode in argon with a through penetration [1]. Samples 20 mm thick were made by tungsten electrode narrow-gap magnetically-impelled arc welding in four passes (Table 2).

The Figure shows the macrostructure and schematics of welded joints. Amount of filler wire in weld metal, made with through penetration, can be calculated proceeding from the ratio of the area of reinforcement to the total weld area, which is equal to

**Table 1.** Composition of filler wires

| *Wire grade* | *Fraction of elements, wt.%* | | | | | $Mo_{eq}$ *wt.%* |
|---|---|---|---|---|---|---|
| | *Al* | *Mo* | *V* | *Nb* | *Zr* | |
| VT203 | 4.5–5.8 | 0.8–1.5 | 1.3–3.2 | 1.7–2.5 | 2.2–3.5 | 3.5 |
| SP15 | 3.5–5.5 | 2.0–3.5 | 2.0–3.5 | 2.5–4.5 | 1.0–2.0 | 5.0 |

*Notes.* 1. In both wires the base is titanium. 2. VT203 wire contains 1–2 % Sn.

**Table 2.** Modes of sample welding

| *Metal thickness, mm* | *Welding current, A* | *Arc voltage, V* | *Welding speed, m/h* | *Wire feed rate, m/h* |
|---|---|---|---|---|
| 8 | 390 | 12.5 | 15.0 | 15.0 |
| 20 | 420 | 11.0 | 8.0 | 85.0 |

*Notes.* 1. Filler wire diameter is 2.5 mm. 2. Magnetic induction in the welding zone in welding of samples 20 mm thick is equal to 9 mT.

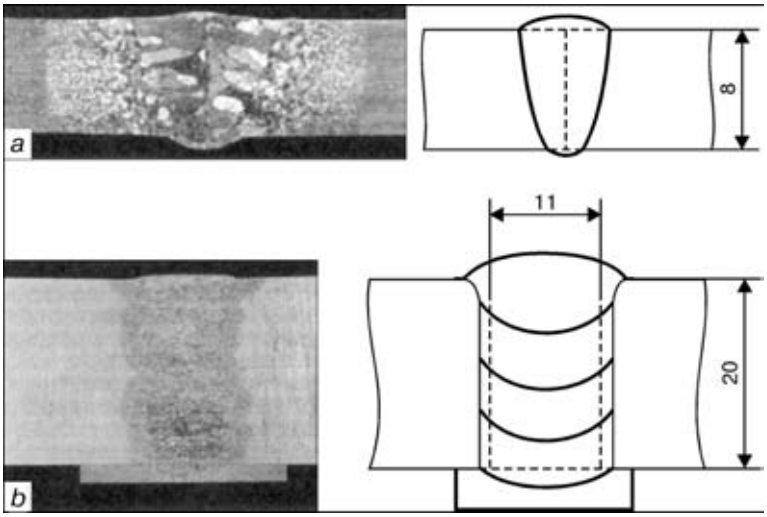


Microstructure of welded joint of alloy VT23 with metal thickness of 8 (*a*) and 20 (*b*) mm

**Table 3.** Composition of weld metal

| *Metal thickness, mm* | *Wire grade* | *Fraction of alloying elements, wt.%* | | | | | | | |
|---|---|---|---|---|---|---|---|---|---|
| | | *Al* | *Mo* | *V* | *Nb* | *Zr* | *Sn* | *Cr* | *Fe* |
| 8 | VT203 | 5.11 | 1.89 | 4.28 | 0.31 | 0.43 | 0.24 | 0.91 | 0.37 |
| | SP15 | 5.02 | 2.03 | 4.26 | 0.67 | 0.22 | – | 0.94 | 0.41 |
| 20 | VT203 | 5.07 | 1.20 | 2.67 | 1.88 | 2.55 | 1.41 | 0.09 | 0.06 |
| | SP15 | 4.43 | 2.15 | 2.56 | 4.07 | 1.36 | – | 0.12 | 0.10 |

*Note.* Titanium is the base.

**Table 4.** Mechanical properties of welded joints

| *Metal thickness, mm* | *Wire grade* | *Heat treatment* | $\sigma_t$, *MPa* | *KCV, J/cm²* | *Location of sample fracture in tension* |
|---|---|---|---|---|---|
| 8 | VT203 | Annealing | 1080–1130 / 1105 | 17–20 / 19 | In weld metal and HAZ |
| | | Annealing and ageing | 1135–1145 / 1138 | 14–18 / 15 | In weld metal |
| | SP15 | Annealing | 1090–1124 / 1109 | 21–24 / 22 | In weld metal and HAZ |
| | | Annealing and ageing | 1137–1142 / 1140 | 19–22 / 20 | Same |
| 20 | VT203 | Annealing | 952–987 / 974 | 21–25 / 22 | In weld metal |
| | | Annealing and ageing | 993–1029 / 1007 | 19–23 / 20 | Same |
| | SP15 | Annealing | 996–1030 / 1020 | 28–32 / 30 | » |
| | | Annealing and ageing | 1070–1100 / 1090 | 24–30 / 27 | In weld metal and HAZ |

*Note.* The numerator gives the scatter of values, and the denaminator — the average value.

≈ 15 %. In narrow-gap welding in the above modes, the gap walls (along their entire length) are melted to the depth of 0.45 mm, and the ratio of the filler and base metal in the weld is practically independent on thickness of the metal being welded. In our experiments the amount of filler metal in the weld should be not less than 90 %. Results of chemical analysis of weld metal confirmed these rough estimates (Table 3).

After welding one part of the joints were annealed at the temperature of 780 °C for 1 h, then cooled in air, and the other part after welding and annealing was subjected to strengthening by two-step ageing [6]. After that their mechanical properties were determined (Table 4).

According to the produced results, strength characteristics of welded joints on 8 mm metal do not depend on the grade of filler wire. Impact toughness of the metal of welds, made with filler wires SP15 and VT203, is also approximately the same. This is related to the fact that in square butt welding with through penetration the proportion of filler metal in the weld metal is small, and the composition of welds, made with different fillers wires, differs only slightly. Level of properties of welded joints in this case is determined by base metal composition and heat treatment mode. Thus, if welding of alloy VT23 is performed in one pass without edge preparation, than in order to produce a full-sized weld wires SP15 and VT203 can be recommended as the filler metal, and proceeding from the findings of [4] — also wire SP15.

As was noted above, in narrow-gap welded joints the weld consists of filler metal by 90 %. Therefore, the properties of welded joints are here determined by wire composition. In the condition after annealing and strengthening heat treatment the strength of welded joints and impact toughness of welds were significantly higher in the case, when welding was performed with filler wire SP15. Obtained results (Table 4) confirm the conclusions of [4] as regards the effectiveness of applying wire SP15 to make welds with edge preparation on alloy VT23.

Evaluation of fatigue life at repeated-static loading was conducted only for welded joints, produced on metal 20 mm thick. Round samples with the gauge diameter of 8.5 mm were used. Maximum cycle stress was 570 MPa. Testing showed that the welded joints, made with filler wire VT203 (irrespective of the heat treatment mode), stood $(44–53)\cdot10^3$ cycles to fracture, and those made with filler wire SP15 — $(26–35)\cdot10^4$ cycles. These results are indicative of the fact that welds, made with filler wire SP15, are characterized by a high level of mechanical properties and better performance at repeated-static loads.

Thus, narrow-gap tungsten electrode welding of alloy VT23 in argon by a magnetically-impelled arc should be conducted with filler wire of grade SP15. Its application provides the strength of welded joints on the level of not less than 90 % of the alloy proper, both after annealing and after strengthening heat treatment, as well as fatigue life to fracture of more than $2\cdot10^5$ cycles.


1. Gurevich, S.M., Zamkov, V.N., Blashchuk, V.E. et al. (1986) *Metallurgy and technology of welding of titanium and its alloys*. Kyiv: Naukova Dumka.
2. Lukin, V.I., Loskutov, V.M., Redchits, V.V. (2002) Filler materials for welding structural titanium alloys. *Svarochn. Proizvodstvo*, **5**, 37–41.
3. Paton, B.E., Zamkov, V.N., Prilutsky, V.P. (1996) Narrow-groove welding proves its worth on thick titanium. *Welding J.*, **5**, 37–41.
4. Topolsky, V.F., Kishkina, S.I., Stronina, L.A. et al. (1983) Strength of VT23 alloy welded joints in repeated-static loading. *Avtomatich. Svarka*, **7**, 42–44.
5. Zamkov, V.N., Topolsky, V.F., Tyapko, I.K. (1996) Wire for welding of $(\alpha + \beta)$-titanium alloys. *Ibid.*, **7**, 51–52.
6. Zamkov, V.N., Kushnirenko, N.A., Topolsky, V.F. et al. (1980) Methods to improve the strength of two-phase titanium alloy welded joints. *Ibid.*, **3**, 49–52.

# THERMAL-PRESSURE JOINING OF TUBES TO TUBE SHEETS OF HIGH-ALLOY STEELS BY THE ELECTRO-HYDROPULSE WELDING METHOD

**L.Yu. DEMIDENKO, N.A. ONATSKAYA** and **E.S. YURCHENKO**
Institute of Pulse Research and Engineering, NASU, Mykolaiv, Ukraine

The quality of joints between tubes and tube sheets made by the thermal-pressure electro-hydropulse process has been estimated from the results of strength tests and metallographic examinations. It is shown that in compact heat exchangers of high-alloy steels a metal bond is formed on an area of more than 50 % of the entire mating surfaces.

***Keywords:*** *thermal-pressure electro-hydropulse welding, tube, tube sheet, electro-hydropulse pressing, strength tests, metallography, metal bond, quality*

The trend in development and upgrading of heat-exchanging equipment is to building high-intensity heat exchangers, i.e. with densely packed tubes and thin inter-tube webs. Decrease in mass and dimensions of heat exchangers is achieved through decreasing thickness of a tube sheet and diameter of tubes. Operational reliability of such equipment can be provided owing to advanced high-strength and corrosion-resistant materials utilised to manufacture them.

High-alloy steels of the martensitic and austenitic grades find wide application in domestic power engineering, as they ensure high performance of power generation units [1]. However, properties of these materials, as high as they are, only partially solve the problem of their reliability.

As proved by experience, the joints between tubes and tube sheets are the first to fail in operation of heat exchangers under conditions of deep thermal cycling [2]. Resistance of the joints to fracture under these conditions can be increased by ensuring predominance of the metal bond, i.e. welding over the entire mating surface area [3].

Thermal-pressure electro-hydropulse (TPEHP) welding [4] is one of the promising methods for joining tubes to tube sheets, providing a joint with the metal bond over almost the entire mating surface area between the components joined. Main peculiarity of this method lies in a certain combination of electro-hydropulse (EHP) pressing [5] and heat treatment. The unique feature of the new method for welding tubes to tube sheets is that it enables realisation of the process similar to diffusion bonding, although with no application of external pressure and no shielding from the environment. The latter, according to the data of physical studies [6], is possible because of the formation of a press joint, as compressive stresses formed between a tube and a tube sheet prevent penetration of air in between them during heating, i.e. this leads to the formation of conditions eliminating oxidation of the mating surfaces, similar to those occurring in autovacuum welding [7]. Efficiency of the method was verified on a number of the tube-to-tube sheet joints in low-carbon, high-temperature and heat-resistant steels [4, 8].

The purpose of this study was to investigate the feasibility of producing a welded joint between a tube and a tube sheet over a major part of the mating surfaces in compact heat exchangers of high-alloy steels. Experiments were conducted on 19 tube mockups with full-scale tubes measuring (10×1) and (8×0.8) mm, thickness of the tube sheets being 35 and 25 mm, respectively (holes in the tube sheet were of a triangular shape and spaced at $13.0 \pm 0.1$ and $10.6 \pm 0.1$ mm). The tubes were made from steels 08Kh18N10T and 03Kh21N32M3B, and tube sheets were made from steels 12Kh18N10T and 08Kh16N11M3.

TPEHP welding of these mockups was performed under conditions which had been preliminarily optimised on corresponding one-tube samples [9]. In particular, EHP pressing was carried out by the method ensuring the maximum possible residual pressure in the joint [5]. Heat treatment of the mockups was conducted in a chamber-type electrical resistance furnace at a temperature of 950 °C.

Quality of the resulting joints was evaluated from the results of strength tests and data of metallographic examinations of templates. The quality criteria were specific shear load $\tau_{sh}$ the procedure of estimation of which is described in [9], and density indicator $Y$ characterising (%) a relative length of the interface in a cross section not more than 1 μm thick. The latter was measured at 100 points located at an approximately equal distance from each other on the circumference by using the X-ray microanalyser JCXA-133 at a ×1000 magnification and a micron ruler with the least division of 0.5 μm. All the 19 joints in a plane normal to the longitudinal axis of a mockup in its central (through thickness of the tube sheet) part after appropriate machining of the mockups were subjected to such examinations.

According to the results obtained, the density indicator for the joints with a tube (8×0.8) mm was $Y = (56.7 \pm 5.8)$ %, while the joints with a tube

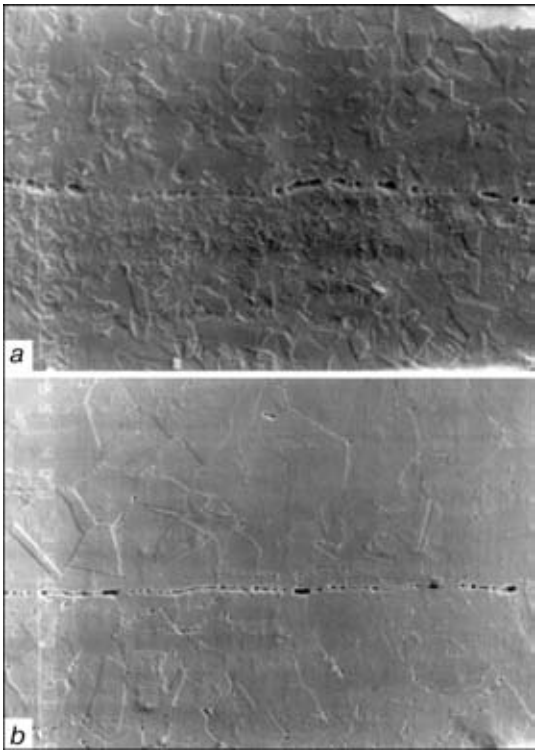


Microstructure of the tube-to-tube sheet joining zone: *a* — mockup with a tube (10×1) mm; *b* — mockup with a tube (8×0.8) mm (×400)

(10×1) μm were characterised by a denser interface, i.e. the length of the interface less than 1 μm wide was (72.3 ± 12.4) %. However, insignificant regions with a gap of 2–4 μm were also noted. The Figure shows characteristic microstructures of welded joints for the combinations of materials investigated. It can be seen that common grains with a chain of defects oriented along the initial contact line remaining in the bulk are formed in the welded joint zone. According to [10], these defects can be eliminated to a substantial degree owing to activation of the diffusion processes through increasing the temperature of heat treatment to an optimal value.

Results of mechanical tests are given in the Table. Analysis of these results showed that the metal bonds were formed at the tube-to-tube sheet interface in all the joints in both mockups, the average shear strength for the joints with a tube (10×1) mm being $\tau_{sh}$ = = (144.8 ± 37.2) MPa, and that for the joints with a tube (8×0.8) mm being $\tau_{sh}$ = (97.9 ± 19.5) MPa. Specific shear strength $\tau_{sh}$ is rather high ($\tau_{sh} \geq 100$ MPa) for the majority of the joints in their central part (templates 2 and 3). The end zone (template 1) is characterised by much lower values of shear stress and a higher inconsistency of the data. This probably is associated with a non-uniform expansion of the tube along the length of the tube sheet, i.e. the tube expansion is lower in the peripheral regions due to energy losses at the tube ends, which leads to decrease in residual pressure and, hence, to decrease in $\tau_{sh}$.

Based on analysis of all the results obtained, it could be noted that TPEHP welding provides the tube-to-tube sheet joints in multi-tube mockups characterised by predominance of the metal bond over the area of not less than half the mating surface one. Temperature and pressure, which are not high in this case, cause no changes in properties of the elements joined, which is particularly important for practical application. The presence of the metal bond between the tube and the tube sheet provides a high relaxation strength of the joints during the entire service period, decrease in heat resistance of the tube-to-tube sheet hole transition, which in turn leads to a drastic decrease in the level of thermal stresses in plane of the joint. This is indicative of a very high technological potential of this type of welding of tubes to tube sheets and, accordingly, of its promising character for the fabrication of high-intensity compact heat exchangers used in shipbuilding.

Another important advantage of this new welding method is that its commercial application requires no extra workshops, as this process can be applied with the available production lines intended for the fabrication of heat exchangers.

Therefore, TPEHP welding makes it possible to produce tube-to-tube sheet welded joints almost over the entire mating surface area in compact heat exchangers of high-alloy steels. This provides a many

Results of shear tests of welded joints in multi-tube mockups

| Joint No. | Shear stress $\tau_{sh}$, MPa | | | | | | |
|---|---|---|---|---|---|---|---|
| | Mockup with tube (10×1) mm | | | | Mockup with tube (8×0.8) mm | | |
| | Template 1 | Template 2 | Template 3 | Mean value | Template 1 | Template 2 | Mean value |
| 1 | 56 | 90 | 130 | 92 | 80 | 110 | 95 |
| 2 | 115 | 195 | 125 | 145 | 112 | 132 | 122 |
| 3 | 72 | 170 | 175 | 139 | 78 | 96 | 87 |
| 4 | 87 | 221 | 241 | 183 | 88 | 100 | 94 |
| 5 | 77 | 135 | 115 | 106 | 69 | 93 | 81 |
| 6 | 33 | 100 | 71 | 68 | 47 | 91 | 69 |
| 7 | 100 | 133 | 205 | 146 | 119 | 121 | 120 |
| 8 | 109 | 189 | 248 | 182 | 108 | 130 | 119 |
| 9 | 85 | 174 | 209 | 156 | 95 | 133 | 114 |
| 10 | 144 | 246 | 209 | 200 | 96 | 124 | 110 |
| 11 | 54 | 100 | 190 | 115 | 51 | 87 | 69 |
| 12 | 186 | 202 | 206 | 198 | 69 | 129 | 99 |
| 13 | 70 | 90 | 143 | 101 | 50 | 94 | 72 |
| 14 | 194 | 210 | 230 | 211 | 81 | 133 | 107 |
| 15 | 35 | 151 | 148 | 78 | 53 | 105 | 79 |
| 16 | 167 | 225 | 198 | 197 | 97 | 135 | 116 |
| 17 | 142 | 194 | 204 | 180 | 120 | 134 | 127 |
| 18 | 75 | 183 | 133 | 147 | 45 | 55 | 50 |
| 19 | 70 | 116 | 135 | 107 | 128 | 134 | 131 |

*Note.* Templates 1–3 were 5 mm thick, they were cut from the external end of the tube sheet at a distance of 5, 15 and 25 mm, respectively.

times increase in reliability and live of the tube-to-tube sheet joints and equipment as a whole.


1. Apolchina, N.M. (1986) *Metals in modern power generation units*. Moscow: Energiya.
2. Promyslov, L.A. (1974) *Failures and performance of ship heat-exchangers*. Leningrad: Sudostroenie.
3. Leskov, G.M., Samusev, N.F., Kotikov, Yu.I. et al. (1990) Influence of the type of the tube-to-tube sheet welded joints on their resistance to fracture in thermal cycling. *Avtomatich. Svarka*, **4**, 21–23.
4. Mazurovsky, B.Ya., Opara, V.S., Demidenko, L.Yu. (1994) Causes of fracture and means for improvement of reliability of nuclear power plant steam generator collectors. *Tyazh. Mashinostroenie*, **8**, 7–9.
5. Mazurovsky, B.Ya. (1980) *Electro-hydropulse pressing of tubes to tube sheets in heat-exchanging equipment*. Kyiv: Naukova Dumka.
6. Demidenko, L.Yu., Opara, V.S., Onatskaya, N.A. (2000) Peculiarities of interaction of mating surfaces in thermal-pressure electro-hydropulse welding. *Tyazh. Mashinostroenie*, **7**, 37–38.
7. Finkelshtejn, M.L. (1978) *Diffusion bonding in liquid media*. Moscow: Metallurgiya.
8. Opara, V.S., Demidenko, L.Yu. (1996) Thermal-pressure welding as a radical way of improving reliability of heat-exchanging equipment. *Tyazh. Mashinostroenie*, **10**, 23–26.
9. Demidenko, L.Yu., Yurchenko, E.S. (1992) Capabilities of thermal-pressure electro-hydropulse welding of tubes to tube sheets. *Ibid.*, **1**, 32–33.
10. Kazakov, N.F. (1976) *Diffusion bonding of materials*. Moscow: Mashinostroenie.


# INFLUENCE OF HYDROSTATIC PRESSURE IN UNDERWATER WET WELDING ON THE PROPERTIES OF WELDED JOINTS

**V.S. BUT** and **S.Yu. MAKSIMOV**
E.O. Paton Electric Welding Institute, NASU, Kyiv, Ukraine

Influence of immersion depth and test temperature on impact toughness of welded joints of 17G1S steel is considered.

***Keywords:*** *wet arc welding, metal, impact toughness, strength, brittleness, HAZ, hydrostatic pressure, flux-cored wire*

Wet underwater welding is performed directly in the water. In this case, the electrode, arc and item are not protected from the impact of the environment, which influences both the nature of running of the metallurgical processes and formation of the structure of welded joint metal.

One of the most important problems of wet arc welding is the hardening effect of the water, leading to embrittlement of weld metal and HAZ and, hence, to a considerable lowering of metal ductility in the above zones. Cooling rate in underwater welding is on average 3 times higher than that in air [1]. In addition, hydrostatic pressure and welding heat input are the significant factors, having the strongest influence on the rate of welded joint cooling [2].

Data of [3] is indicative of difficulties encountered, when attempting to alloy the welds with the purpose of a significant increase of the indices of their strength properties during welding directly in the water, which is due to a considerable loss of the alloying elements, increasing with the increase of immersion depth.

At PWI it was possible to optimize the composition of the slag- and gas-forming components of the flux-cored wire, which allowed ensuring satisfactory welding-technological properties in welding at the depth of 20–100 m and reaching the level of base metal of 17G1S type steel by the strength properties of weld metal.

The influence of immersion depth in wet welding on impact toughness of the metal in different sections of welded joints was studied taking into account the information about an insufficiently high level of impact toughness of the metal in welded joints, made under the water [3].

Investigations were conducted in a hyperbaric chamber of GK-80 type at internal pressure of 0.2, 0.5 and 1.0 MPa, which corresponded to 20, 50 and 100 m depth of water environment. Welds were made in U-shaped grooves 5 mm deep on plates of 17G1S steel 14 mm thick with flux-cored wire of 1.6 mm diameter, using charge of $TiO_2$–$SiO_2$–$Fe_2O_3$–FeO–$MnO_2$ system in the following modes: $I_w$ = 180–200 A, $U_a$ = 29–32 V, $v_w$ = 18 cm/s. Welding heat input was 32–33 kJ/cm.

The lines for making the notches were marked on templates, cut out of the plates with deposits, after grinding and appropriate etching of weld contours, in such a way that the notch tip was located in the studied zone, i.e. in the weld or coarse-grained section of the HAZ (GOST 13585). Then, the templates were used to make samples for impact bend testing of Mesnager type (GOST 6996, VIII type). To evaluate the HAZ metal resistance to brittle fracture 6–7 samples were made at the same temperature taking into account the complexity of making the notch by the mechanical method in the above zone. Proceeding from test results, the lowest values of HAZ metal impact toughness at a specific temperature were cho-

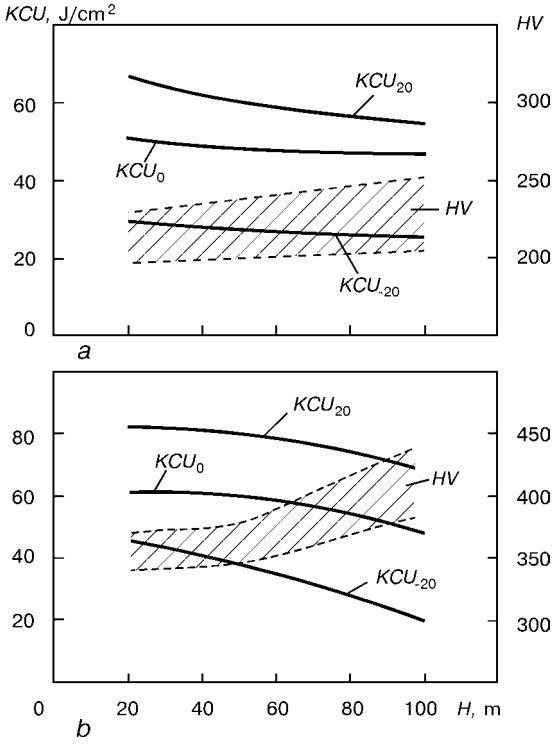


**Figure 1.** Influence of the immersion depth $H$ in wet underwater welding on indices of impact toughness of weld metal (*a*) and coarse-grain section (*b*)

sen. The most brittle metal in the welded joint is located in the coarse-grain section. Now, the nature of sample fracture at impact loading is determined by the properties of the metal, which is in the notch tip [4].

Graphic interpretation of the obtained results, as well as the zones of distribution of maximal hardness in the studied sections of welded joints, determined in Vickers instrument at 50 N load (GOST 2999), are shown in Figures 1 and 2.

It is obvious that the impact toughness of weld metal changes only slightly depending on the depth, at which welding is performed, and has quite good values at room temperature testing of samples (similar to wet underwater arc welding). However, at negative temperature its indices do not meet the standard requirements of guaranteed brittle fracture resistance (below 30 J/cm$^2$). For HAZ metal embrittlement, depending on immersion depth is more pronounced, particularly at testing samples at −20 °C. The fact of embrittlement of the HAZ metal is confirmed by the results of hardness measurement, which in this zone may reach *HV* 430.

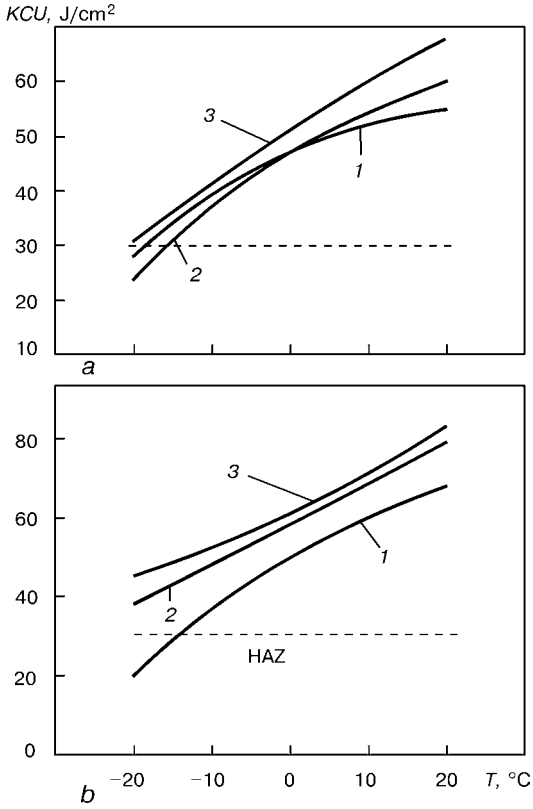


**Figure 2.** Nature of variation of impact toughness depending on testing temperature for weld metal (*a*) and HAZ (*b*) in welding at different depths: *1* — 100; *2* — 50; *3* — 20 m

Figure 2 shows the nature of variation of brittle fracture resistance depending on the temperature of testing both the weld metal and HAZ metal. It is seen from the Figure that the required impact toughness of the metal in the above sections of welded joints, made by wet arc welding with flux-cored wire at the depth of 20–100 m, is ensured at operating temperatures of structure service above −10 °C. This satisfies the requirements of construction of underwater pipelines and allows expansion of the area of application of wet underwater repair technologies.

1. Gretsky, Yu.Ya., Maksimov, S.Yu. (1995) Structure and properties of low-alloy steel joints in wet underwater welding with covered electrodes. *Avtomatich. Svarka*, **5**, 7–11.
2. Gretsky, Yu.Ya., Maksimov, S.Yu. (1994) Metallurgical properties of wet underwater welding with covered electrodes. *Ibid.*, **12**, 10–14.
3. Szelagowski, P., Stugff, H., Loebel, P. et al. (1989) Properties of wet welded joints. In: *Proc. of 21st Ann. OTC, Houston*, May 1–4, 1989.
4. Ivashchenko, G.A., Novikova, D.P. (1988) Structural and mechanical inhomogeneity of HAZ and impact strength of structural steels welded joints. *Avtomatich. Svarka*, **12**, 5–9, 15.

Developed at PWI

# MULTIPURPOSE POWER SOURCE FOR CONSUMABLE ELECTRODE ARC METHODS OF WELDING

The arc methods of welding and surfacing with consumable electrodes in the machine-building branches of industry are leading among all known methods both in volume and cost of products and also in available manpower and operating equipment. The wide range of materials being welded, high requirements to the quality of welding and surfacing jobs, cause demands for application of different methods of arc welding and surfacing.

The multipurpose power source, developed at the E.O. Paton Electric Welding Institute, is suitable in realization of all known methods of automatic, mechanized, manual electric arc consumable electrode welding and surfacing of products made from different materials, providing the high quality. The list of methods of electric arc welding and surfacing, for which the multipurpose power source is designed, types of materials welded and advantages as compared with known power sources are given in the Table.

**Main technical characteristics of the developed multipurpose power source**

| | |
|---|---|
| Voltage of three-phase mains, V | $380^{+19}_{-38}$ |
| Rectified open-circuit voltage, V | $90 \pm 5$ |
| Primary open-circuit current, A | $< 8$ |
| Ranges of smooth adjustment of welding current, A | 40–500 |
| Ranges of smooth adjustment of operating voltage, V | 16–60 |
| Amplitude of current pulses, smoothly, A | up to 800 |
| Duration of current pulses, smoothly, s | $(1–5)\cdot10^{-3}$ |
| Frequency of smooth following of current pulses, Hz | 30–300 |
| Ranges of smooth adjustment of duration of modulated current, s | 0.01–1.00 |
| Ranges of smooth adjustment of modulation frequency, Hz | 0.5–30.0 |

| *Method of arc welding* | *Materials welded* | *Advantages as compared with known sources* |
|---|---|---|
| DC Mechanized and automatic $CO_2$ welding | Steels | Reduction in losses for spattering of electrode metal by 40–50 %, decrease in spatter of products, increase in productivity and decrease in cost of works due to decrease in expenses for cleaning products from spatters and consumption of welding wire |
| Mechanized and automatic $CO_2$ welding with modulated current | Same | Control of sizes, shape and appearance of welds, improvement of mechanical properties of weld metal, HAZ and service characteristics of welded joints |
| Mechanized and automatic welding in gas mixtures Ar + $CO_2$, Ar + $CO_2$ + $O_2$, Ar + $O_2$, Ar + $N_2$ at direct and modulated current | » | Widening the range of welding currents with a stable process without spattering of metal, decrease in requirements to assembly precision, welding along increased gaps and edge displacements, improvement of appearance and service characteristics of welded joints |
| Mechanized automatic flux-cored wire surfacing without arc zone protection using direct and modulated current | » | Providing feasibility of surfacing worn-out parts of both large and small thickness, increase in hardness and wear resistance of deposited metal |
| Pulsed-arc consumable electrode welding in inert gases, mixtures of inert and active gases | Alloys on base of aluminium, copper, titanium, ordinary and high-quality steels | Providing high-quality welded joints on critical products made from different materials in wide range of thicknesses welded, welding in different spatial positions |
| Pulsed-arc consumable electrode welding and surfacing with frequency-, width- and pulse-amplitude modulation of parameters of welding process condition | Alloys on base of copper (bronze, brass), aluminium, titanium, ordinary and high-quality steels | No analogues. Decrease in requirements for the quality of preparation of edges welded; providing welding at increased gaps; decrease in amount of defects in welds, increase in values of their service properties; improvement of appearance of welded joints |
| DC manual electric arc welding with rod coated electrodes of all diameters | Steels | Widening of ranges of welding currents with a stable quality process by 20–30 %, elimination of starting porosity of welds |
| Manual electric arc welding with modulated current | Same | Making vertical welding easier; improvement of mechanical properties of weld metal, HAZ and service characteristics of joints |

| | |
|---|---|
| Operation condition (duty cycle) at 10-minute cycle and rated welding current 500 A, % | 60 |
| Operation condition (duty cycle) at 10-minute cycle and rated welding current 315 A, % | 100 |
| Dimensions, mm: | |
| length | 650 |
| width | 620 |
| height | 1600 |
| Mass, kg | 570 |

The use of one versatile multipurpose power source in realizing many methods of arc welding and surfacing allows attaining, except advantages indicated in the Table, an abrupt decrease in expenses for purchase of a gamma of power sources, saving in electric energy, reduction in working time for wiring and resetting, effective and economic use of working areas that is especially important in the conditions of ship building and repair.

As to the complex of welding-technological capabilities, parameters and advantages (see the Table), there are no similar multipurpose power sources for fulfillment of welding, surfacing, repair and restoration works using different materials in Ukraine, CIS and abroad.

***For additional information, please, address:***

Dr. P.P. Shejko, V.M. Pavshuk,
V.E. Puzanenko, A.M. Zhernosekov
Tel.: (380 44) 227-4478, 261-5231
Fax: (380 44) 268-0486
E-mail: office@paton.kiev.ua